①

GL-TR-89-0306

The Study of Plasma Clouds Around Large
Active Space Structures

AD-A230 634

Daniel Hastings

Massachusetts Institute of Technology
Department of Aeronautics and Astronautics
Cambridge, MA 02139

DTIC
ELECTE
JAN 0 2 1991
D

7 November 1989

Final Report
May 1986–December 1989
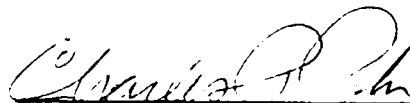
Approved for public release; distribution unlimited

GEOPHYSICS LABORATORY
AIR FORCE SYSTEMS COMMAND
UNITED STATES AIR FORCE
HANSCOM AIR FORCE BASE, MASSACHUSETTS 01731-5000

" This technical report has been reviewed and is approved for publication "
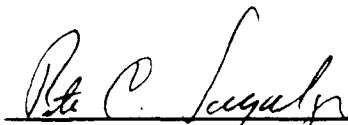

DAVID L. COOKE
Contract Manager

CHARLES P. PIKE
Branch Chief

FOR THE COMMANDER

RITA C. SAGALYN
Division Director

This report has been reviewed by the ESD Public Affairs Office (PA) and is releasable to the National Technical Information Service (NTIS).

Qualified requestors may obtain additional copies from the Defense Technical Information Center. All others should apply to the National Technical Information Services.

If your address has changed, or if you wish to be removed from the mailing list, or if the addressee is no longer employed by your organization, please notify AFGL/DAA, Hanscom AFB, MA 01731. This will assist us in maintaining a current mailing list.

Do not return copies of this report unless contractual obligations or notices on a specific document requires that it be returned.

REPORT DOCUMENTATION PAGE

Form Approved
OMB No. 0704-0188

1a REPORT SECURITY CLASSIFICATION UNCLASSIFIED	1b RESTRICTIVE MARKINGS
2a. SECURITY CLASSIFICATION AUTHORITY	3 DISTRIBUTION / AVAILABILITY OF REPORT Approved for public release; distribution unlimited
2b. DECLASSIFICATION / DOWNGRADING SCHEDULE	

4. PERFORMING ORGANIZATION REPORT NUMBER(S)	5. MONITORING ORGANIZATION REPORT NUMBER(S) GL/TR-89-0306

6a. NAME OF PERFORMING ORGANIZATION Mass. Institute of Technology	6b. OFFICE SYMBOL (If applicable) GL/PHK	7a. NAME OF MONITORING ORGANIZATION Geophysics Laboratory
6c. ADDRESS (City, State, and ZIP Code) Cambridge, MA 02139		7b. ADDRESS (City, State, and ZIP Code) Hanscom AFB, MA 01731-5000

8a. NAME OF FUNDING / SPONSORING ORGANIZATION	8b. OFFICE SYMBOL (If applicable)	9 PROCUREMENT INSTRUMENT IDENTIFICATION NUMBER F19628-86-K-0018
8c. ADDRESS (City, State, and ZIP Code)		10. SOURCE OF FUNDING NUMBERS

PROGRAM ELEMENT NO	PROJECT NO.	TASK NO	WORK UNIT ACCESSION NO.
62101F	LCPD	6H	AB

11. TITLE (Include Security Classification)
(U) THE STUDY OF PLASMA CLOUDS AROUND LARGE ACTIVE SPACE STRUCTURES

12. PERSONAL AUTHOR(S)
Daniel Hastings

13a. TYPE OF REPORT Final	13b. TIME COVERED FROM May 1986 TO Dec1989	14. DATE OF REPORT (Year, Month, Day) 11/7/89	15. PAGE COUNT 86

16. SUPPLEMENTARY NOTATION

17. COSATI CODES			18. SUBJECT TERMS (Continue on reverse if necessary and identify by block number) · Plasma clouds, active space structure
FIELD	GROUP	SUB-GROUP	
20	09		
22	02		

19. ABSTRACT (Continue on reverse if necessary and identify by block number)
Large spacecraft such as the space shuttle perturb the natural environment by releasing contaminants into the atmosphere through outgassing, chemical dumps and thruster firings. A fluid model has been developed to describe the large scale structure of the contaminant plasma cloud. The model is two dimensional with the structure along the magnetic field being averaged out. The model predicts that an important parameter is the parallel length scale of the cloud since this determines the effective length over which electrons can be drawn to short out the ions flowing perpendicular to the magnetic field. In addition, a significant amount of work has been done on the small scale kinetic processes that occur in the contaminant cloud and that cannot be explained by the fluid model. These small scale processes include instabilities in the cloud, ion acceleration by the cloud and anomalous ionization in the cloud.

20 DISTRIBUTION / AVAILABILITY OF ABSTRACT [X] UNCLASSIFIED/UNLIMITED ☐ SAME AS RPT ☐ DTIC USERS	21 ABSTRACT SECURITY CLASSIFICATION UNCLASSIFIED
22a NAME OF RESPONSIBLE INDIVIDUAL Dr. David Cooke	22b TELEPHONE (Include Area Code) 617 377-2931	22c OFFICE SYMBOL GL/PHK

DD Form 1473, JUN 86   Previous editions are obsolete

Contents

iii

1 Summary

Large spacecraft such as the space shuttle perturb the natural environment by releasing contaminants into the atmosphere through outgassing, chemical dumps and thruster firings. A fluid model has been developed to describe the large scale structure of the contaminant plasma cloud. The model is two dimensional with the structure along the magnetic field being averaged out. The model predicts that an important parameter is the parallel length scale of the cloud since this determines the effective length over which electrons can be drawn to short out the ions flowing perpendicular to the magnetic field. In addition, a significant amount of work has been done on the small scale kinetic processes that occur in the contaminant cloud and that cannot be explained by the fluid model. These small scale processes include instabilities in the cloud, ion acceleration by the cloud and anomalous ionization in the cloud.

2 Personnel Involved and Outline

This work has involved thesis research by four graduate students. Mr. N. Gatsonis produced the two dimensional fluid model of the plasma cloud. His work resulted in two papers in the Journal of Geophysical Research which are included as appendices to this report. In addition he received the S. M. degree on this topic. Mr. T. Mogstad worked on a theory of low frequency instabilities for the plasma cloud. He obtained the S. M. degree for his thesis which was entitled " Stability Theory of Plasma Clouds about Large Space Vehicles ". Currently, Mr. R. Biasca is working on a doctoral dissertation on the possibilities of anomalous ionization in the contaminant plasma cloud and Mr. D. Rivas is working on a doctoral dissertation exploring other kinetic effects in the contaminant plasma cloud. These include a theory of ion acceleration and high frequency instabilities in the cloud. The aim is to explain some of the experimental observations which cannot be explained by a fluid theory. In addition, Mr. N. Gatsonis is working on a doctoral dissertation on a three dimensional theory of the plasma cloud. Finally, Dr. Michael Gerver spent some time working on

this prgram and contributed to the work of Mr. David Rivas.

The outline of the report is as follows:

1) Kinetic plasma mechanisms in contaminant plasma clouds (D. Rivas and M. Gerver)

2) Anomalous ionization in contaminant plasma clouds (R. Biasca)

3) Low frequency instabilities in contaminant plasma clouds (T. Mogstad)

4) Three dimensional fluid theory of contaminant plasma clouds (N. Gatsonis)

5) Two dimensional fluid theory of contaminant plasma clouds (N. Gatsonis)

3 Kinetic Plasma Mechanisms in Contaminant Plasma Clouds

3.1 Introduction

In low earth orbit the space shuttle releases neutral water or ions through outgassing, water dumps or thruster firings and thus perturbs the ambient ionosphere. Neutrals and ions undergo chemical reactions and form a contaminant plasma cloud within the perturbed environment of the shuttle. Various authors (Hastings et al., 1989; Eccles et al., 1988) have studied the composition and evolution of this cloud by using two-dimentional fluid models. These studies, however, did not adequately model the small scale-length structure of the cloud. In this report we therefore extend the theory of the shuttle's plasma cloud by studying some of the kinetic processes that have been observed to occur in orbit.

We are mainly interested in explaining observations of high energy ambient O^+ ions (Paterson et al., 1989; Pickett et al., 1985; Shawhan et al.,1984) that were detected in the cloud by the Plasma Diagnostic Package (PDP) flown aboard the third Space Shuttle flight (STS-3). In these experiments O^+ ions with energies up to 10's of eV were observed in the cloud and up to 100 eV during primary and vernier thruster firings. Since these populations of ions have energies at least one order of magnitude larger than the expected 5 eV ram kinetic energy, they could significately affect the structure of the cloud. The mechanism that accelerates these ions is described in the section that follows.

2

3.2 Fermi-like Ion Acceleration Mechanism

The acceleration of charged particles to very high energies is also a problem of interest in the study both of cosmic rays and hot plasmas. Fermi has proposed a method for accelerating particles to cosmic ray energies. In the proposed mechanism, a charged particle is moving in a magnetic field between two interstellar clouds. If the magnetic field in the clouds is assumed to be greater than in the intervening region, the particle is trapped between two magnetic mirrors. Such trapping will occur of course, only for particles whose velocity is inclined to the magnetic field at a sufficient angle. The clouds comprising the two mirrors are assumed to be moving toward each other at some relative velocity. A charged particle now gains energy on each reflection from the mirror. This acceleration may be computed from the constancy of the longitudinal adiabatic invariant (second adiabatic invariant).

In our work we explain the mechanism that accelerates the O^+ ions to high energies by extending this Fermi acceleration concept to the case of the shuttle's plasma cloud. We show that the ambient O^+ ions can be accelerated by interacting with the irregular electrostatic potential structure of the cloud. Some of the electrostatic potential irregularities of interest to us are those due to the partial shielding of the motional electric field $\vec{V} X \vec{B}$ by the dense plasma cloud and those resulting from the electrostatic noise, instabilities, electron density enhancements, and pressure increases observed in such events as flash evaporator system releases and primary and vernier thruster firings (Pickett et al., 1985; Shawhan et al., 1984).

The mechanism that fermi-accelerates the ambient ions can be described as follows. Due to the orbital motion, from a frame of reference moving with the shuttle, the ambient O^+ ions are seen to flow with a 5 eV ram kinetic energy. Those ions in front of the cloud will go through the cloud and interact with its irregular potential structure. In cloud regions with large potential gradients, specifically with potential increases greater than 5 eV, the ions will not have enough kinetic energy to overcome the potential 'barrier' and will therefore bounce off it. Now, if we examine this event from a stationary frame (fixed to the ground), we will see that in this frame the ion energy increases. Figure 1 illustrates this situation, it can be seen that this situation is analogous to the case of a ping-pong ball, which is initially at rest, being overrun by a brick wall (or barrier) moving at the

3

orbital speed. By linear momentum conservation it can be shown that after the first bounce the ion will gain a velocity equal to two times the orbital velocity (V_s). Moreover, further increases in kinetic energy will be possible since after the first bounce the magnetic field will deflect the ion trajectory and make it bounce off other potential barriers. As illustrated in Fig. 1, in each bounce the ion velocity will be incremented by as much as $2V_s$ until the ion kinetic energy will be larger than the potential barrier.

3.3 Kinetic Theory

A rigorous theoretical analysis of the processes described in the previous section would require the derivation of a kinetic model of the ambient O^+ ions interacting with the plasma cloud. One of our major tasks would then be to determine how the electrostatic potential structure of the cloud (which to zeroth order is already known from fluid models (Hastings et al., 1989)) is affected by the accelerated ion population. Specifically, we would be interested in determining whether the electrostatic potential gradients due to the shielding of the motional electric field are indeed the driving forces that accelerate the ambient O^+ ions. If so, we would then calculate the resulting self-consistent structure of the electrostatic potential with high energy ion populations taken into account.

The derivation of a 'closed form' kinetic model of the cloud, however, is a rather difficult if not impossible task. A reasonable kinetic model of the self-consistent shielded potential structure of the cloud would require consideration of collisions and charge exchange reactions between the various species (four neutral and three ion species) and this would complicate the mathematics enormously. It is therefore useful to borrow some of the tricks and short cuts that are often used in solving other problems similar to ours. In the next section we shall review some of the standard techniques that are used in the derivation of kinetic models for strong field gradient problems where the gradients are in the magnetic field and collisions can be neglected. Then we shall apply some of these techniques to our problem and we will derive an approximate constant of motion for particle motion in strong electrostatic potential gradient regions which will be useful to analyze the processes that occur there.

4

3.4 Kinetic Solution to Strong Field Gradient Problems.

There is a great deal of interest at present in acceleration processes in large gradients in the magnetic field which usually occur in critical regions such as in shock structures, in the magnetopause or in other sheet regions such as in the magnetotail. These regions are important because they are often bounderies separating different plasmas, and also because they are frequently the location of particle acceleration.

The standard technique used in solving these strong B-field gradient problems self-consistently is the integration of the Vlasov equation in terms of the single particle constants of the motion. In these problems we therefore seek solutions of the Vlasov equations for ions and electrons, which are expressible in terms of the available constants of motion, and are suitable to represent the particle distributions in the strong field gradient configuration. It should be pointed out that this is not the same as providing general integrals to the Vlasov equation. For instance, in the case of the two-dimenitonal Vlasov equation, the general integral of this equation in five independent variables (two spatial and three velocity components) is expected to contain an arbitrary function of four independent arguments, not of two only (which is the number of available constants of motion). Therefore, these standard techniques are restricted to the study of a subclass of possible solutions, in the hope, of course, that it is relevant to the actual problem.

In the case of the magnetotail, many authors (Grad, 1961; Harris, 1962; Bird and Beard, 1972) showed how solutions could be obtained by using the Poisson and Ampere equations after expressing the plasma distribution functions in terms of the constants of the motion. In the adiabatic limit the constants of motion in the magnetotail are the particles total energy and canonical momentum component perpendicular to the field gradient. In two-dimensional field gradients, however, the canonical momentum is no longer constant. Nevertheless, Propp and Beard (1984) and Beard and Cowley (1985) used the same techniques to calculate ion orbits in a two-dimentional model of the tail. In the latter two papers the authors found that adiabatic theory predictions were generally valid in spite of 'violation of the adiabatic limit'. On the other hand, Roggers and Whipple (1988) were able to derive a more accurate model of the two-dimentional structure of the magnetotail current sheet by deriving a new constant of the motion, the generalized first adiabatic invariant.

which is an extension of the magnetic moment for regions of large magnetic field gradients.

Finally, going back to our problem, we should recall that in the analysis of the acceleration of O^+ ions in the shuttle's cloud we are interested in strong gradients in the electrostatic potential (with the magnetic field constant everywhere). Since any constant of the motion that can be found for the particle motion in such regions would be very useful in analyzing the physical processes that occur there, we shall derive a generalized first adiabatic invariant for the case of the cloud by using the same method that Roggers and Whipple (1988) have used in their analysis of the geomagnetic tail. The procedure for obtaining generalized adiabatic invariants was invented by M. Kruskal (1962) and we shall therefore denote it as the Kruskal method. Latter on, we shall integrate numerically for the O^+ ion orbits and for the electrons we shall use the generalized adiabatic invariant along with energy conservation to predict and model the electron behaviour.

3.5 The Generalized Adiabatic Invariant for Electrons in Regions of Strong Field Gradients.

3.5.1 The Kruskal Method

Before describing the Kruskal method let us first of all recall from classical mechanics that whenever a system has a periodic motion the action integral $\oint pdq$ (taken over a period) is a constant, where p is the generalized momentum and q is the generalized coordinate. If a slow change is made in the system so that the motion is not quite periodic, the constant in the motion does not change and is then called the adiabatic invariant.

The Kruskal method (M. Kruskal, 1962) is a systematic method for finding asymptotic solutions of (and) any adiabatic invariant associated with coupled differential equations having the form

$$\frac{dX}{dt} = f(X, \varepsilon) \tag{1}$$

where X is a N-dimentional vector and ε is a small parameter. Furthermore, $\frac{dX}{dt} = f(X, 0)$ has closed (periodic) solutions that are closed in X-space.

The difficulty in treating eq.(1) is that f is in general both large and (through its dependence on X) rapidly varying in time.

6

The Kruskal method is a transformation procedure for splitting off the rapid time variation of X into a single angle variable $\phi(X)$ leaving an (N-1)-dimentional vector $Z(X)$ which varies slowly. By construction, Z and ϕ have equations of the form

$$\frac{dZ}{dt} = \epsilon h(Z, \epsilon)$$

$$\frac{d\phi}{dt} = \omega(Z, \epsilon) \tag{2}$$

The important feature of the transformation is that ϕ does not appear in h or ω, so that Z varies smoothly with time (with a time derivative of the order of the small parameter ϵ) rather than showing oscillations at the frequency of the ϕ variable.

Equations (2) are the new equations of motion, equivalent to Eq.(1), and thus the solutions of Eqs.(2) when converted back to X-space are solutions of Eq.(1). There exist closed curves ('rings') in X-space on which Z is constant. The ϕ variable is periodic about the ring and specifies position on it (phase angle). The real trajectory differs slightly from a ring and it is not closed in X-space. If equations (1) are canonical equations, derived from a hamiltonean, then there exists an adiabatic invariant in addition to the asymptotic solutions (in ϵ) of the set (1). The invariant is an integral over a ring, not over any segment of an actual particle trajectory:

$$J = \oint_{ring} p(Z, \phi) \frac{\partial q(Z, \phi)}{\partial \phi} d\phi \tag{3}$$

p being the canonical momentum and q the generalized coordinate. For an adiabatic invariant to exist, it is not necessary that eq.(1) itself be of canonical form only that it be possible to convert it to that form.

The transformation X to (Z, ϕ) is actually made by way of intermediate variables (Y, ν), where Y is constant on the closed unperturbed (i.e. for $\epsilon = 0$) curve ('loop') and ν is some phase angle about the loop. The distinction among actual trajectories, loops, and rings can be further classified as follows: an actual trajectory (i.e. for $\epsilon \neq 0$) is generally not even a closed path in the N-dimentional space of X. In the special case (unperturbed case) where $\epsilon = 0$, the trajectory in X is required to be closed in order to apply the Kruskal theory. Only in this case a loop coinsides with a ring.

7

3.5.2 Derivation of the Generalized Adiabatic Invariant for the Electrons.

Let us now use the Kruskal method to derive a generalized adiabatic invariant for regions with strong electrostatic potential gradients. We define our coordinate system to be moving with the shuttle, with the x-axis pointing towards the wake, the y-axis pointing towards the motional electric field direction $\vec{V}X\vec{B}$ and the z-axis pointing towards the $\vec{B}$-field direction.

In order to apply generalized adiabatic theory, the motional electric field $\vec{V}X\vec{B}$ must be assumed to be small and will be denoted by ε. Since the dimentionless quantity which must be small is the ratio (ε/B) drift speed (which in our case is equal to the orbital velocity, i.e. $\ulcorner$ Km/sec) to the particle thermal velocity ($v_{the} = 132.$ Km/sec, $v_{hi} = 0.8$ Km/sec), this derivation will be valid only for the electrons.

We define $\Phi(x)$ as the electrostatic potential and assume that it only changes strongly with x. This potential does not include the potential distribution due to the motional electric field $\vec{V}X\vec{B}$). The equations of motion then are

$$\frac{dx}{dt} = v_x$$

$$\frac{dv_x}{dt} = \frac{e}{m}v_y B - \frac{e}{m}\nabla\Phi(x) \qquad (4)$$

$$\frac{dv_y}{dt} = \frac{e}{m}[\varepsilon - v_x B]$$

where the charge e equals to -e for the electrons. These equations are of the form of eq.(1) with $X = (x, v_x, v_y)$. When $\varepsilon = 0$, the particle does not drift gradually accross the shock in $\Phi(x)$, and all the three components of X are periodic as required.

The next step in the Kruskal procedure is to use the constants of the zeroth-order equations (i.e. eqs(1) with $\varepsilon = 0$) as starting points for constructing the 'Z-variables' that are useful when ε is finite. In our case, these constants are the generalized transverse energy W and the canonical y-momentum p

$$W = K + 2e\Phi/m$$

$$p = p_y = mv_y + eA_y$$

where $K = v_x^2 + v_y^2$ and $A_y = xB$. The quantities W and p are called 'Y-variables' in Kruskal's terminology; it can be shown that these variables have time derivatives of order ε. The phase angle

8

ν may be defined by

$$\tan \nu = -\frac{v_x}{v_y} = \frac{\pm \{m^2(K + \frac{2e\Phi}{m}) - (p - eBx)^2\}}{(p - eBx)}$$

The Y-variables can be improved by the Kruskal procedure to obtain 'nice Z-variables', which have the property that they do not oscillate at the gyrofrequency as do the Y-variables. We denote these improved quantities by $(\tilde{W}, \tilde{p})$ and by following the Kruskal procedure find them to be

$$\tilde{W} = W + 2\varepsilon \int_0^\nu \frac{[< v_y >_t - v_y]}{B} d\nu'$$

$$\tilde{p} = p = mv_y + eA_y$$

where $< v_y >_t$ is the gyro averaged y-component of velocity, and ν is an appropiatly defined phase angle for the gyromotion. The advantage of the Z-variables is that they are strictly drift parameters, varying slowly and smoothly as the particles drift in the x-direction. It can be shown that the time-derivatives of the Z-variables are non-oscillatory and of order ε. Moreover, to zeroth order in ε the phase angle ϕ is equal to ν.

The particle's motion accross the layer can be described in terms of the drift parameters and the generalized invariant. The generalized invariant is constant throughout a particle's orbit through first order in ε even in the region with the strong gradient in the electrostatic potential. In our case the action integral eq.(3) in terms of the Z-variables reduces to

$$J = \oint_{ring} p_x dx$$

In order to estimate this constant of the motion for a very strong potential gradient, which we shall model as a step function in the potential, we first define $Q = 2e\triangle\Phi/mW$ where $\triangle\Phi$ is the potential jump. We must distinguish particles that reflect from the discontinuity from those that cross. Reflection occurs when $\sin^2 \nu_0 < Q$ for $e\triangle\Phi > 0$ (a repulsive potential jump). Here, ν is the phase angle $\tan^{-1}(-v_x/v_y)$ as mentioned above, and ν_0 is the value of ν as the particle is incident on the discontinuity from the upstream side. The angle ν jumps discontinously for both reflected and transmitted particles because v_x changes discontinously as a consequence of the infinite acceleration at the potential jump. The invariant is given by

$$J = \frac{m^2 \tilde{W}}{eB} [\nu_0 - \sin \nu_0 \cos \nu_0]$$

9

for reflected particles, and

$$J = \frac{m^2 \bar{W}}{e} [\frac{(\nu_0 - \sin \nu_0 \cos \nu_0)}{B}$$

$$+ \frac{(1 - Q)\{\pi - \cos^{-1}[p/m(\bar{K}(1 - Q))^{1/2}]\}}{B}$$

$$+ \frac{\cos \nu_0 (\sin^2 \nu_0 - Q)^{1/2}}{B}]$$

for transmitted particles. The reflected particles will continue to 'bounce' against the discontinuity, drifting tangentially, and gradually gain energy until they are able to overcome the potential barrier and propagate across it.

3.6 Acceleration of Ambient Ions by the Cloud Shielding of the Motional Electric Field

In the reference frame moving with the shuttle and in the absence of any electric field perturbation an observer will see the unshielded motional electric field $\vec{E}_m = \vec{V} \times \vec{B}$. However, within a plasma cloud density perturbation the electric field and consequently the drift velocity will be determined by the balance between Pederson and Hall currents, diamagnetic currents, "pickup" currents as well as parallel currents carried by the Alfven wings. The self consistent interaction of these currents will create a polarization field which will shield the imposed motional electric field. Consequently, the electric field within the plasma cloud will be $| \vec{E} | < | \vec{E}_m |$ and the ions will drift backward (in the shuttle frame) with a speed which is less than the orbital. In the case that the motional electric field is entirely shielded, the plasma cloud will be stationary or it will be moving with the shuttle velocity in a fixed frame.

Caledonia et al. (1987) showed that experimental measurements of the contaminant plasma cloud were consistent with an ion residence time in the vicinity of the shuttle of 40 ms. Theoretical work on the plasma cloud about the space shuttle started with the suggestion that the plasma cloud could be highly polarized leading to a long residence time for the ions in the shuttle frame (Katz et al., 1984). A model for the unsteady motion of the plasma cloud was developed by Hastings et al. (1988), where it was shown that for the densities around the shuttle the polarization of the cloud was highly dependent upon the ion density. Recently, Hastings et al.(1989) have extended

10

this model (1988) to include the coupling of the cloud to Alfven waves which can carry current parallel to the magnetic field. Another study of the plasma cloud which takes into account the effect of Hall and Pederson currents was undertaken by Eccles et al. (1988). The Hall currents are shown to rotate the polarization t   hat it is not antiparallel with the motional electric field.

In the following sections we wi.   .ine whether a cloud that shields the motional electric field could have a self consistent potential structure that could fermi accelerate the ambient O^+ ions to the energies observed in the experiments. We will also make an effort to estimate the electrostatic effects of the accelerated particles; therefore, we will try to determine a cloud potential configuration which will be self consistent with all the cloud and ambient species including the accelerated ions. Our approach to the problem will be to use Hastings et. al. (1989) 2-D fluid model to model the cloud and neutral ambient species and to treat the ambient O^+ ions by using kinetic theory techniques. This will therefore allows us to take Fermi acceleration effects into account. In the following section we start by analysing the parts of the 2-D fluid model relevant to our problem.

3.6.1   Two-dimensional Fluid Model of the Cloud

Hastings and Gatsonis (1989) developed a two-dimensional fluid model for the motion of the contaminant cloud perpendicular to the magnetic field lines. They assumed that the contaminant cloud consisted of ions such as O^+, H_2O^+, H_3O^+ and neutrals such as O, H, OH and H_2O. Their numerical solution examined the effects of Alfven wave coupling, neutral water density, ion temperature and initial conditions in the cloud motion. Their results show that in low density neutral water clouds ($\leq 10^9$ cm^{-3}) the shielding of the electric field was small. On the other hand, in neutral water clouds with densities of interest for shuttle conditions ($\sim 10^{10}$ cm^{-3}) the shielding was predicted to be of the order of the motional electric field and the ratios of the line averaged densities of the ions was consistent with experimental data.

Hastings et al. (1989) have solved the fluid equations for a 5 Km by 5 Km square region using a uniform 101 by 101 cartesian mesh. It is useful to review the algorithm that they have used, latter on we shall modify it to include kinetic effects. This algorithm is as follows:

1) With the density profiles $n_{H_2O^+}(x,y)$, $n_{H_3O^+}(x,y)$ and $n_{O^+}(x,y)$ given at some time, inte-

grate the current balance equation

$$\nabla \cdot \vec{J} = 0 \tag{5}$$

to determine the potential $\phi(x, y)$.

2) Use the obtained potential $\phi(x, y)$ in the momentum equations to determine the ion velocities.

3) Use the obtained ion velocities in the continuity equations to advance the densities by one time step. Then, go back to (1).

It is also useful to examine the current balance equation of Hastings et al. (1989). This will enable us to rigorously determine the physical parameters that contribute to the shielding of the motional electric field. Due to the small collisionality assumption in the model ($\nu/\Omega \ll 1$, which restricts the model to water densities below 10^{11} cm^{-3}), the electron current canceled out with the zeroth order ion current (Hall current) and thus the current balance was made between the first order perpendicular ion current and the parallel current carried by Alfven wings. The current balance equation, which in Hastings model is solved for ϕ, can be put to the familiar form:

$$\nabla \cdot (\epsilon \nabla \phi) = \rho_{ext} \tag{6}$$

where ϵ and ρ_{ext} are independent of ϕ. This two dimensional equation has already been integrated along the Alfven characteristics; ρ_{ext} contains terms due to the diamagnetic ion currents and to currents that arise from the friction forces between ion and neutral species. The parameter ϵ which can be thought of as a dielectric constant has the form

$$\epsilon \simeq 1 + \int \frac{ds}{v_a} \bar{\nu}_i \tag{7}$$

where v_a is the Alfven velocity and $\bar{\nu}_i$ is the effective ion-neutral plus reactive collision frequency. The first term in this equation represents the current carried by Alfven waves and the second the pederson current.

The parallel interaction length to perform the parallel integration over can be estimated as

$$L_{\parallel} \simeq 2 r_{cloud} \frac{v_a}{v_\perp} \tag{8}$$

where r_{cloud} is the radius of the cloud in the perpendicular direction and $v_\perp$ is the average perpendicular drift velocity of the cloud. This expression is the distance an Alfven wave can travel in the

12

time the cloud takes to convect across the magnetic field line. If we use eq.(8) in eq.(7) we obtain the dielectric constant as

$$\epsilon \simeq 1 + 2 r_{cloud} \frac{\bar{\nu}_i}{v_\perp} \tag{9}$$

For plasmas with low neutral density the collision frequency is small and the drift velocity is of the order of the orbital speed. In this case, $\epsilon \simeq 1$ and the electric field in the plasma is the motional electric field since the plasma does not shield out the field. Physically, the parallel current carried by Alfven waves is so large that no significant field can built up in the plasma cloud to shield out the imposed motional electric field. For a plasma where neutral water density is high, the collision frequency is large and the drift velocity is small. We find that $\epsilon \ll 1$ and so the electric field is highly shielded. In this case the perpendicular ion current is sufficiently large to give rise to a substantial change in the motional electric field.

3.6.2 Fluid Model Results Suggesting the Need of a Kinetic Model

The electrostatic potential configuration obtained by Hastings et al.(1989) 2-D fluid model for a cloud with an initial water density of $10^{10} cm^{-3}$ which decreases radially away from the shuttle as $(50 m./r)^2$ is shown in Figure 2. In the model the inertia terms in the ion momentum equations were neglected and therefore to zeroth order in (ν/Ω) the "fluid" ions drifted along the equipotential lines at the $\vec{E} \times \vec{B}$ drift velocity. A closer inspection of Figure 2b, however, suggests that it is possible that the O^+ ions could not really drifted along the equipotential lines. This is because, from basic guiding center theory, we know that the only time that the ion larmor motion can be ignored and the guiding center drift be described in terms of the local $\vec{E} \times \vec{B}/B^2$ velocity (guiding centers moving along the equipotential lines) is when the electric field gradients are small in a larmor radius distance. In the case of the cloud, however, the ion larmor radius at the orbital speed (V_0/Ω_{O^+}) is about 40 meters and in this distance, referring to Hastings results (Fig. 2b), we see sizable gradients in the electric field. Therefore, it is questionable whether in Hastings model it was right to assume that the ion trajectories would follow the equipotential lines.

Referring to Fig. 2b, we can see that if the ambient O^+ ions in front of the shuttle structure were not to follow the equipotential lines but instead they were to follow straight trajectories, by

13

the time they would have completed one gyroperiod (0.035 sec. in low earth orbit) they would have drifted 250 meters at the orbital velocity and seen potential increases of as much as 35 eV. Although this situation is impossible, since the O^+ ions have kinetic energies of only 5 eV and therefore do not have enough energy to follow straight trajectories, this fictitious experiment suggests that if the real ion trajectories would lie somewhere between straight lines and the equipotential lines we would expect some kind of bouncing off potential "barrier" or Fermi acceleration to occur.

All this suggests the need of the derivation of a kinetic model of the the cloud where ion larmor motion effects and thus the possibility of fermi acceleration would be taken into account. If fermi acceleration were to occur or the ion trajectories be different from those of the 2-D fluid model this analysis would help us to determine a more accurate self-consistent potential configuration (self-consistent with the cloud and ambient species including the accelerated ions).

3.6.3 Kinetic Treatment of the Cloud

In this section we describe an analysis of the cloud which extends the 2-D fluid model to include the kinetic effects of the ambient ions. As we discussed in the last section, it is very difficult to attempt to derive a 2-D kinetic model of the cloud that would include the shielding of the motional electric field. Since the dominant mechanism for shielding are the ion-neutral collisions (see sec 5.1), a kinetic model that would be useful to investigate fermi acceleration due to this shielding would have to include collisions and this would complicate the mathematics enormously. In our discussion of the previous section, however, we argued the possibility of O^+ ion fermi acceleration in a shielded cloud and that a kinetic treatment of the cloud was necessary in order to obtain accurate self consistent models of the potential structure.

We have therefore found it convenient to use the 2-D fluid model of Hastings et al. (1989), which accurately models ion-neutral and reactive collisions and Alfven currents (crucial for modeling the shielding), to model the cloud ions and neutrals and ambient neutrals but to treat the ambient O^+ ions in a different manner. The ions are treated as individual particles and their behaviour is obtained by numerically integrating their equation of motion. Therefore, ion inertia and larmor motion effects are now taken into account. These kinetic ambient ions are then merged into the

fluid cloud model as follows: First, the O^+ equation of motion is numerically integrated for various particles and the divergence of the O^+ current ($\nabla \vec{J}_{O^+}$) is calculated by using PIC-code particle weighting techniques. Then, the fluid value of $\nabla \vec{J}_{O^+}$ in Hastings current balance equation (eq. 5) is replaced by our kinetic value of $\nabla \vec{J}_{O^+}$. Finally, the potential is obtained by integrating the resulting current balance equation which now includes fermi acceleration effects and the calculations are advanced in time by using the algorithm described in section 3.5.1.

In section 3.5.5 we will show that this kinetic analysis should lead to the same results as those of the fluid analysis (Hastings et al. 1989). We will show that in shuttle cloud models ion larmor motion effects can be ignored, fermi acceleration cannot occur and thus fluid models give an accurate description of the shielding of the motional electric field by the cloud. In the next section we determine the conditions necessary for shielding the motional electric field. We will find this analysis to be useful in understanding the physics of various plasma clouds which we will test in section 3.5.5 for fermi acceleration.

3.6.4 Cloud Effective Radius and Densities for Shielding the Motional Electric Field

In order to determine the values of the cloud parameters (ion and neutral densities, effective cloud radius, etc.) that are needed for the cloud to shield the motional electric field, we consider a simple cloud model. We assume the cloud to be spherical in shape and with a finite effective radius denoted by R_c. Moreover, inside the cloud we assume the ion (n_{ic}) and neutral (n_{H_2O}) densities to be uniform. Therefore, for this cloud to shield the motional electric field the following conditions must be satisfied:

1) the sheath impedance has to be greater than the Alfven impedance

2) the sheath impedance has to be greater than the resistance across the cloud

Here we are referring to the sheath along the magnetic field.

If (1) is violated, the parallel current carried by Alfven waves will be so large that no significant field can build up in the cloud to shield the motional electric field. In this case the current flowing through the cloud will be limited by the Alfven impedance rather than by the saturation current of the ambient plasma, Alfven wings will become charged up to the same potential as the cloud

15

The ions will therefore flow along the equipotential lines.

If (2) is violated, then cloud will be unable to short out the motional electric field in the ambient plasma and thus the cloud ions and electrons will drift downstream of the structure with velocities near the orbital.

Now, the Alfven impedance is (in cgs units)

$$\frac{V_A}{c^2} = c^{-1}(\omega_{ci}/\omega_{pi})_{ambient} \tag{10}$$

and the sheath impedance is the potential across the cloud

$$\frac{V_0 B_0 R_c}{c}$$

divided by either the saturation current from the ambient plasma to the cloud, or the saturation current from the cloud to the ambient plasma, whichever is less. The reason being that the cloud will always develop a potential to keep the net current into the cloud equal to zero. The saturation current into the cloud is

$$e(n_i v_i)_{ambient} + e(n_e v_e)_{cloud} \simeq e(n_e v_e)_{cloud}$$

and the saturation current out of the cloud is

$$e(n_i v_i)_{cloud} + e(n_e v_e)_{ambient}$$

The latter is clearly less than $e(n_e v_e)_{cloud}$, since, as we shall see, $n_{ec} \gg n_{ea}$, while T_{ec} is not that much less than T_{ea} and thus $v_{ea} \simeq v_{ec}$. Therefore, the sheath impedance is

$$\frac{V_0 B_0 R_c}{c(2\pi R_c^2)} [e(n_i v_i)_{cloud} + e(n_e v_e)_{ambient}]^{-1}$$

$$\simeq \frac{V_0 B_0}{c R_c e(n_{ic} v_{ic} + n_{ea} v_{ea})} \tag{11}$$

Now, since the largest current across the cloud is the Pederson current, the resistance across the cloud is

$$\frac{\omega_{ci}}{\omega_{pic}^2 R_c} \left(\frac{\omega_{ci}}{\nu_{in}} + \frac{\nu_{in}}{\omega_{ci}} \right) \tag{12}$$

16

where ν_{in} is the ion (O^+) neutral (H_2O) collision frequency. In our case,

$\nu_{in} = n_{H_2O}\sigma_{H_2O}v_{O^+}$ where $\sigma_{H_2O} \simeq 10^{-15}cm^2$ and v_{O^+} can be taken as the orbital velocity,

thus $\nu_{in} \simeq 5 \times 10^{-11}n_{H_2O}sec^{-1}$ (n_{H_2O} can range anywhere between $10^8 - 10^{14}cm^{-3}$).

The first criterion is then

$$\frac{\omega_{ci}}{c(\omega_{pi})_{ambient}} < \frac{V_0 B_0}{cR_c e(n_{ic}v_{ic} + n_{ea}v_{ea})} \qquad (13)$$

Using $c = 3 \times 10^{10}$ cm/sec, $\omega_{ci} = eB_0/m_ic = 2 \times 10^2$/sec for O^+, $B_0 = 0.3$ Gauss,

$(\omega_{pi})_{ambient} = (4\pi e^2 n_{ea}/m_i)^{1/2}$, $n_{ea} \simeq 5 \times 10^5$ cm^{-3} (dayside), $v_{ea} \simeq 10^7$ cm/sec

(for $T_{ea} = 0.1$ eV), $V_0 = 8 \times 10^5$ cm/sec, $e = 5 \times 10^{-10}$ statcoul,

and $v_{ic} = 5 \times 10^4$ cm/sec for H_3O^+ at 500^0 K, this becomes

$$R_c < \frac{10^{13}}{n_{ic} + 10^8}cm. \qquad (14)$$

The second criterion is

$$\frac{V_0 B_0}{cR_c e(n_{ic}v_{ic} + n_{ea}v_{ea})} > \frac{\omega_{ci}}{\omega_{pic}^2 R_c}\left(\frac{\omega_{ci}}{\nu_{in}} - \frac{\nu_{in}}{\omega_{ci}}\right) \qquad (15)$$

Using $\omega_{pic}^2 = 4\pi n_{ic}e^2/m_i = 10^6 n_{ic}$, it can be shown that this inequality can be satisfied only for

$n_{H_2O} > 10^{10}cm^{-3}(\nu_{in} \geq 0.5sec^{-1})$, for $n_{H_2O} \simeq 10^{11}cm^{-3}$ this becomes

$$\frac{0.32}{n_{ic} + 2 \times 10^7} > \frac{0.08}{n_{ic}}$$

or

$$n_{ic} > 5 \times 10^6 cm^{-3} \qquad (16)$$

Finally, by combining eqs.(14) and (16) we can see that the two criteria for shielding will be satisfied

for $n_{H_2O} > 10^{10}cm^{-3}, n_{ic} > 5 \times 10^6cm^{-3}$, and $R_c < 1$ Km.

Before comparing these results with those from 2-D fluid models, let us note that if the cloud is

elongated by a factor A the conductivity across the cloud would also increase by this factor, then

from eq.(12) n_{ic} times n_{H_2O} can be reduced by A, and the cloud would still be able to short out the

electric field, up to a factor $A = V_A/V_0$ which is a few hundred in low earth orbit. What is really

relevant is the scale length, along the magnetic field, of n_{H_2O} times n_{ic}, not just of n_{ic}. However,

since the neutral density is spreading out in all directions it is questionable wether the elongation

17

would be a few hundred. Hastings et al. (1989) have found substantial shorting out of the electric field for slightly lower densities since they assumed that A is greater than V_A/V_0.

It should be mentioned that T_{ec} will be close to T_{ic}, since the electron cooling time by coulomb collisions with ions, $\sim (\nu_e m_e/m_i)^{-1} \simeq 6 \times 10^{-2}$ sec, is shorter than the escape time of the electrons from the cloud, which is $\frac{n_{ec}R_c^3}{n_{ea}v_{ea}R_c^2} \simeq 10^{-1}$ sec; or at least they are comparable. This confirms that $n_{ea}v_{ea} < n_{ec}v_{ec}$, so the cloud will develop a positive potential to hold electrons in.

3.6.5 Ion Larmor Motion Effects in Clouds that Shield the Motional Electric Field

In this section we determine the larmor motion effects on ambient O^+ ion which go through various types of clouds that shield the motional electric field. We do this by comparing the fluid model ion trajectories and velocities with those of a kinetic model. In the analysis of various types of clouds we consider the trajectory that is most likely to be affected by larmor motion effects, as we shall see, this trajectory will usually be that for ions which are initially traveling towards the center of the cloud.

Figs. 2 a an b show, respectively, the potential configuration and equipotential contours of a cloud after 0.2 sec of being released with an initial central neutral water density of $10^{10}cm^{-3}$ which decreases radially as $(50 \text{ m}/r)^2$ (Hastings et al. 1989). Now, the dominant ion species in the cloud is the ambient O^+ ion, with a density of $n_{O^+} \simeq 2 \times 10^5 cm^{-3}$ which is almost uniform throughout the cloud. Therefore, since the other cloud ion species (H_2O^+ and H_3O^+) are the products of reactive collisions between O^+ and H_2O, they will also have densities more or less uniform throughout the cloud. The ion densities $n_{H_2O^+} \simeq 10^5 cm^{-3}$ and $n_{H_3O^+} \simeq 10^4 cm^{-3}$ decrease more slowly than $(50 \text{ m.}/r)^2$, the water density; in fact, at r=500 m they are down by only one order of magnitude. Consequently, because the total cloud ion density (which is dominated by the ambient ions) decreases radially very slowly, we can see that the resultant potential configuration (Fig. 2a) is smooth and thus the gradients in the potential are small (Fig. 2b) even though the motional electric field is entirely shielded at the structure.

Fig. 2c shows a guiding center or fluid model trajectory (an equipotential line) of an ion which is initially in front of the shuttle. Fig. 2d shows the trajectory of the same ion obtained by numerically

integrating the equation of motion

$$m_{0^+} \frac{d\vec{V}}{dt} = e(\vec{E} + \vec{V} \times \vec{B})$$ (17)

Therefore, the trajectory in Fig. 2d includes ion larmor motion, the ion temperature is assumed to be 0.1 eV. Figs. 2e and 2f show the corresponding velocities. It is interesting to note that the fluid (fig. 2c) and kinetic (fig.2d) trajectories coincide (or almost coincide since $V_0 \gg v_{th}$) and that the ion velocity (or 'kinetic velocity') (fig. 2f) has an average velocity equal to the fluid $\vec{E} \times \vec{B}/B^2$ drift (fig. 2e). We can therefore see that the fluid approximation is accurate for modeling this cloud since the potential gradients are smooth enough so that ion larmor motion can be disregarded. Obviously, no fermi acceleration occurs in this case.

In Fig.3 we examine the case of a cloud with larger potential gradients due to the shielding of the background electric field. We consider a very small cloud with a central neutral density same as that of the cloud in fig. 2, $10^{10} cm^{-3}$, but which decreases much faster, as $(10 \text{ m.}/r)^2$. Figs. 3c and d show, respectively, the fluid and kinetic trajectories and figs. 3e and f show the corresponding fluid and kinetic velocities of an ambient ion which is initially in front of the structure. Although the motional electric field at the structure is almost entirely shielded and the gradients in the potential due to the shielding (potential increases as large as 20 eV in a larmor radius distance, 40 m. at the orbital velocity) are in this case five times larger than those in fig. 2, we can see that the ion trajectory (fig. 2d) adjusts itself to follow the equipotential line (fig. 2c). Therefore, the fluid model is also accurate for describing this cloud: the kinetic trajectory (Fig.3d) coincides with the equipotential line (fig.3c) and the kinetic velocity (fig. 3f) has an average velocity equal to the local $\vec{E} \times \vec{B}/B^2$ drift velocity (fig. 3e). Nevertheless, a small larmor radius effect can be noticed in fig. 3f, in the wake of the cloud the ion larmor speed is two times greater than upstream of the cloud and thus the ion temperature is four times greater. This, however, is not expected to change the potential configuration significantly since the fluid quantities (figs. 3 c and e) are still equal to the average of the kinetic quantities (figs. 3 d and f) and ion neutral collisions will tend to keep the ion temperature down (although they will be unable to keep it equal to the background neutral temperature since the cooling time $\nu_{in}^{-1} > 2R_c/V_0$, the time for ions to travel $2R_c$). It is also interesting to note that in the cloud the total (drift +larmor) ion velocity goes up to 15 Km/sec

19

with corresponding energies of 15 eV. This could therefore explain some of the peaks in the O^+ ion energy distribution near this value observed by Paterson et al. (1989).

Figs. 4 a and b show, respectively, the potential configuration and equipotential contours of a non self consistent or artificial potential of a cloud with an outer region where the potential is smooth and an inner region which exhibits large potential gradients. In this artificial case the cloud not only shields the motional electric field but, from the reference frame of the earth, the cloud is seen to develop an E-field that is even greater in magnitude than the motional electric field. Numerical studies of the cloud show that this type of potential configuration (although not as exaggerated as in fig. 4) can occur in some particular cases where Alfven currents are taken into account (Gatsonis, 1989).

Figs. 4 c and d show, respectively, the fluid and kinetic trajectories and figs. 4 e and f show the corresponding fluid and kinetic velocities of the ion which is likely to experience the largest ion larmor motion effects. It is interesting to note that if the outer region of the cloud (especially upstream of the cloud) has a smooth potential structure, then the majority of the upstream ion, even those initially in front of the structure, will drift at the local $\vec{E} \times \vec{B}/B^2$ velocity along the smooth equipotential lines that surround the inner region. Therefore, only very few ions will enter into the inner cloud region and be fermi accelerated by the sharp potential gradients there.

The above analysis of the three different clouds (figs. 2, 3, and 4) shows that in water clouds with central neutral densities less than $10^{12} cm^{-3}$ the dominant ion species will be the ambient O^+ ion with a fairly uniform density distribution. Furthermore, since the other ion species in the cloud are the products of reactive collisions between the O^+ ions and water neutrals, the overall cloud ion density will decrease slowly in the radial direction (more slowly than the neutral density). Therefore, although near the shuttle the motional electric field will be shielded, the resulting potential structure will always be smooth with weak potential gradients in the outer region of the cloud. Consequently, the ions will just drift according to the local $\vec{E} \times \vec{B}/B^2$ velocity and no fermi acceleration will be possible from the shielding of the clouds with $n_{H_2O} \leq 10^{12} cm^{-3}$.

It might be possible, however, that in a small dense cloud, with a central water density of $10^{14} cm^{-3}$ which decreases radially as $(10 \text{ m}/r)^2$, the H_2O^+ and H_3O^+ ions (products of reactive

20

collisions between O^+ and H_2O) could outnumber the O^+ ions in the cloud and decrease radially in density almost as fast as the neutral water density. This in turn could lead to large potential gradients in the outer region of the cloud that could Fermi accelerate the ambient ions. We could not consider this case because Hastings et al. (1989) fluid model is restricted to $(n_{H_2O})_{central} \leq 10^{12}$ cm^{-3}.

3.7 Acceleration of Ambient O^+ Ions by the Plume of Primary and Vernier thrusters.

Since most of the very high energy ions ($\simeq 100\,eV$) observations (Pickett et al. 1985) were during primary and vernier thruster firings, in this section we examine the possibility of fermi acceleration of the ambient ions in the plume of a primary thruster. The space shuttle fires the primary thrusters in pulses of 80 ms. These thrusters have the following characteristics: thrust=3925 N, I_{sp}=281 sec, c=2753 m/sec, P=1 Mpa, Nozzle diameter= 60 cm, mass flow= 800 g/sec of LO_2 + 150 g/sec of LH_2. Now, since the plume exhaust neutral density is about $10^{17}cm^{-3}$, therefore much higher than the cloud neutral density, large number of exhaust neutrals could be ionized due to reactive collisions with ambient ions. Then, it might be possible that the resulting high plasma density ($\simeq 10^9 cm^{-3}$) could shield the motional electric field inside the plume. If the plume axis would be directed perpendicular to both the B-field and the direction of orbital motion, sharp gradients in the electrostatic potential of the cloud could exist in the plume region. These gradients could then fermi accelerate the ambient ions even for low water cloud densities. Next, we determine whether this situation could happen.

3.7.1 Analysis of the Shielding of the Motional Electric Field in the Plume of the Primary Thruster

In this section we make a basic calculation of the shielding of the motional electric field $\vec{E}_\perp$ in the primary thruster plume to determine whether the density in the exhaust is high enough to short out the background electric field significantly. Assuming that the axis of the plume is perpendicular to both the magnetic field and the direction of orbital motion and neglecting the exhaust velocity

(since $c \simeq V_0/4$), the perpendicular current density is

$$J_\perp = (\omega_{pi}^2 \tau_{loss} + \frac{\omega_{pe}^2}{\tau_{loss}\omega_{ce}^2})E_\perp \qquad (18)$$

where $\tau_{loss} \approx 10^{-3}$ sec is the time an ion takes to go out of the plume, and the ion density in the plume is $n_{ip} \approx 2.5 \times 10^9 cm^{-3}$. This density is based on the ionization rate from collisions of ambient oxygen atoms with plume neutrals, and τ_{loss}. The electron contribution to $J_\perp$ turns out to be much less than the ion contribution, which is

$$J_\perp = \omega_{pi}^2 \tau_{loss}E_\perp = n_{ip}e(\frac{eE_\perp}{m_i}\tau_{loss}) \qquad (19)$$

Note that the expression in parentheses is just the velocity that the ion gets accelerated to in a time τ_{loss}. We use this expression for $J_\perp$, rather than $\frac{\omega_{pi}^2}{\omega_{ci}^2\tau_{loss}}E_\perp$ (the pederson current), because $\tau_{loss}\omega_{ci} \ll 1$. We then find that $J_\perp = 4 \times 10^{-5}$ A/cm^2. By contrast, $J_\parallel$ due to electrons streaming out of the plume (in the absence of an ambipolar potential) would be $n_e e v_e \approx 10^{-2}$ A/cm^2, which is much greater. It follows that $\nabla \cdot J = 0$ can be satisfied only by having $J_\parallel \approx 0$ everywhere, i.e. the potential of the plume on each field line must adjust itself so that electron losses on that field line are balanced by incoming ambient electrons and ion losses. This is in contrast to the case of a big dense plasma cloud, where $\nabla \cdot J = 0$ is satisfied by having $J_\parallel \approx J_\perp$, and $E_\perp$ is shorted out. If we assume the plume electrons to be Maxwellian, the plume potential will then have to be a few T_e above the ambient potential everywhere. This is to keep the electrons from flowing out of the plume and thus $J_\parallel \approx 0$ as is required. T_e will be some fraction of 5 eV, since the electrons are produced by ionization of exhaust atoms and incoming ambient oxygen atoms which collide with an energy of about 5 eV. Therefore, the plume potential will be on the order of 5 V. Whether or not incoming ambient O^+ ions can reflect from the plume potential depends on whether it is greater than or less than 5 V. To answer this depends on a more detailed calculation, but at least it is plausible that fermi acceleration (only one bounce) occurs.

However, it is possible that the plume potential be much larger than 5eV since it is very sensitive to the electron temperature in the plume, and for that matter to the electron distribution function. Because, it is not obvious that the electron distribution function is maxwellian, even a small deviation from a maxwellian, e.g. an extended tail, can have a big effect on the potential

22

which will adjust itself to keep the electrons from flowing out of the plume, if the potential is a few times greater than the bulk temperature. This will depend on the velocity distribution at which electrons are born (from ionization by collisions between exhaust molecules and incoming ambient atoms, and any other ionization source that is important), and on any instabilities that occur in the initial distribution, and how these affect the distribution. Also, ambient electrons coming in along the magnetic field, and accelerated by the potential may contribute significantly to the electron distribution and instabilities.

3.7.2 Trajectories of Ambient Ions across a Shielded Primary Thruster Plume

Figs. 5 a and b show, respectively, the potential configuration and potential contours of a plume fired in the direction of the motional electric field (negative y-direction). Figs. 6 a and b show these same quantities but for a plume which is fired in the direction opposite to the motional electric field. These potential characteristics are (artificial) non self consistent (with the plume and cloud plasma) and the plume is assumed to shield the motional electric field at a potential equal to the potential at the structure. Therefore, to the left of the shuttle (in the negative y-direction)the ambient ions will see a potential hill at the plume (fig. 5) and to the right of the shuttle they will see a potential well (fig. 5). For simplicity, we have studied these two cases separately and only considered 1-D potential shocks (variations in the plume potential along the y-direction were ignored). Figs. 5c and 6c show the (fluid) $E \times B$ drift O^+ ion trajectories (which is of course coincide with the equipotential lines) and figs. 5e and 6e show the corresponding guiding center drift velocities (equal to the local $\vec{E} \times \vec{B}/B^2$). Figs. 5d and 6d show the particle (or 'kinetic') trajectories of the ambient O^+ ions (obtained by numerically integrating the equation of motion) and figs. 5f and 6f show the corresponding particle velocities . In figs. 5 and 6 the potential shocks caused by the plume shielding were assumed to be equal in magnitude but opposite in sign and relatively smooth.

We can see that in the case of a potential well (fig. 6) the ion larmor motion does not affect the trajectory and thus a fluid description of the ambient ions would be relatively accurate in this case The small increase in the ion temperature downstream of the plume should not in reality

23

be that high due to ion-neutral collisions at the plume. On the other hand, in a potential shock equal in magnitude but opposite in sign (a potential hill, fig. 5) we can see that ion larmor motion effects become significant. Although we do not see the ion bounce off the shock and upstream of the shock (up to the plume axis) the fluid description seems to be accurate, the sharp potential gradient at the plume axis makes the ion guiding center leave the equipotential line and accelerate to very high velocities.

Finally, in fig. 7a we show the potential of a plume with a potential hill of about 6 V but with large potential variations in distances of the order of the ion larmor radius at the thermal velocity ($\triangle \phi \approx 6$ V in distances of 5 meters). Figs. 7 b and c show the ambient ion fluid an kinetic trajectories and figs. 7 d and e show the corresponding velocities. In this plume we see that ion larmor motion and ion inertia effects are important since we see the ion bouncing off the plume (fig. 7 c) and thus fermi accelerating to velocities three times larger than the orbital in one bounce. It is interesting to note that if the background motional electric field were not present the particle would fermi accelerate only to velocities twice the orbital (fig. 1). However, in our case, after the first bounce the background motional electric field does work on the ion and thus the ion ends up with energies of more than 6 times its initial (not only 4 times as predicted by fermi acceleration). This agrees with the observed peak in the O^+ energy distribution near 30 eV (Paterson et al., 1989). It is also interesting to note in fig. 7e, that after the first bounce, due to the work of the background motional electric field on the ion, the second time the ion encounters the shock it has a velocity of 2.3 times V_0 (corresponding to a kinetic energy of 26 eV.). Nevertheless, the second time the ion encounters the shock it could still bounce off it, even if the potential increase at the shock is less than 26 V, as long as the ion kinetic energy component perpendicular to the shock is less than that of the potential increase at the shock. Therefore, more than one bounce could be possible with plume shielding potentials not much larger than 5 V above the background potential. If the ion could bounce three times it could readily be accelerated to energies of about 100 eV's.

24

3.8 Summary and Conclusions

A basic analysis of the shielding of the motional electric field by a spherical plasma cloud shows that, when Alfven currents are taken into account as well as the sheath along the B-field, the motional electric field will be shielded for $n_{H_2O} > 10^{10} cm^{-3}$, $n_{ic} > 5 \times 10^6 cm^{-3}$, and $R_c < 1$ Km (R_c is the effective radius of the cloud which could be defined as the distance at which the neutral water density is three orders of magnitude lower than the density at the center). If the cloud is elongated by a factor A, then the requirements of n_{H_2O} times n_{ic} decrease by this factor up to V_A/V_0 which is a few hundred in low earth orbit.

The self consistent study of the acceleration of ambient ions by the potential of a polarized cloud requires a kinetic treatment. Analytical kinetic models pose difficult mathematical problems since collisions must be taken into account. These models are also complicated by the fact that when considering fermi acceleration problems, regions of strong field gradients must be included. Nevertheless, it is possible to derive a constant of the motion of the electrons in these regions for studying the processes that occur there.

A study that is based on a self consistent fluid model of the cloud but that takes into account O^+ ion kinetic effects shows that water clouds with central neutral water densities less than $10^{12} cm^{-3}$ will have smooth potential distributions for all values of R_c, the effective radius. In these clouds the dominant ion species is the ambient O^+ with a density distribution that is more or less uniform throughout the cloud. Since the other cloud ion species, H_2O^+ and H_3O^+, are products of reactive collisions between O^+ and the cloud's H_2O neutrals, they will have density profiles that do not fall as fast as the n_{H_2O} profiles and for $n_{H_2O} < 10^{13} cm^{-3}$ will be at the most of the order of magnitude of n_{O^+}. This will lead to smooth potential configurations that will be unable to fermi accelerate the ambient ions.

Large and medium size water clouds ($R_c > 600$ m) with $(n_{H_2O})_{central} \geq 10^{13} cm^{-3}$ will have potential configurations that will be smooth in the outer region of the cloud for the same reason as the less dense clouds. Therefore, no fermi acceleration is expected to occur in these cases either. On the other hand, very small polarized clouds ($R_c \approx 100$ m) with $(n_{H_2O})_{central} \geq 10^{13} cm^{-3}$ can have potential gradients that are sharp enough in the outer region of the cloud to fermi accelerate

25

the ambient ions.

The plume of a primary thruster of the shuttle has a neutral density of $10^{17} cm^{-3}$ and is ionized by reactive collisions with the ambient atomic oxygen to plume ion densities of $10^9 cm^{-3}$. Due to the fact that the time an ion takes to go out of the plume is small (10^{-3} sec), the perpendicular current in the plume is small. Charge conservation therefore requires that the parallel current be also small. Consequently, the plume potential has to adjust itself to hold the electrons in and is very sensitive to the electron distribution function. If the plume electrons were Maxwellian the plume potential would be about 5 V above the background potential and this could lead to one bounce or fermi accelerating the O^+ ions to 26 eV. However, because of instabilities and ionization processes that take place in the plume the electron distribution function is not expected to be Maxwellian and this could lead to much larger plume potentials. Therefore, ambient ions could bounce two or three times off the plume and easily end up with energies of about 100 eV. (because the motional electric field also does work on the ions that bounce off).

Finally, it is important to mention that the major problem in the self consistent study of fermi acceleration lies in modeling the strong potential gradients or shocks self consistently. If these shocks are due to the shielding of the motional electric field, as in the case of polarized clouds and primary thruster plumes, a self consistent model must have to take ion-neutral collisions into account. Therefore, since conventional PIC codes and particle tracking codes do not include collisions, they cannot be used in modeling these problems. A hybrid treatment, such as the one described in this report (using the 2-D fluid model of the cloud and kinetic O^+ ions), seems to be a good way to approach the problem of the plume.

3.9   References

Beard, D.B. and Cowley, S.W.H., Electric and magnetic drift on non-adiabatic ions in the earth's geomagnetic tail current sheet., Planetary Space Sci., 33, 1985.

Bird, M.K. and Beard, D.B., Self-consistent description of the magnetotail current system., J. Geophys. Res. 77, 1972.

Eccles J.V., Raitt W.J., and Banks P.M., A numerical model of the electrodynamics of plasma within the contaminant gas cloud of the space shuttle orbiter at LEO., J. Geophys. Res., 1989.

Gatsonis N.A.,(private communication), Dept. of Aeronautics and Astronautics, M.I.T., 1989.

Grad H., Boundary layer between a plasma and a magnetic field, The Physics of Fluids, 4, 1961.

Harris E.G., On a plasma sheath separating regions of oppositely directed magnetic field., Il Nuovo Cimento, 29, 1962.

Hastings D.E., and Gatsonis N.A., The motion of contaminant water plasma clouds about large active space structures., J. Geophys. Res., 94, 1989.

Kruskal M., Asymptotic theory of hamiltonean and other systems with all solutions nearly periodic., J. of Mathematical Phys., 3, 1962.

Paterson W.R., and Frank L.A., Hot ion plasmas from the cloud of neutral gases surrounding the space shuttle., J. Geophys. Res., 94, 1989.

Pickett J.S., Murphy G.B., Kurth W.S., and Goertz C.K., Effects of chemical realeses by the STS3 orbiter on the ionosphere., J. Geophys. Res., 90, 1985.

Propp K., and Beard D.B., Solar wind access to the plasma sheet along the flanks of the magnetotail., J. Geophys. Res., 89, 1984.

Roggers S.H., and Whipple E.C., Generalized adiabatic theory applied to the magnetotail cur-

rent sheet., Astrophysics and Space Science, 144, 1988.

Shawhan S.D., Murphy G.B., and Pickett J.S., Plasma diagnostic package initial assessment of the space shuttle orbiter plasma environment., J. Spacecraft, 21, 1984.

4 Anomalous ionization in contaminant plasma clouds

The computational simulation of medium and low frequency plasma processes can aid greatly in developing an understanding of the interactions between a spacecraft and the plasma environment of the upper atmosphere. The usual method of accomplishing time-dependent plasma simulations is the particle-in-cell (PIC) code. These PIC codes simulate a plasma which, in reality, may consist of between 10^{20} and 10^{25} particles by integrating the equations of motion of between, typically, 10^3 and 10^5 'macro-particles'. In the usual explicit electrostatic PIC code, the Lorentz force law is used to 'push' particles along their trajectories over some small time step ($\omega_{p,e}\Delta t \ll 1$, where $\omega_{p,e}$ is the electron plasma frequency). The particles are then weighted to a grid to determine a charge density distribution over the domain, and Poisson's equation is solved to determine the potential and electric field. This electric field is used to push the particles to new positions, and the process repeats. Plasma properties such as density and temperature are found by taking the appropriate moments of the distribution function of the macro-particles.

Numerical stability requirements, however, restrict the typical explicit PIC code to time steps of $\omega_{p,e}\Delta t < 2$. Hence, available computer processing power restricts explicit PIC codes to simulations of processes with frequencies on the same order as the electron plasma frequency. For simulating low and medium frequency phenomena ($\omega \ll \omega_{p,e}$), implicit methods must be used. The implicit method uses a modified form of Poisson's equation which results in an algorithm that is stable for all time steps and can therefore be used to simulate low frequency processes.

The objective of the current research is to develop an implicit PIC code capable of simulating low and medium frequency plasma phenomenon. The code is to be developed in a manner commiserate with the ultimate goal of studying spacecraft-upper atmosphere interactions. Work towards this objective has continued over the last year. An explicit code (used as a baseline model)
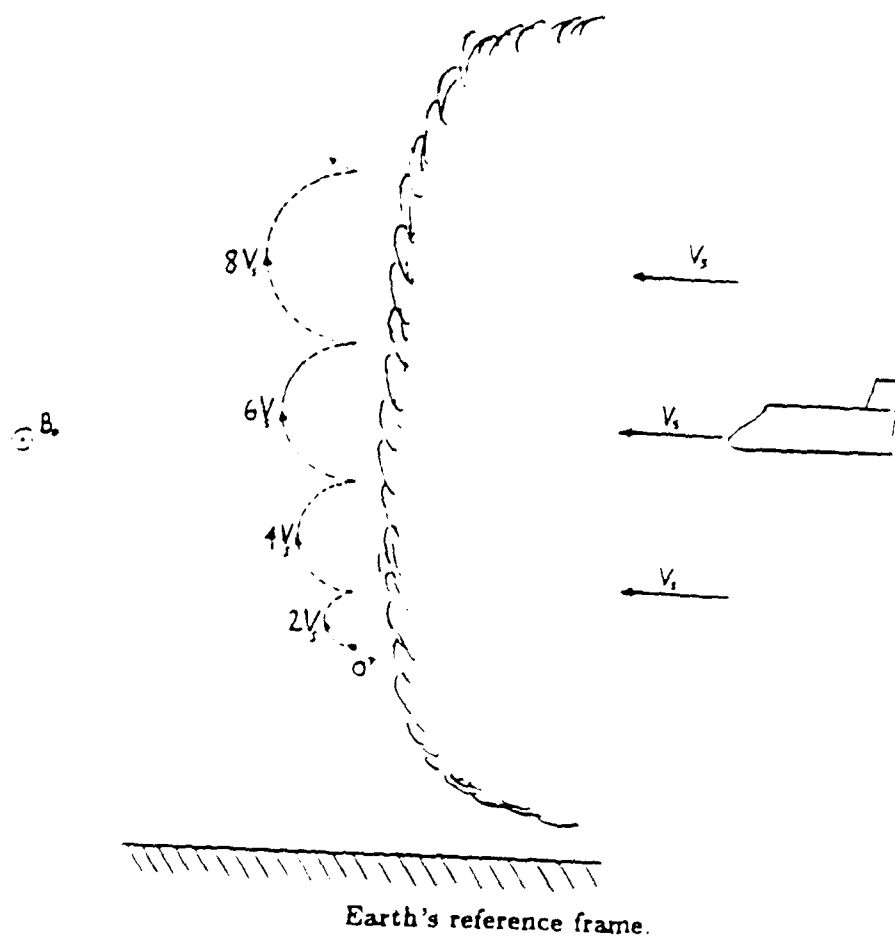
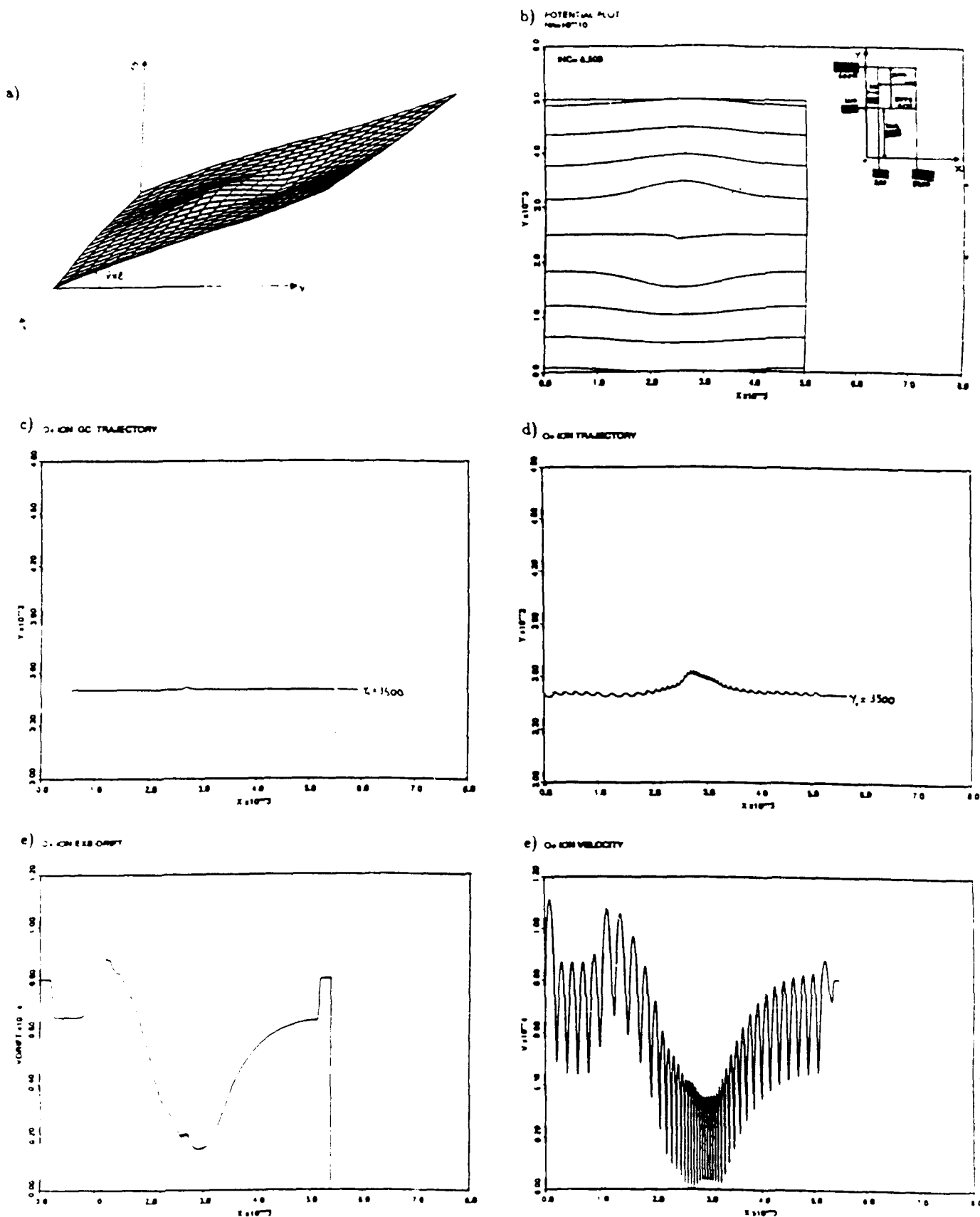Figure 1. Fermi-like acceleration of ambient O^+ ions.

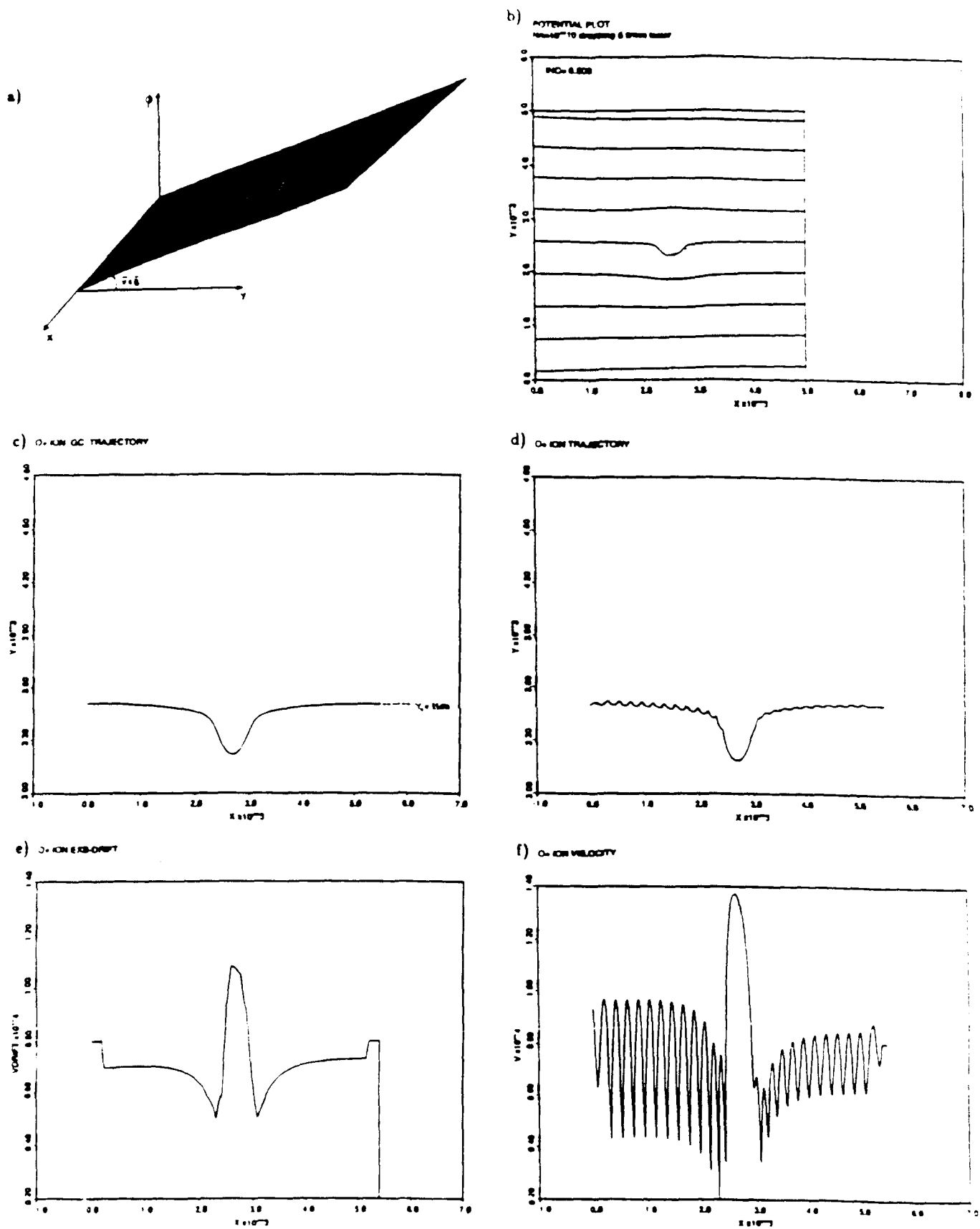Figure 2. Fluid and kinetic descriptions of an ambient ion going through a large water cloud (SI units)

Figure 3. Fluid and kinetic descriptions of an ambient ion going through a small water cloud (SI units).
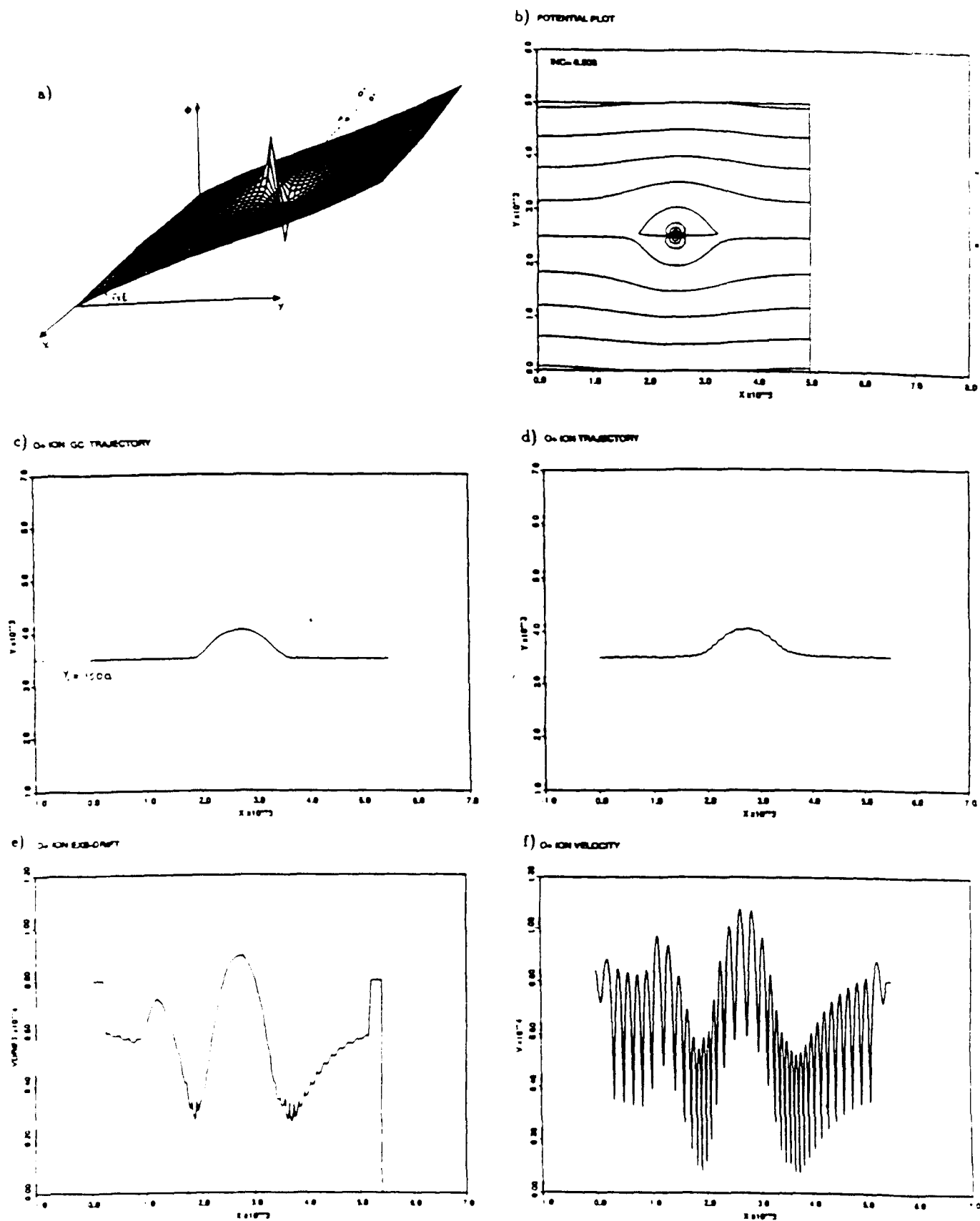
Figure 4. Fluid and kinetic descriptions of an ambient ion going through a water cloud with a smooth potential in the outer region and sharp potential gradients in the inner region (SI units)
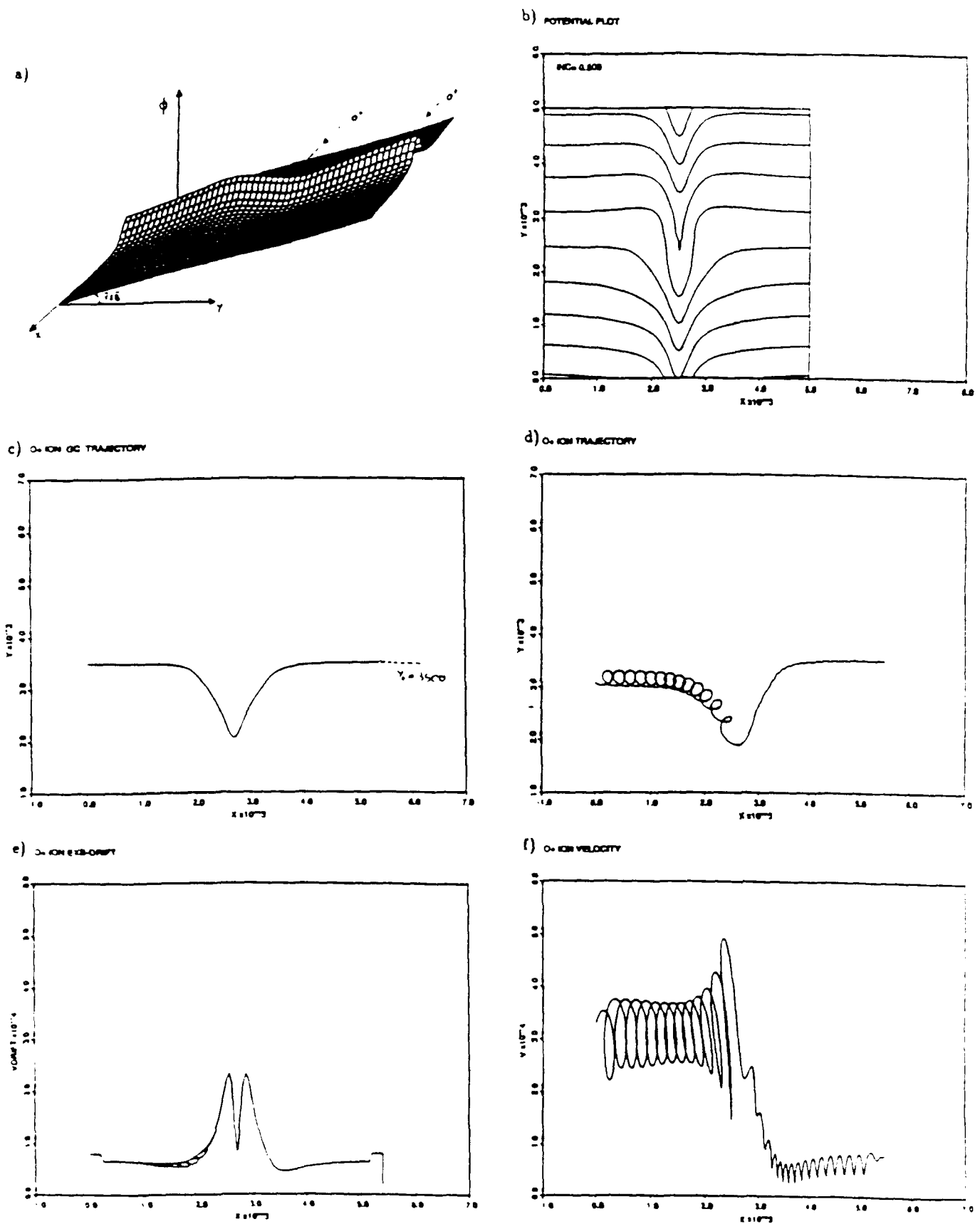
Figure 5. Fluid and kinetic descriptions of an ambient ion going through a plume with smooth potential variations (SI units).
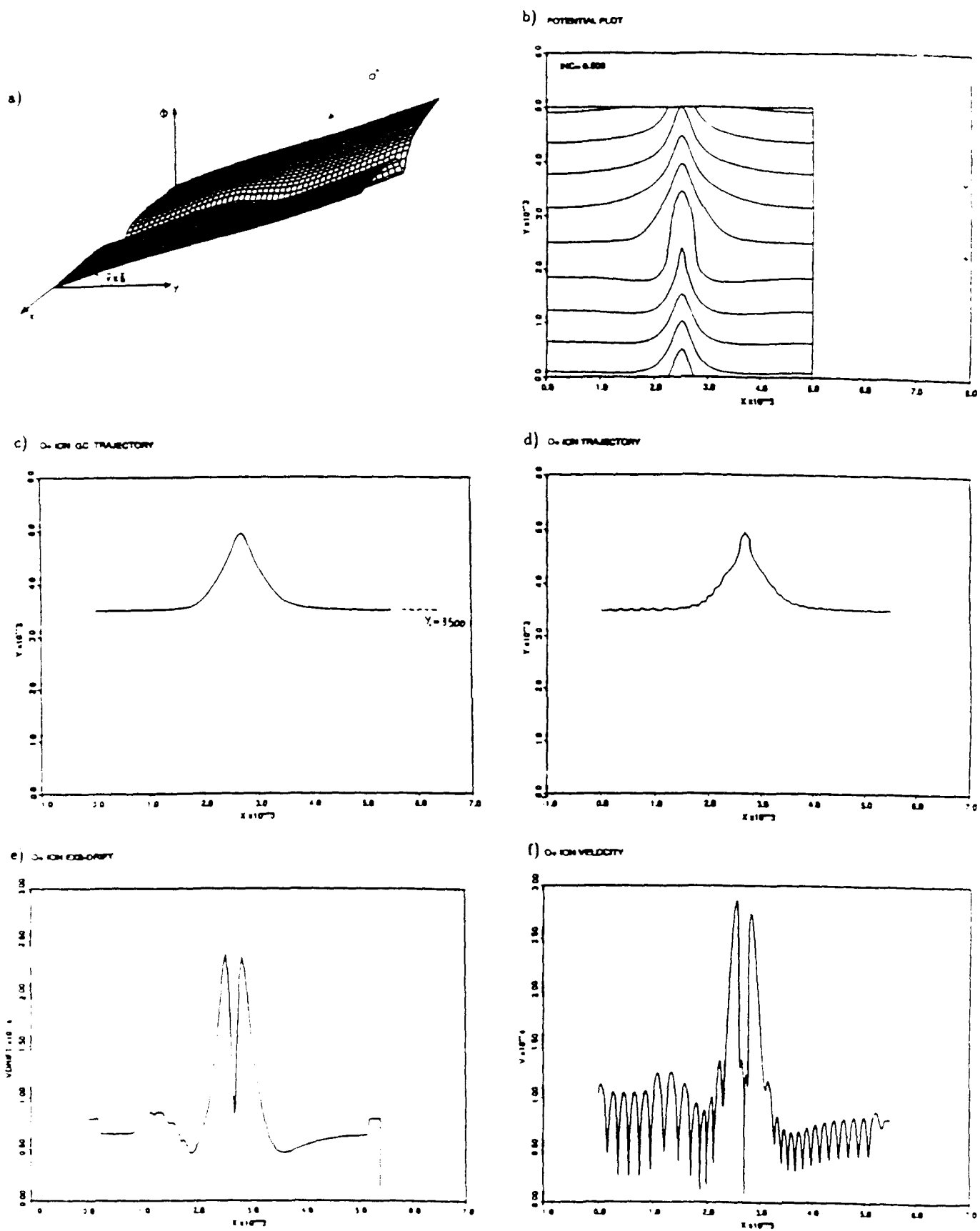
Figure 6. Fluid and kinetic descriptions of an ambient ion going through a plume with smooth potential variations (SI units)
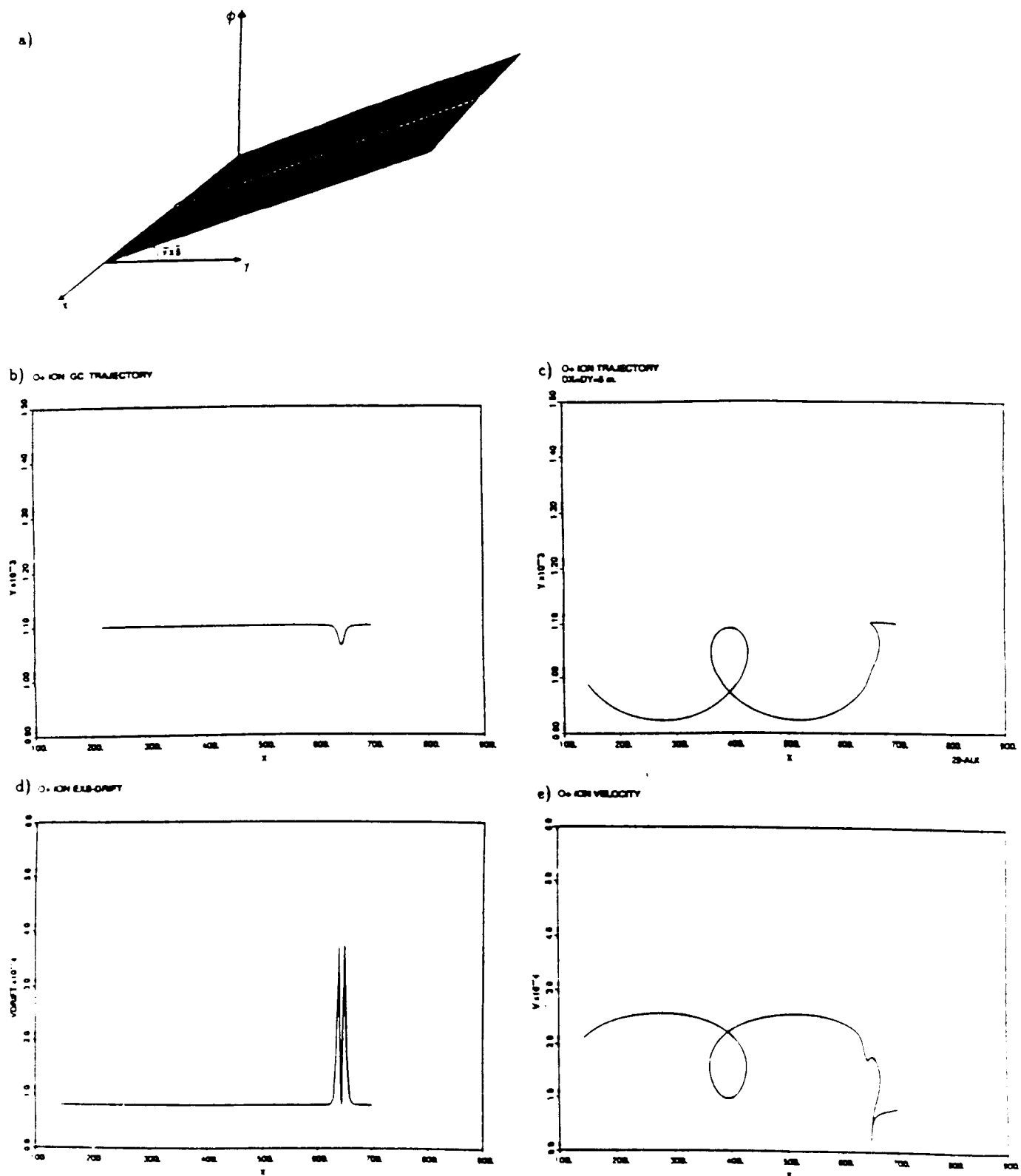
Figure 7. Fluid and Kinetic descriptions of an ambient ion going through a plume with large potential gradients (SI units).

35

and an implicit code ca⁻ıble of modelling low and medium frequency phenomena have both been developed and are currently functional. Presently, the codes are doubly periodic. Development of bounded, explicit and implicit codes is currently underway. Further validation of all the codes is also continuing by comparing the results of the codes which each other and with examples from the literature. Extensions of the code to include more complex geometries and chemical reactions are planned for the future.

5 Low frequency instabilities in contaminant plasma clouds

In this section, the abstract of Mr. Mogstad's thesis is reproduced. For more detail, the thesis can be referenced (T. Mogstad, S. M. Thesis, Dept. of Nuclear Engineering, MIT, 1987).

It has been observed that the Space Shuttle in its ionospheric orbit has a relatively dense plasma cloud associated with it. The Shuttle is releasing water, and the plasma cloud is generated when ambient O^+ ionizes the water through a charge exchange reaction. Electrostatic noise at frequencies between 0-30 kHz has been recorded in the Shuttle vicinity. We have performed a stability analysis of the plasma cloud with respect to the $\vec{E} \times \vec{B}$ instability. We model the cloud density distribution as a cylindrical step function along the geomagnetic field, and the Shuttle is travelling in the west-east direction. This modtion with respect to the magnetic field generates an electric field in the moving Shuttel frame, which triggers a destabilizing electric polarization field inside the cloud. By applying linearized continuity equations, momentum balance, charge conservation and quasinuutrality we obtain a local dispersion realtion. The dispersion relation is solved analaytically and indicates that the instability growth rate exhibits a maximum at the backside($\theta = 180°$) of the cloud, wheras the oscillating frequency is greatest at $\theta = 90°$. By increasing the parallel wavenumber k_z, the temperature, the parallel conductivity or the collision frequency, the instability is reduced. Increasing the Shuttle velocity makes the cloud more unstable. In addition to local modes, we consider global modes and we find that exponentially growing eigenmodes can build up on the backside of the cloud.

The local dispersion relation is solved numerically, and the results support the findings from the analytic analysis. we also show that a steep density gradient is inherently unstable in crossed

$\vec{E}$ and $\vec{B}$ fields and that the cloud has steady state solutions only when linearized.

The poloidal localization of instability modes suggests that Shuttle carried sensors operating inthe very low frequency regime (i. e. below 100 Hz) should not be used at poloidal angles of $\theta = \pm 90°$. Also, radio communications at all frequencies can be scattered by striations at the anisotropic backside of the cloud where the instability growth rates are the greatest. the growth rate frequency is estimated between 1-1000 Hz and the oscillating frequency between 1-100 Hz. The latter can induce signal degradation of radio waves of frequencies less than 100 Hz only.

6 Two and three dimensional fluid theory of contaminant plasma clouds

Finally in this report we include two published papers on two dimensional fluid theory and a recent AIAA paper on three dimensional fluid theory.

A Simple Model for the Initial Phase of a Water Plasma Cloud About a Large Structure in Space

D. E. Hastings, N. A. Gatsonis, and T. Mogstad

Department of Aeronautics and Astronautics, Massachusetts Institute of Technology, Cambridge

Large structures in the ionosphere will outgas or eject neutral water and perturb the ambient neutral environment. This water can undergo charge exchange with the ambient oxygen ions and form a water plasma cloud. Additionally, water dumps or thruster firings can create a water plasma cloud. A simple model for the evolution of a water plasma cloud about a large space structure is obtained. It is shown that if the electron density around a large space structure is substantially enhanced above the ambient density then the plasma cloud will move away from the structure. As the cloud moves away, it will become unstable and will eventually break up into filaments. A true steady state will exist only if the total electron density is unperturbed from the ambient density. When the water density is taken to be consistent with shuttle-based observations, the cloud is found to slowly drift away on a time scale of many tens of milliseconds. This time is consistent with the shuttle observations.

1. Introduction

Since the dawn of shuttle flights to the ionosphere it has been realized that the ambient ionosphere is strongly perturbed by the presence of a large body in space [*Green et al.*, 1985]. Several experiments on board the space shuttle have been devoted to the measurement of the plasma parameters in the vicinity of the spacecraft [*Murphy et al.*, 1986; *Reasoner et al.*, 1986]. It has been found that the shuttle or any body in space affects the ambient environment through the interaction of its associated contaminant cloud with the environment. The contaminant cloud arises from surface outgassing, leaks from life support systems, thruster firings, and water dumps. The contaminant cloud can undergo several different types of interactions with the ambient environment ranging from physical interactions such as momentum transfer to chemical interactions such as charge exchange. The result is that the self-consistent environment around a large body in space may be significantly different from the ambient environment. We choose to put the emphasis on large bodies since large bodies can have an associated contaminant cloud which makes an $O(1)$ change to the ambient environment. By an $O(1)$ change we mean that the composition of the ion density is substantially changed. For example, observations around the shuttle [*Pickett et al.*, 1985] indicate that the observed environment differs considerably from the expected ambient environment.

It is important to study the self-consistent environment around large space vehicles such as the shuttle for several reasons. The major reason is to understand the noise that will be observed on any sensors carried on the vehicle [*Pickett et al.*, 1985]. This will directly affect the utility of the sensors for purposes of observation. Another important reason is to build understanding of the space plasma environment and some of the processes that can occur in it. Finally, study of the self-consistent environment will help in understanding such basic design issues as how to mitigate spacecraft charging in low Earth orbit.

In this paper we develop a simple model for the motion of a water plasma cloud around a large structure in the ionosphere. In section 2 we derive the equations that describe the

large-scale plasma flow around the body. In section 3 we obtain a analytic solution for the case where there is no electrostatic modification of the motional potential. This case corresponds to a plasma cloud which does not enhance the ambient density. In section 4 we perform a multiple scale analysis and obtain the equations for the field line averaged densities and potential. For the case where the cloud density exceeds the ambient density we show that the equations of motion do not allow steady state solutions and suggest that the cloud may be unstable to the growth of $\mathbf{E} \times \mathbf{B}$ gradient instabilities. We then solve the model equations numerically with a flux conserving transport (FCT) numerical method and show the long time behavior of the plasma cloud. We obtain the ion residence time for a range of cloud densities. For densities typical of what is observed around the shuttle, the residence times are consistent with the measurements. Finally in section 5 we conclude with a discussion of the significance of these results for measurements from large space vehicles such as the shuttle. Although the equations of the water plasma cloud are generally applicable, we choose to concentrate on the dynamic behavior of an initial water plasma "puff" which could arise from a magnetoplasmadynamic (MPD) thruster firing or a plasma source.

2. Derivation of the Equations for the Plasma Cloud

Plasma clouds in the ionosphere have been studied both theoretically and experimentally for a number of years [*Perkins et al.*, 1973; *Zabusky et al.*, 1973; *Mitchell et al.*, 1985]. The major motivation has been to understand the dynamics of such clouds since they have been used for tracing the magnetic field lines and they may interfere with communications. In this work we shall follow a similar path to obtain the equations for the plasma and self-consistent electrostatic potential around a large body.

We work in a frame attached to the space structure and start by assuming that the space structure is emitting neutral water into an ambient background of oxygen ions and neutrals. The spacecraft is taken to be moving at orbital velocity with respect to the ambient environment ($\simeq 8$ km s^{-1} for low Earth orbit). For an ambient environment whose neutral density is of the order of 10^8 cm^{-3} the mean free path of the water molecules is many kilometers. Hence for length scales of

up to a few kilometers we can take the water molecules as freely expanding with their thermal velocity and write the steady state neutral water density as

$$n_{H_2O} = n_{H_2O}{}^0 (r_0/r)^2 \qquad (1)$$

This assumption about the neutral density is reasonable for low water densities (water density much less than the ambient neutral density) but will have to be modified for higher densities. However, since we wish to concentrate on the plasma dynamics, we shall leave more detailed modeling of the neutrals for future work. In (1) we have approximated the structure as a sphere of radius r_0 and taken r as the radial distance from the center of the sphere. This approximation will be reasonable for any body shape as long as we are several body dimensions from the body. So for example, the space shuttle, whose longest dimension is of the order of 40 m, can be reasonably approximated in this manner at distances of the order of 100 m and beyond. The density $n_{H_2O}{}^0$ is the density of water at the surface. The assumption that the neutral species is water is based on observations from the space shuttle, where the dominant contaminant species was observed to be H_2O [Caledonia et al., 1987].

The ionic water may be formed by the charge exchange reaction

$$O^+ + H_2O \xrightarrow{k_{cx}} O + H_2O^+ \qquad (2)$$
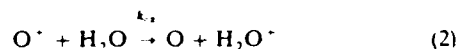
where in the frame moving with the space structure the oxygen ions sweep through with an energy of up to 5 eV. At this energy the reaction rate k_{cx} has been measured and is $k_{cx} = 6 \times 10^{-10}$ cm^3/s [Murad and Lai, 1986a], and for O^+ the charge exchange collision frequency is $v_{cx} = n_{H_2O}k_{cx}$.

We assume for simplicity that the body is moving perpendicular to the magnetic field with velocity in a fixed frame of V. We define a wind velocity in the moving frame as $V_w = -V$ and then define a Cartesian coordinate system (x, y, z) in the moving frame by taking the distance x to be along the direction of $-V_w$, the distance y to be along the direction of $-V \times B$, and the distance z to be along the direction of the magnetic field B. We note that the negative y direction is along the direction of the unshielded motional electric field that will be seen in the far field from the moving frame. The frame is illustrated in Figure 1.

We take the oxygen and water ions to be mainly moving across the magnetic field due to their large gyroradii while the electrons are taken to dominantly flow along the magnetic field due to their small gyroradii. This assumption on the ion motion is true on the large scale where the ions have a chance to complete their gyroorbits. In the work by Caledonia et al. [1987] the ions were taken to be almostly perfectly shielded from the motional electric field, and hence in the moving frame the only motion available to them was parallel motion. In this work the potential is being calculated in a self-consistent manner so that the ions can move across the magnetic field. The perpendicular velocity of the oxygen ions can be obtained from the steady state momentum balance equation [Krall and Trivelpiece, 1973] and is

$$v_{O^+} = (\kappa_{O^+}F_- - \kappa_{O^+}{}^2 F_- \times b)(1 + \kappa_{O^+}{}^2) \qquad (3)$$

where b is the unit vector in the magnetic field direction with κ_{O^+} being the Hall parameter given

$$\kappa_{O^+} = \Omega_{O^+}/(v_{O^+ - H_2O} + v_{cx}) \qquad (4)$$
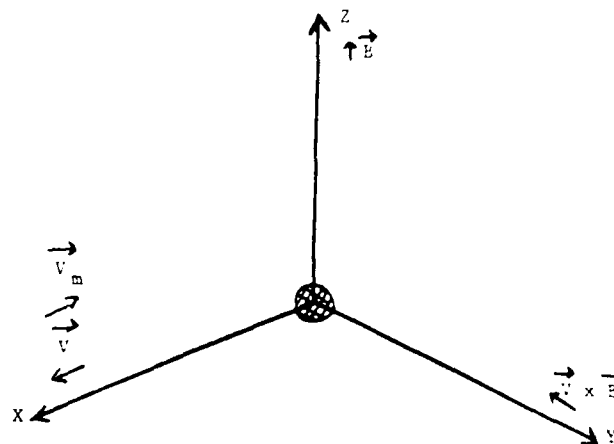
and Ω_O, being the oxygen cyclotron frequency while $v_{O^+ - H_2O}$ is the oxygen ion-neutral water momentum exchange collision frequency. The vector F_- is given by

$$F_- = -(cT_i/eB)\nabla_- \ln n_{O^+} + (ce/B)E - v_{O^+ - H_2O}v_{H_2O}/\Omega_{O^+} \qquad (5)$$

In (5). T_i is the ion temperature, which we take to be constant, and the first term is the force due to the ion pressure. E is the electric field seen from the moving frame and gives the electric force on the ions in the moving frame, and v_{H_2O} in the third term is the velocity of the water, a term that expresses the force on the oxygen ions due to collisions with the water neutrals. In the derivation of the force on the oxygen ions the dominant collisions for these ions have been taken to be collisions with the neutral water molecules (rate constant $\simeq 1.2 \times 10^{-9}$ cm^3/s). Collisions with oxygen neutrals (rate constant $\simeq 3 \times 10^{-9}$ cm^3/s) have been neglected for simplicity since we anticipate little differential velocity between oxygen neutrals and ions. In (3) the first term gives rise to the well-known Pedersen conductivity while the second contains the $E \times B$ drift and the Hall current. We note that the Hall parameter takes very large values for parameters typical of the ionosphere ($v_{O^+ - H_2O} \simeq 2 \times 10^{-3}$ s^{-1} and $\Omega_{O^+} \simeq 1.8 \times 10^2$ s^{-1}, so that $\kappa_{O^+} \simeq 9 \times 10^4$). This suggests that the dominant motion for the oxygen ions will be the $E \times B$ drift. Hence we can write the continuity equation for the oxygen ions as

$$\frac{\partial n_{O^+}}{\partial t} - \frac{c}{B}\nabla \phi \times b \cdot \nabla n_{O^+} = -n_{O^+}v_{cx} \qquad (6)$$

where the electric field in the moving frame is $E = -\nabla \phi$ and the boundary condition on (6) is that for $r \to \infty$ the oxygen density approaches the ambient density.

The electrons will mainly flow along the magnetic field but will also have an $E \times B$ drift across the field. In addition, electrons will be lost as a result of dissociative recombination of the water ion. This occurs with a rate k_{recom} which we shall specify later. Hence we can write the electron continuity equation as

$$\frac{\partial n_e}{\partial t} - \frac{c}{B}\nabla \phi \times b \cdot \nabla n_e + \nabla \cdot \Gamma_- = -n_e n_{H_2O}k_{recom} \qquad (7)$$

where Γ_- is the parallel electron flux given by

$$\Gamma_- = \frac{cn}{m_e v_c}\nabla v_- \qquad (8)$$

Fig. 1. Coordinate system

and the potential ψ_e is defined as

$$\psi_e = \varphi - \frac{T_e}{e} \ln (n_e / n_{ambient}) \tag{9}$$

In (9), φ is the self-consistent potential which is modified by the electron pressure. The parallel current is related to the parallel electric field through the resistivity (η_e):

$$j_\| = -e\Gamma_e = \frac{1}{\eta_e} (-\nabla_\| \psi_e) \tag{10}$$

where the resistivity is given by

$$\eta_e = \frac{m_e \nu_e}{n_e e^2} \tag{11}$$

In (8) the collision frequency ν_e is the electron momentum exchange frequency due to collisions with the neutrals or the ions. The physical content of this equation is that the electrons flow along the field lines and are swept across it by the self-consistent potential in the plasma cloud. We note that for any steady state to exist for this equation it is necessary that there be a convection of electrons across the field lines. This implies that the potential contours must be open. This is because closed potential contours will cause the plasma to rotate [Daly and Whalen, 1979] but will not lead to any net loss. This implies that the symmetry breaking part of the electrostatic potential will be crucial in determining the motion of electrons. This part of the potential will arise from the fact that the system is moving and hence sees a motional potential.

Once we have the equations for the oxygen ions and the electrons, the equation for the water ions follows from the requirement that the plasma remain quasi-neutral.

$$n_{H_2O^+} = n_e - n_{O^+} \tag{12}$$

As an alternative to using (6), (7), and (12) we could use (6) and (12) coupled with the equation for the water ions

$$\frac{\partial n_{H_2O^+}}{\partial t} - \frac{c}{B} \nabla \varphi \times b \cdot \nabla n_{H_2O^+} = n_{O^+} \nu_{cx} - n_e n_{H_2O^+} k_{recom} \tag{13}$$

Finally, we need an equation to determine the self-consistent potential. This equation comes from the requirement of quasi-neutrality for all times. This means that in addition to (12) we require that we have charge conservation $(\nabla \cdot j = 0$ where j is the current flowing in the plasma). We take the perpendicular current to be given by the perpendicular ion flows (equation (3) and the analogous equation for the perpendicular water velocity) and the parallel current to be given by the electron flows (equation (10)) and obtain the equation [Drake and Huba, 1986]

$$\frac{c}{B} \nabla \cdot \left(\left(\frac{n_{H_2O^+}}{\kappa_{H_2O}} + \frac{n_{O^+}}{\kappa_{O}} \right) \nabla \varphi \right) - \nabla (D_{,H_2O} n_{H_2O^+}$$

$$- D_{,O} n_{O^+}) + \left[b \times v_{H_2O} \cdot \nabla \left(n_{O^+} \frac{v_{O^+ H_2O}}{\Omega_{O^+}} \right) \right.$$

$$\left. + b \times v_{,o} \cdot \nabla \left(n_{H_2O^+} \frac{v_{H_2O}}{\Omega_{H_2O^+}} \right) \right] + \nabla \left(\frac{1}{e\eta_e} \nabla \psi_e \right) = 0 \tag{14}$$

In this equation for charge conservation the perpendicular ion diffusion coefficient is

$$D = \frac{1}{\kappa} \frac{cT}{eB} \tag{15}$$

where the Hall parameter for the water ions is

$$\kappa_{H_2O^+} = \Omega_{H_2O^+} n_{H_2O^+ O} \tag{16}$$

We note that in this expression all the $E \times B$ drifts have canceled out since they do not give rise to any net current. The first term on the left-hand side of (14) arises from the Pedersen current due to the electric field, the second term due to the diffusion of ions down the density gradients, and the third due to the Hall current, while the fourth is the electron flow to balance the ions. This equation must be solved subject to the boundary condition that in the far field the electric field in the moving frame is the motional electric field. This requires that for $|r| \to \infty$ we have $\nabla \varphi = -V \times B/c$. We can interpret the first two terms in the potential equation (equation (14)) as giving the shielding from the plasma cloud while the last term is the charge neutralization by the parallel flow of electrons from far away in the ionosphere.

3. ANALYTIC SOLUTIONS OF THE CLOUD EQUATIONS

The set of equations for the potential and densities cannot in general be solved analytically. However, it is possible to obtain a special solution and draw some general conclusions from the structure of the equations.

If the density of the cloud is very low, then we expect that the motional potential will be only weakly shielded by the cloud. In this case we approximate the electric field everywhere by the boundary condition on (14) and write $\nabla \varphi = -V \times B/c$ for all space. If we require that $\phi = \phi(r)$ (i.e., we do not allow any parallel electric fields), then in the absence of recombination we have from (7) in steady state that

$$-V \cdot \nabla_{,} n_e = 0 \tag{17}$$

which has only two possible solutions, either that $n_e = n_{ambient}$ everywhere or that n_e varies in only one direction in space, which is physically unreasonable. The oxygen equation is

$$-V \cdot \nabla_{,} n_{O^+} = -n_{O^+} \nu_{cx} \tag{18}$$

which has the solution

$$n_{O^+} = n_{ambient} \exp \left\{ -\frac{n_{H_2O}{}^0 k_{cx}}{V} \frac{r_0{}^2}{(y^2 + z^2)^{1/2}} \right.$$

$$\left. \left[\arctan \left(\frac{-x}{(y^2 + z^2)^{1/2}} + \frac{\pi}{2} \right) \right] \right\} \tag{19}$$

This shows the product of the water column density traversed by an O^+ ion and the charge exchange cross section. Hence the electron density is constant everywhere while the oxygen ion density is depleted and partially replaced by the water ion density. The contours of constant water ion density relative to the ambient electron density are shown in Figure 2 for a typical case of an outgassing structure which is emitting water from a central region of 100 m in radius. We choose to look on these large length scales since there is evidence from plasma diagnostics package (PDP) measurements around the shuttle of water ions out to a kilometer from the shuttle (G. Murphy, private communication, 1987). We see that most of the depletion for the oxygen density occurs on the wake side of the structure, and for this case, somewhat less than half of the oxygen ions are converted to water ions. Hence for this case the water plasma cloud is actually a depletion relative to the ambient electron density.
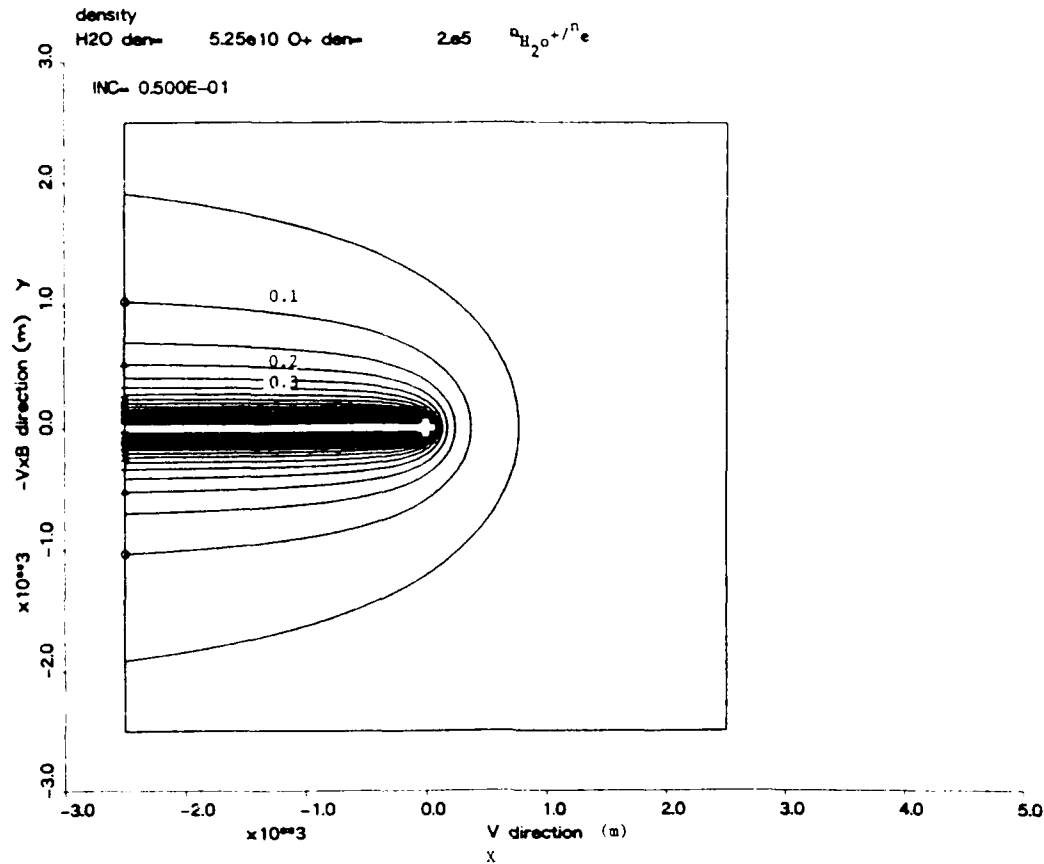
40

density
H2O den=   5.25e10 O+ den=   2.e5 $n_{H_2O^+}/n_e$

INC= 0.500E-01

Fig. 2   Steady state water ion density contours for a uniform electron density. Water ion density is normalized to the electron density

4. Derivation and Numerical Solution of the Averaged Cloud Equations

Since the plasma flow along the magnetic field is extremely rapid compared to the perpendicular flow, we can simplify the equations describing the plasma by doing a formal multiple scale analysis. Physically, we expect the cloud to take a cigar shape along the magnetic field. The equations for the field line averaged density and field line averaged potential can be obtained by averaging the density and potential equations where the averaging operator is given by

$$ F = \left(\int dl\, B \right)^{-1} \int f\, \frac{dl}{B} $$

Hence from this point, N_e, $N_{H_2O^+}$, N_{O^+}, and Φ refer to the field line averaged electron density, water ion density, etc. The field line average operator annihilates the parallel terms in the electron density and potential equations and gives for the density equations (from (6) and (7))

$$ \frac{\partial N_{O^+}}{\partial t} - \frac{c}{B} \nabla_\perp \Phi \times \mathbf{b} \cdot \nabla N_{O^+} = - N_{O^+} \nu_{ii} \tag{20} $$

$$ \frac{\partial N}{\partial t} - \frac{c}{B} \nabla_\perp \Phi \times \mathbf{b} \cdot \nabla n_i = - N_e N_{H_2O^+} k_{recom} \tag{21} $$

while the potential equation (equation (14)) is

$$ \frac{c}{B} \nabla_\perp \cdot \left[\left(\frac{N_{H_2O^+}}{\kappa_{H_2O^+}} + \frac{N_{O^+}}{\kappa_{O^+}} \right) \nabla_\perp \Phi \right] + \nabla_\perp $$

$$ (D_{\perp H_2O^+} N_{H_2O^+} + D_{\perp O^+} N_{O^+}) $$

$$ + \left[\mathbf{b} \times \mathbf{v}_{H_2O^+} \cdot \nabla \left(N_{O^+} - \frac{v_{O^+ H_2O}}{\Omega_{O^+}} \right) \right. $$

$$ \left. + \mathbf{b} \times \mathbf{v}_{O^+} \nabla \left(N_{H_2O^+} - \frac{v_{H_2O^+ O}}{\Omega_{H_2O^+}} \right) \right] = 0 \tag{22} $$

In obtaining these equations we have used the multiple scale assumption to say that the densities and potential have a strong dependence on the perpendicular direction and a weak dependence on the parallel direction. This is a reasonable assumption for the plasma quantities but cannot be applied to the neutrals. Therefore in (20), (21), and (22) we have evaluated the neutral water density in the plane $z = 0$. This assumption enables us to obtain a closed set of equations for the field line averaged quantities and still contains the appropriate physics. We note that in (22) we have neglected the parallel current carried by Alfven waves. This point will be addressed in future work.

This set of equations describes the dynamic evolution of a water plasma cloud as seen from a moving frame and with the

potential calculated self-consistently. We shall use these equations to study the evolution of a water plasma cloud where the initial density may be larger than the ambient electron density. As pointed out by *Caledonia et al.* [1987], such an enhanced density cannot arise self-consistently solely by chemical processes such as charge exchange. Therefore in those cases where the water plasma density exceeds the ambient density we assume that the water plasma has been injected at the initial time due to some mechanical mechanism such as the firing of a plasma source.

This set of field line averaged equations for a plasma cloud around a space structure still cannot be solved analytically, but it can be shown that the only steady state solution allowed is the one previously discussed where the electron density is uniform everywhere. The proof of this statement is given in the appendix and follows a similar proof in work by *Dungey* [1958]. Since in the far field the electron density must match the ambient density, we conclude that plasma clouds whose density exceeds the ambient density cannot be steady state structures. Therefore the enhanced densities seen around the shuttle [*Pickett et al.*, 1985] must be transient phenomena. The fact that a plasma cloud whose density exceeds the ambient will continuously evolve is also suggested by the following physical arguments: Such a plasma cloud will have a density distribution which will probably peak toward the center of the cloud. The moving cloud will have Pedersen currents in it which act to modify the imposed motional field. These Pedersen currents are density dependent since they arise from the bulk motion of ions due to the potential gradients. Therefore we expect, and (22) confirms this, that the highest-density regions of the cloud will modify the motional potential most effectively. Hence the low-density cloud edges will see a self-consistent $E \times B$ drift different than the higher-density regions. This leads to a velocity shear through the cloud which causes it to continuously distort. Therefore no steady state will exist. The time scale on which this distortion will take place will be a function of density. It can be estimated on the basis of the arguments given by *Perkins et al.* [1973] if we assume that the dominant effect of the cloud is to shield the potential. If the cloud has density $n_c \gg n_{ambient}$, then the electric field in the cloud is $E_\gamma \simeq n_{ambient} n_c E_0$, where $E_0 = V \times B c = E_0 e$. From $\nabla \times E = 0$ we obtain

$$E_x \simeq -(n_{ambient} \; n_c^{-2})(dn_c \; dx)E_0$$

The cloud velocity is $V = c E \times B B^2$, which gives

$$v_x \simeq -V(n_{ambient} \; n_c)$$

$$v_x \simeq -V(n_{ambient} \; n_c^{-2})(dn_c \; dx)$$

We see that in the moving frame the cloud will drift backward with a velocity which depends on the density and will drift sideways with a velocity which depends both on the density and on how sharp the density gradient is in the direction of the neutral wind. From these estimates we can see that distortion will occur on a time scale of L_n $[V(n_{ambient} \; n_c)]$ where L_n is the density length scale. For the case of the space shuttle if we take the density length scale to be the shuttle length $(\approx 50$ m) and take a water ion cloud of 10^6 cm^{-3} in an ambient density of 10^4 cm^{-3}, then for a velocity of 8 km s the distortion time is 0.6 s.

We have solved the averaged cloud equations (equations (20), (21), and (22)) for a 5 km by 5 km square region using a uniform 101 by 101 Cartesian mesh. The center of the square was fixed on the structure. With $N_{H_2O}(x, y)$ and $N_0(x, y)$ given at some time we calculate the potential from (22) and use that result to obtain the flow field velocities. Then that information is used in (20) and (21) to advance the densities by one time step.

Successive point over relaxation (SPOR) was used to solve the elliptic current balance equation. This scheme introduces a relaxation parameter into the equation, which then allows an iterative solution of the problem [*Roach*, 1976]. The derivatives were approximated by second-order finite differences, and iterations were carried out until the maximum error was less than 10^{-5} between two successive iterations. Neumann boundary conditions were applied in both the x and y directions. We required the potential to match the following boundary conditions in the far field:

$$\nabla_\perp \phi = -\frac{V \times B}{c}$$

in the $V \times B$ direction and

$$\nabla_\perp \phi = 0$$

in the direction of motion. The potential of the central structure was taken to be 4 V, which is consistent with measurements taken from the shuttle.

For the convective equations we used the two-dimensional flux correction method (FCT) of *Zalesak* [1979]. The high-order scheme was a leapfrog trapezoidal [*Roach*, 1976] with fluxes calculated with the flux formulae developed by *Zalesak* [1984], while a donor cell scheme [*Roach*, 1976] was used for the lower scheme to complete the FCT algorithm. Symmetric boundary conditions were applied on the density distributions, and the flux limiter was applied on every iteration. No assumptions were made about the symmetry of the solutions so that the computations were carried out through the whole mesh. The oxygen ion density approached the ambient ion density (taken to be 2×10^4 cm^{-3}) at the edges of the square. The water ion density was assumed to have an initial Gaussian profile falling off on a length scale of 500 m

$$N_{H_2O} = N_{H_2O}(x = 0) \exp\left[-\left(\frac{|r - r_c|}{R_t}\right)^2\right]$$

where $|r_c| = 50$ m and $R_t = 500$ m. This simulates a large-scale ionic water injection. The initial water ion profile for a typical simulation is shown in Figure 3, where the central density for this case was $N_{H_2O}(x = 0) = 10^6$ cm^{-3}. In this figure the x direction corresponds to the negative wind velocity direction. That is, the neutral wind is blowing from positive x to negative x in this figure. The negative x direction is the direction of the motional electric field.

In Figures 4-6 we show the initial distribution of potential for a density profile as given in Figure 3 and for three initial ion water densities. In Figure 4 the initial water density was $N_{H_2O}(x = 0) = 10^4$ cm^{-3}. In this figure we see the shielding (electric field decreases) that arises when the total ion density exceeds the ambient oxygen ion density and the cloud behaves
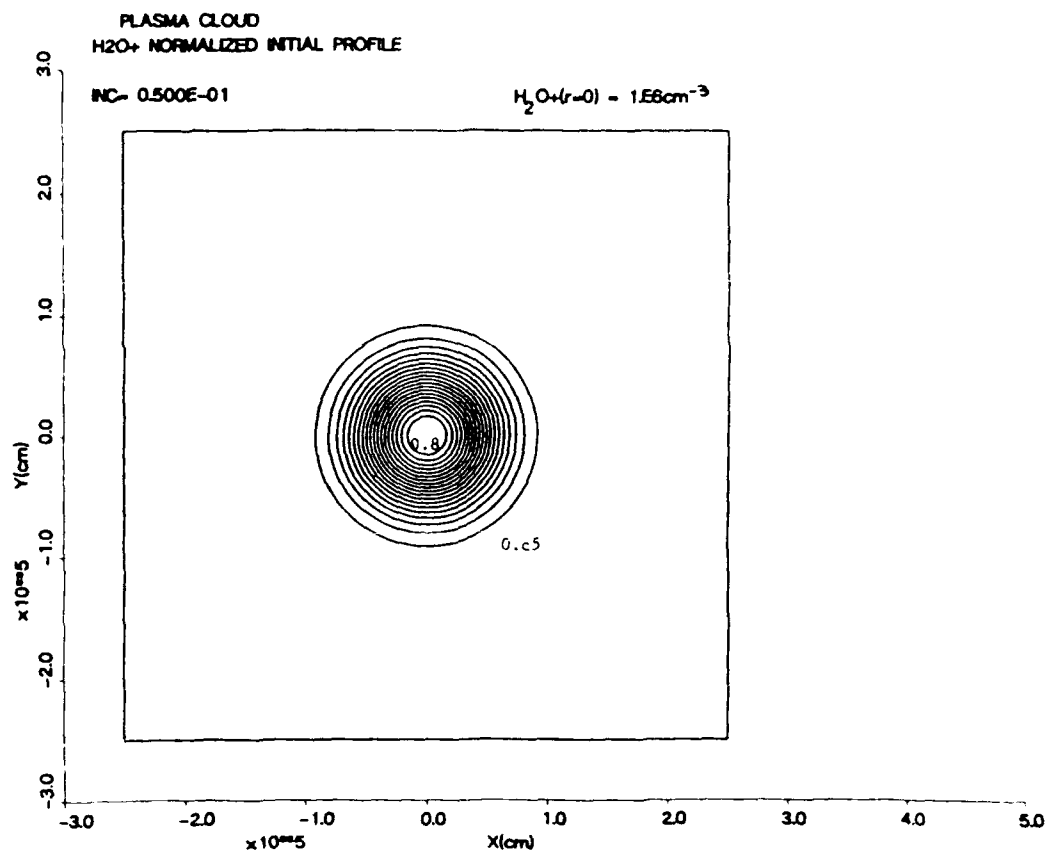
PLASMA CLOUD
H2O+ NORMALIZED INITIAL PROFILE

INC= 0.500E-01 $H_2O+(r=0) = 1.66cm^{-3}$

Fig. 3   Initial water ion density contours for numerical simulations. This corresponds to an initial puff of water plasma
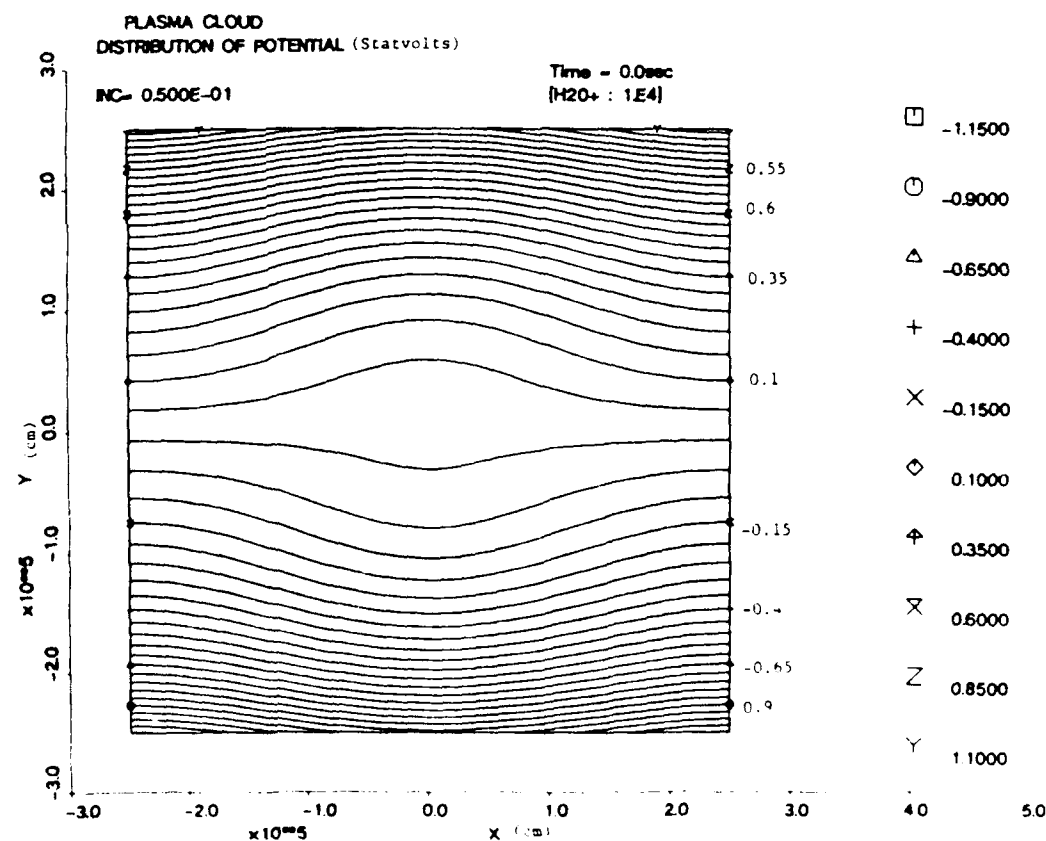Water ion density is normalized to the far field electron density.

PLASMA CLOUD
DISTRIBUTION OF POTENTIAL (Statvolts)

INC= 0.500E-01   Time = 0.0sec
                                            (H2O+ : 1.E4)

☐	-1.1500
⊙	-0.9000
△	-0.6500
+	-0.4000
✕	-0.1500
◇	0.1000
⟁	0.3500
⊠	0.6000
Z	0.8500
Y	1.1000

Fig. 4   Initial potential contours for a central water ion density of 10^4 cm^{-3} where water plasma has the contours of
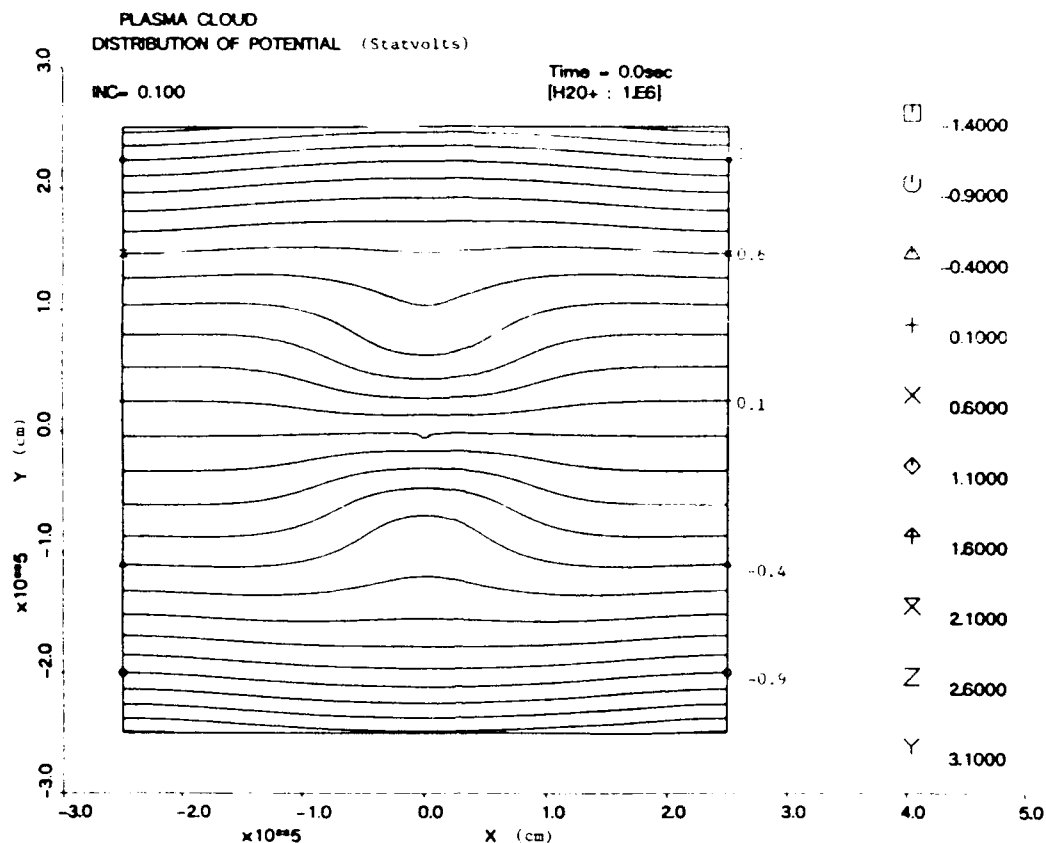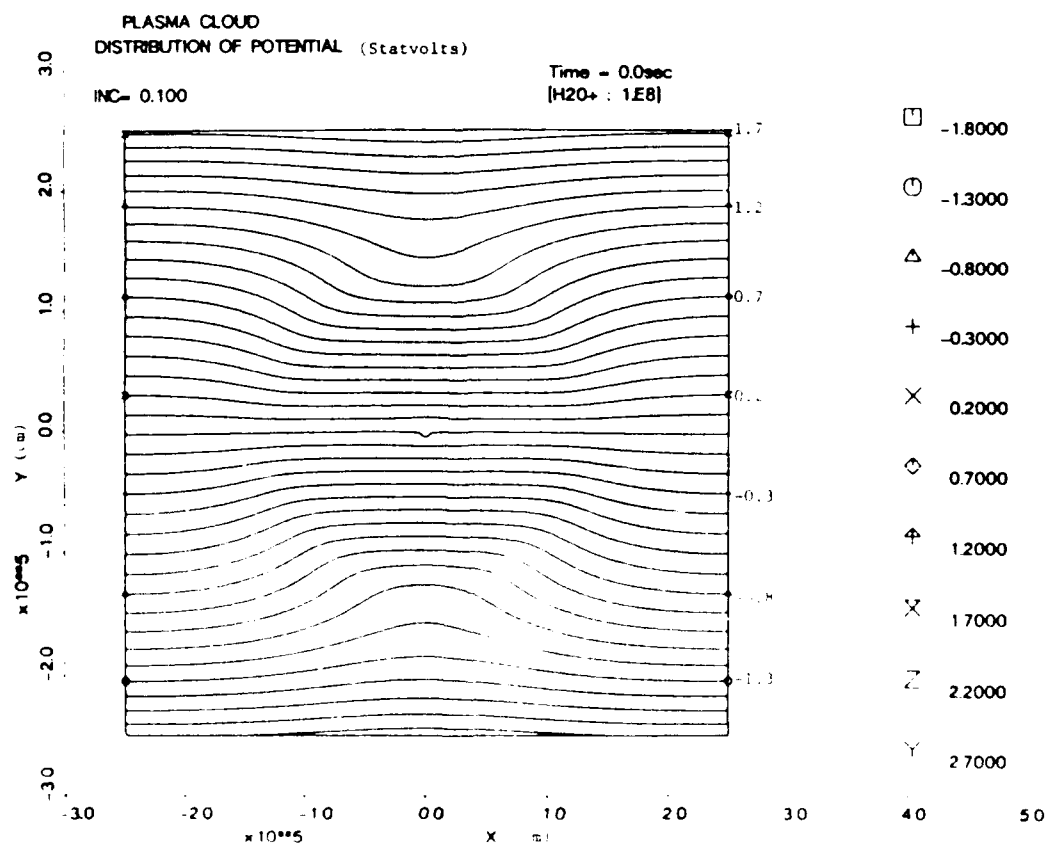Figure 3. The electric field is the gradient of these potential contours.

43

PLASMA CLOUD
DISTRIBUTION OF POTENTIAL (Statvolts)

Time = 0.0sec
INC= 0.100   [H2O+ : 1.E6]

Fig 5   Initial potential contours for a central water ion density of 10^6 cm^{-3} where water plasma has the contours of Figure 3 The electric field is the gradient of these potential contours

PLASMA CLOUD
DISTRIBUTION OF POTENTIAL (Statvolts)

Time = 0.0sec
INC= 0.100   [H2O+ : 1.E8]

Fig 6   Initial potential contours Hastings for a central water ion density of 10^8 cm^{-3} where water plasma has the contours of Figure 3 The electric field is the gradient of these potential contours
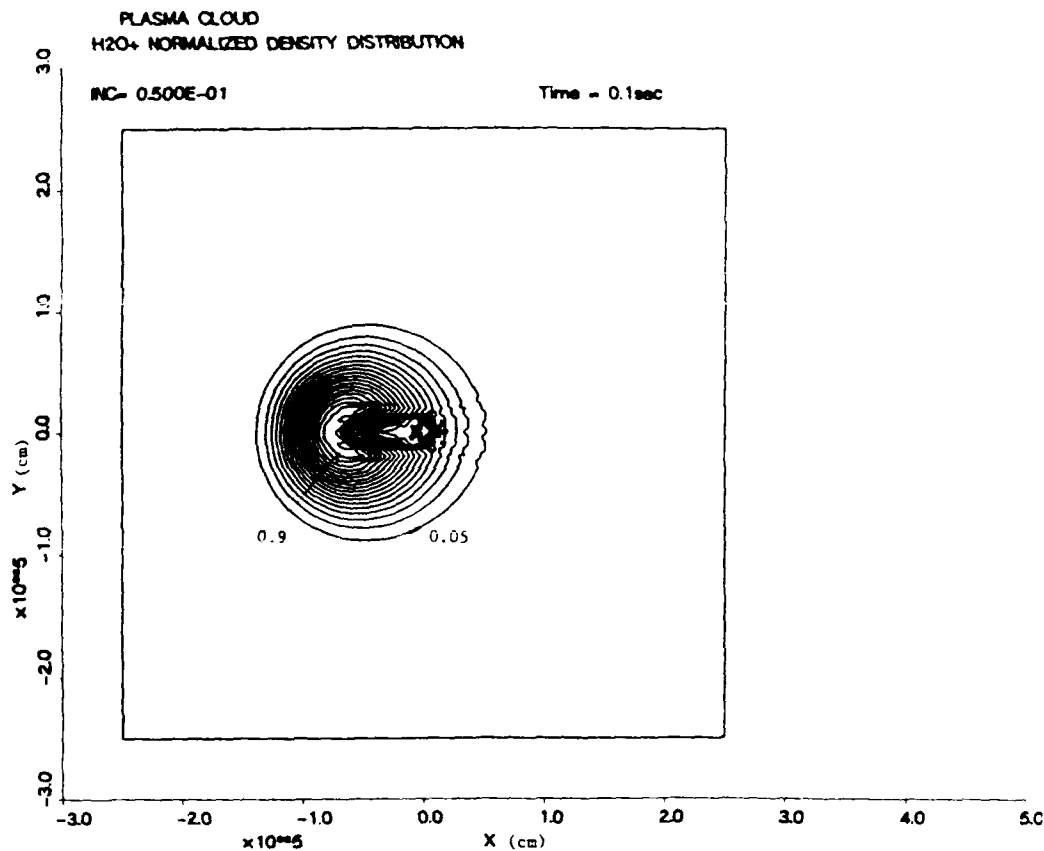
44

Fig. 7. Water ion density contours at 0.1 s for an initial central water ion density of 10^6 cm^{-3}. Water ion density is normalized to the far field electron density.

as a classical dielectric. In Figure 5 the central water density was taken to be $N_{H_2O}.(x = 0) = 10^6$ cm^{-3}. Here we see exactly the opposite tendency from Figure 4. The electric field inside the cloud increases rather than decreases. This occurs because the density gradient terms in the current balance equation are large enough to overcome the natural polarization which occurs due to the imposed motional electric field. The electric field increases since a large mobility driven electric flux is necessary to balance the density gradient driven ion flux. This tendency is confirmed in Figure 6, where we give the potential distribution for $N_{H_2O}.(x = 0) = 10^8$ cm^{-3}. The potential contours here can be well modeled as due to a uniform motional field and a positive charge on the positive y side of the cloud and a negative charge on the negative y side of the cloud. This suggests that the picture of the plasma cloud around large objects in the ionosphere as being a dielectric shield [Katz et al., 1984] is too simplistic a model. The important effect of the plasma density gradients must also be taken into account.

A typical simulation is shown in Figures 7–13 for the initial water ion puff given in Figure 3 and with an initial density of $N_{H_2O}.(x = 0) = 10^6$ cm^{-3}. Since an enhanced density of this magnitude would have to be caused by some means such as a plasma source which would probably emit warm electrons, we took the recombination rate for the water as $k_{recom} \approx 3 \times 10^{-8}$ cm^3 s^{-1} [Murad and Lai, 1986b], which corresponds to an electron energy of 1 eV. The neutral water is assumed to have the form given in (1). In Figure 7 we show the water ion density contours at 0.1 s after the start of the simulation. This corresponds to 16 gyroperiods which is enough time so that a substantial $E \times B$ drift can occur. The water ion cloud is seen to be drifting backward and to be undergoing some distortion

on the backside of the cloud. The central region of the cloud is seen to be breaking into two regions with very steep gradients on the backside of the central region. The fact that most of the distortion is concentrated on the backside of the cloud can be understood by noting that the high-density core of the cloud will drift more slowly than the rear fringes of the cloud so that the back edge of the cloud will collide with the central core, thus leading to the observed distortion. Also, around the source, ionic water is still being formed due to charge exchange and then immediately drifting backward so that a very steep density gradient in the ionic water is observed near the source. The distortion on the backside of the cloud may be the development of the $E \times B$ instability. In barium cloud studies where the equations [Perkins et al., 1973] for the barium cloud are very similar to the ones used here the cloud was observed to break up into filaments both experimentally and numerically [Zabusky et al., 1973]. For barium clouds it is believed that the filaments may be associated with the formation of $E \times B$ instabilities [Drake and Huba, 1986]. This leads us to suggest that the filaments may be due to a similar reason. This important topic of possible instabilities is the subject of ongoing research and will be reported in a future publication. This also suggests that long-wavelength, low-frequency electrostatic noise may be inextricably linked with the large water densities observed around large objects. In Figure 8 we show the associated oxygen density contours at the same time. This region delimits the area where new ionic water is being created from the area where ionic water exists because it has come from the initial conditions. Comparison of this figure with the last figure suggests that part of the break-up of the central core may be due to the creation of ionic water there in an asymmetric manner. In this figure we also
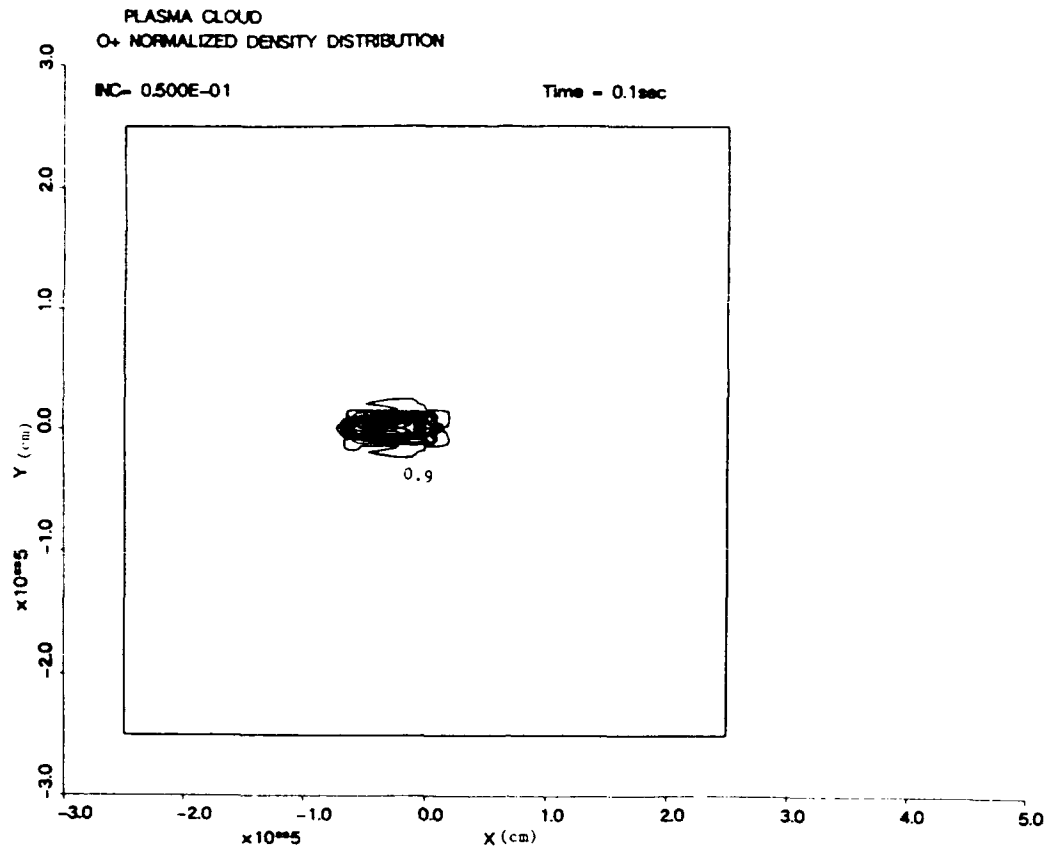
45

Fig. 8. Oxygen ion density contours at 0.1 s for an initial central water ion density of 10^6 cm^{-3}. Note that the region of oxygen depletion is much smaller than the water density enhancement in the previous figure. Oxygen ion density is normalized to the far field electron density.
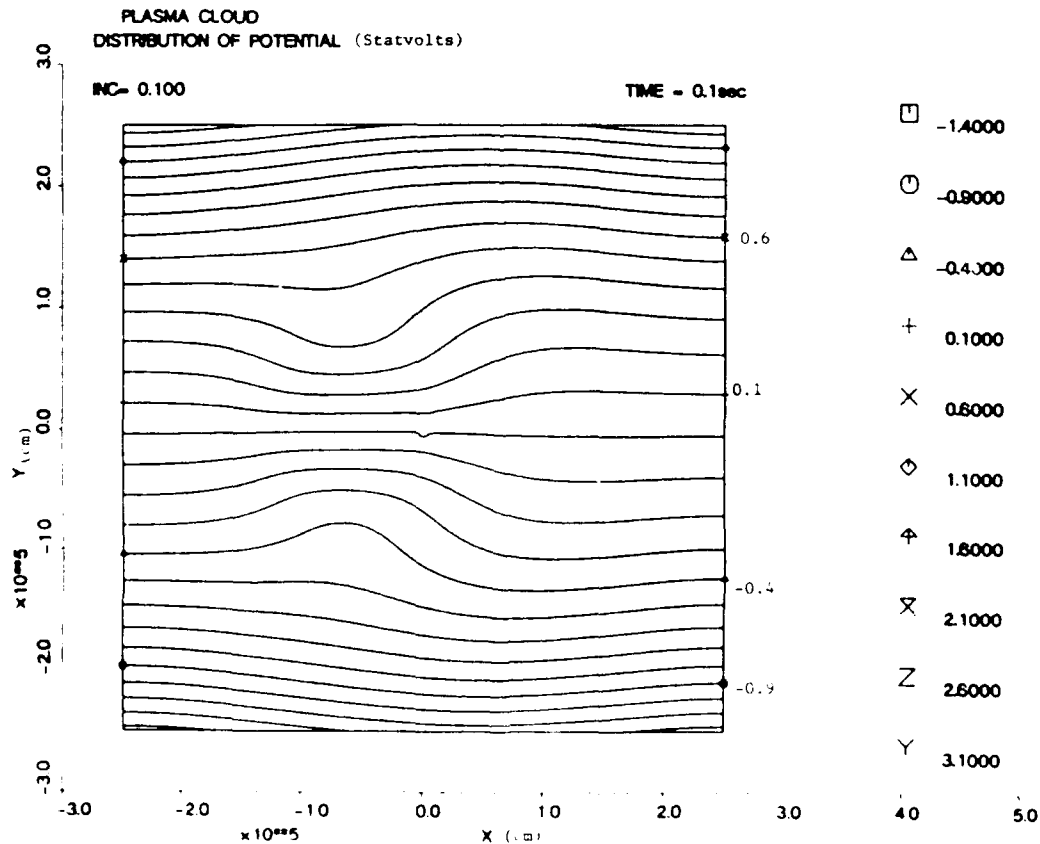

Fig. 9. Potential contours at 0.1 s for an initial central water ion density of 10^6 cm^{-3}. Potential at the origin is taken to be 4 V.
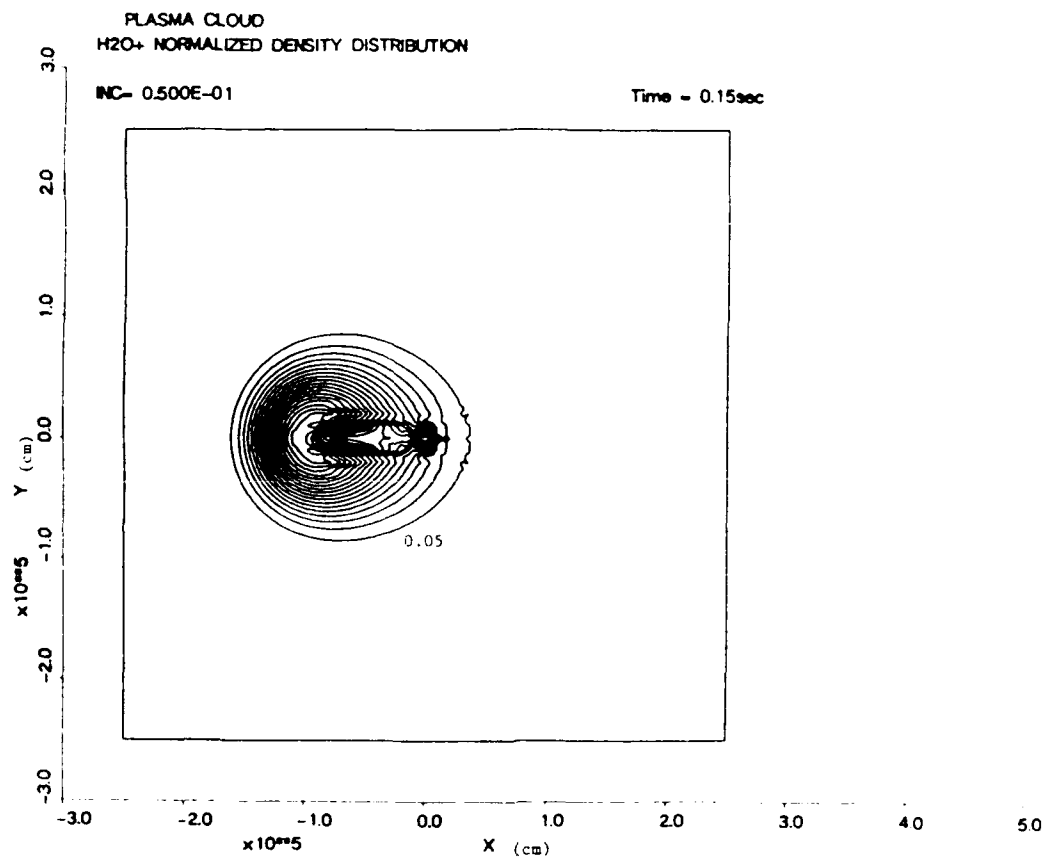
PLASMA CLOUD
H2O+ NORMALIZED DENSITY DISTRIBUTION

INC- 0.500E-01   Time - 0.15sec

Fig 10   Water ion density contours at 0.15 s for an initial central water ion density of 10^6 cm^{-3} Water ion density is
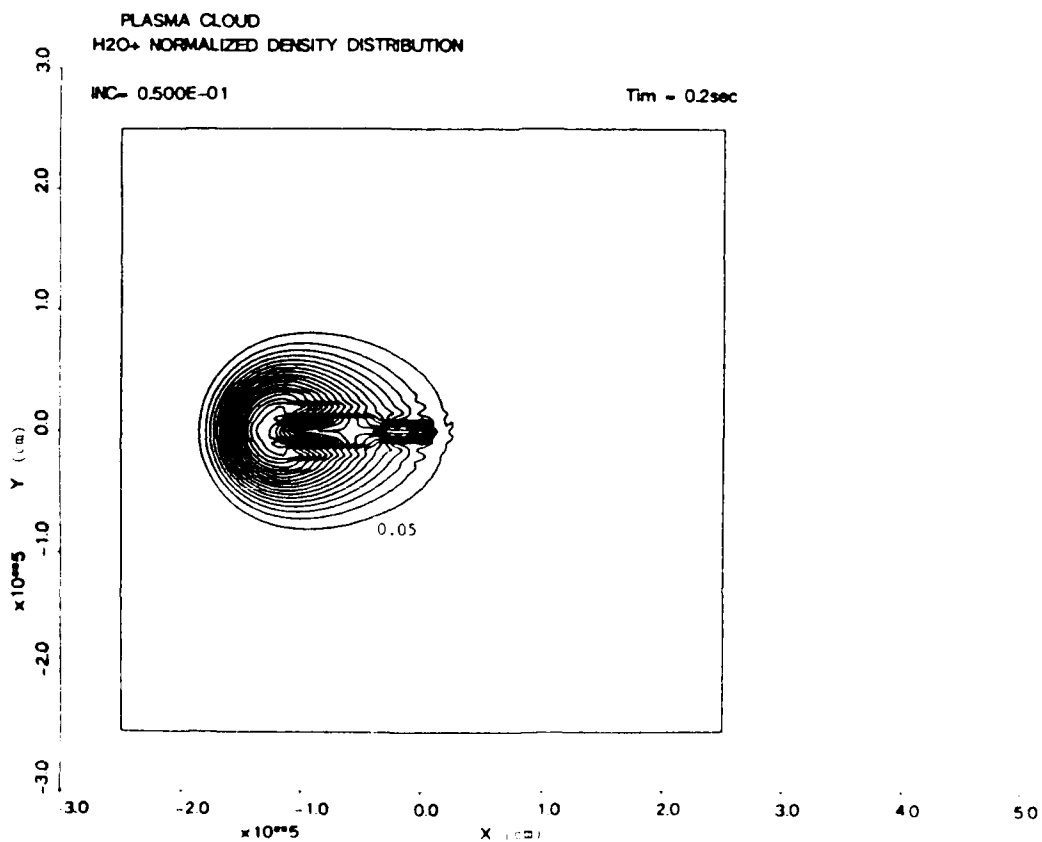normalized to the far field electron density.

PLASMA CLOUD
H2O+ NORMALIZED DENSITY DISTRIBUTION

INC- 0.500E-01   Tim - 0.2sec

Fig 11   Water ion density contours at 0.2 s for an initial central water ion density of 10^6 cm^{-3} Water ion density is   47
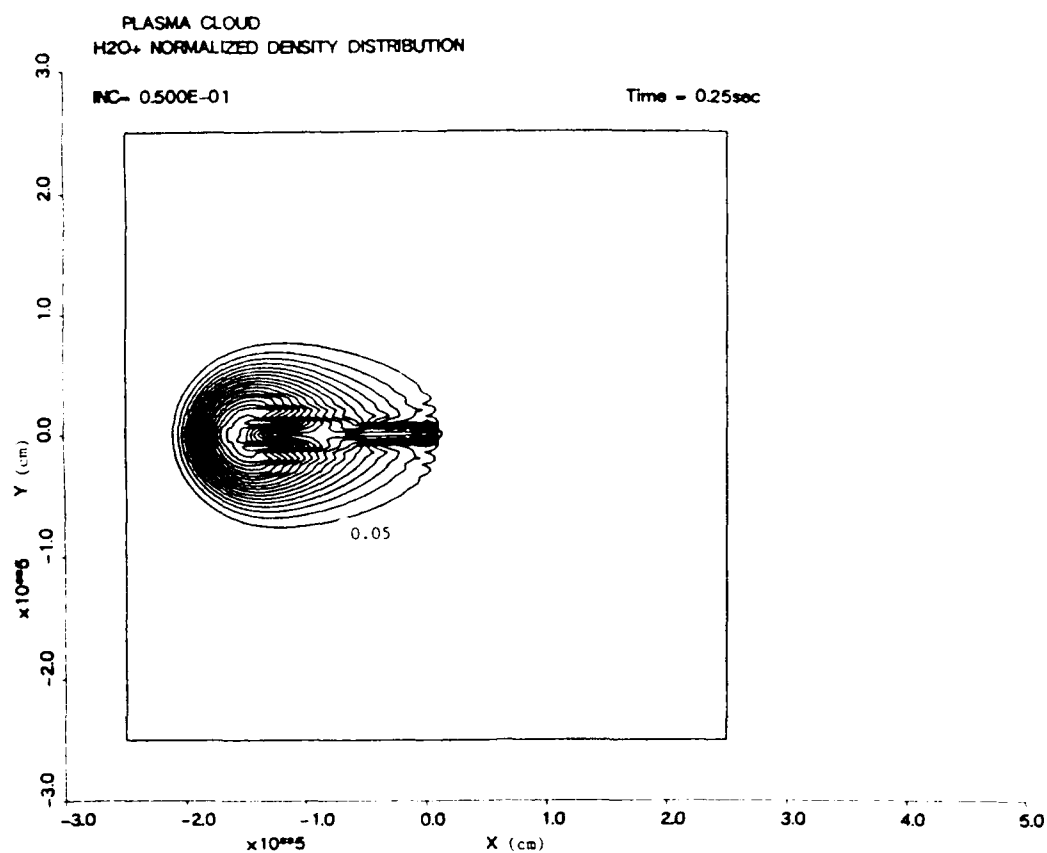normalized to the far field electron density

PLASMA CLOUD
H2O+ NORMALIZED DENSITY DISTRIBUTION

INC= 0.500E-01   Time = 0.25sec

Fig. 12. Water ion density contours at 0.25 s for an initial central water ion density of 10^6 cm^{-3}. Water ion density is normalized to the far field electron density.
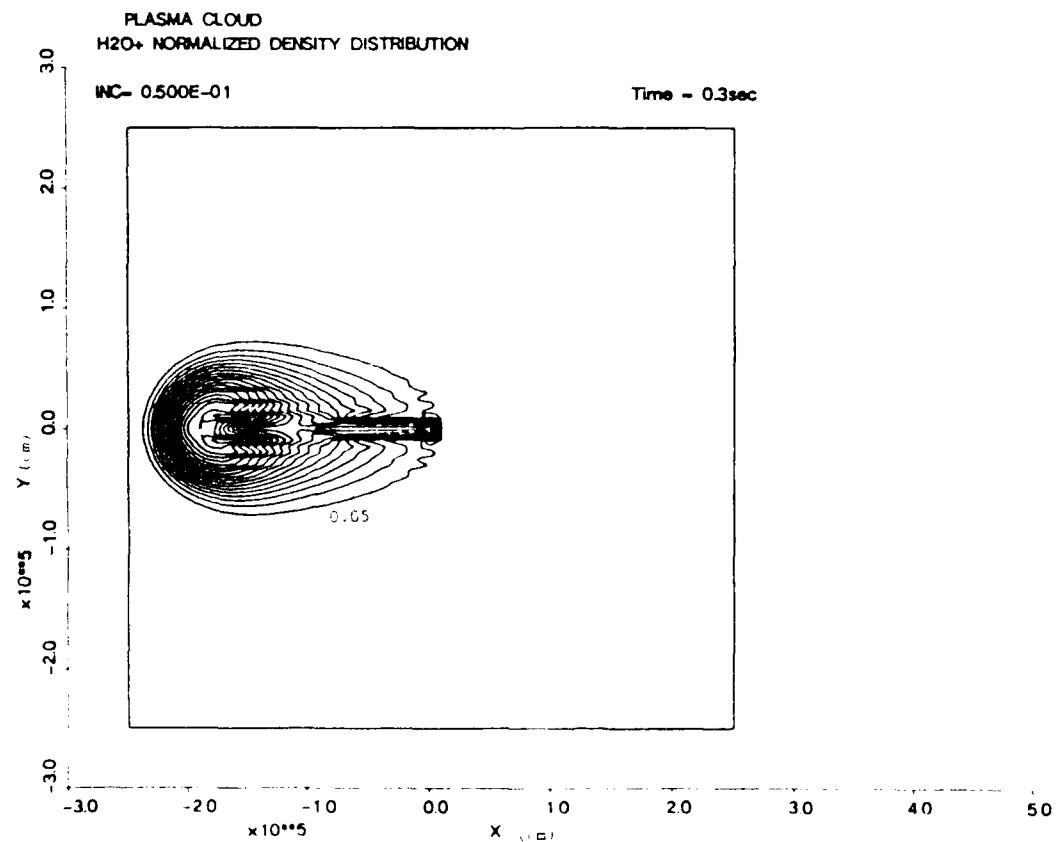
PLASMA CLOUD
H2O+ NORMALIZED DENSITY DISTRIBUTION

INC= 0.500E-01   Time = 0.3sec

Fig. 13. Water ion density contours at 0.3 s for an initial central water ion density of 10^6 cm^{-3}. Water ion density is normalized to the far field electron density.   48

see the very sharp density gradients in the oxygen density along the edges of the oxygen hole. In 0.1 s the region of oxygen depletion extends back behind the structure a distance of approximately 0.7 km. This suggests that the center of the water cloud is moving with a drift velocity of approximately 7 km s. This is less than the velocity at which an individual ion would drift backward if it saw only the motional electric field and occurs because the ions in the cloud are being affected by the self-consistent electric field and not the motional electric field. In Figure 9 we show the potential contours at 0.1 s. The fact that the cloud has moved relative to the structure is clearly seen in this figure since the region where the potential contours are distorted has moved backward. For Figures 10-13 we show the time development of the water ion cloud at 0.15, 0.2, 0.25, and 0.3 s. The cloud continues to develop a tadpole-like shape in the direction of cloud motion, and the central breakup and gradients become more pronounced. The instability on the backside of the cloud has entered a nonlinear state where distinct fingers have formed on the backside of the cloud. This has also been seen in barium cloud releases in the ionosphere. The cloud distribution over this period of time suggests that measurements of the cloud density from the structure will see a density that is both time dependent and spatially anisotropic. This suggests that density measurements from the space shuttle must be interpreted with care.

The time that ions spend in the vicinity of the structure is critical to determining the range of chemical reactions that they can undergo. This question is of substantial interest since there is evidence that chemical reactions can occur over surfaces in space [Green et al., 1985]. In Table 1 we give an estimate of the residence time of a water ion in the vicinity of the space shuttle as a function of the initial central water ion density. The residence time τ was defined as $\tau = L \, v_D$ where L is the length of the shuttle, taken as 50 m, and v_D is the cloud drift velocity determined from the simulation. We see that the residence time of the ions is in the millisecond to tens of milliseconds range and furthermore the higher-density cases lose ions substantially faster than the low-density cases. This suggests that measurement of the decay rate of a puff of plasma will not give a unique answer for the ion residence time [Sasaki et al., 1985]. Rather the ion residence time is a function of the density, as we would expect for a loss process which is not linear. For the low-density case the residence time is consistent with measurements from the shuttle [Caledonia et al., 1987]. In the work by Caledonia et al. [1987] it was shown that a signal of n_{H_2O} n_O of 0.1 was consistent with a loss time for the water ions of 40 ms. We also note that these times are consistent with results from Spacelab 2, where enhanced ionic densities were not seen and substantial shielding of the motional potential was not observed (J. Raitt, private communication, 1986)

TABLE 1. Residence Time Against Central Ion Water Density

N_{H_2O}, n_O cm^{-3}	τ ms
10^4	44
10^5	19
10^6	8
10^7	5

5. CONCLUSIONS

We have formulated a simple model for the plasma cloud around a large structure in the ionosphere. One such structure is the space shuttle, and another may be a system like the space station. The model has been applied to an ionic water puff, and the dynamic behavior of the cloud followed.

A number of important conclusions can be drawn. First is that the cloud possesses no steady state if the electron density is enhanced above the ambient density. The second is that the effect of density gradients in the cloud may actually enhance the electric field that the cloud sees, so that the picture of the cloud always acting as a shield against the motional potential is too simplistic. The third is that the cloud may be subject to electrostatic instabilities which will grow and saturate with distortion of the cloud structure. This will mean that electrostatic noise and turbulence may always accompany these clouds. Finally, we conclude that the cloud structure will be highly anisotropic, which suggests that measurements of the cloud density from the structure must be treated with care.

Future work will concentrate on elucidation of the electrostatic instabilities associated with the cloud and on resolution of the ion residence times with the observed chemistry around the shuttle.

These conclusions indicate that sensors or board systems like the space shuttle or a space station will have to cope with a background which is spatially anisotropic, temporally varying, and also electrostatically noisy. These issues will also be studied in future work.

APPENDIX: ANALYTIC PROOF THAT CLOUD EQUATIONS HAVE NO STEADY STATE

We consider equations (20), (21), and (22) with recombination in the electron equation ignored for simplicity. We define two potentials by

$$\psi_{O^+} = \frac{\phi}{k_{O^+}} + \frac{B}{e} D_{e O^+} \ln n_{O^+} \qquad (23)$$

$$\psi_{H_2O^+} = \frac{\phi}{k_{H_2O^+}} + \frac{B}{e} D_{e H_2O^+} \ln n_{H_2O^+} \qquad (24)$$

We assume that the density equations for the oxygen and water possess a steady state and that the plasma cloud is moving with some constant velocity V. With this assumption we can write

$$\frac{\partial n_{O^+}}{\partial t} = -V \cdot \nabla n_{O^+} + n_{O^+} \, \dot{} \qquad (25)$$

$$\frac{\partial n_{H_2O^+}}{\partial t} = -V \cdot \nabla n_{H_2O^+} + n_{O^+} \, \dot{} \qquad (26)$$

We substitute (25) and (26) into (20) and the equivalent equation for the water ions and use the definitions of the potentials in (23) and (24) to obtain

$$-V \cdot \nabla n_{O^+} = \frac{1}{B} (\nabla \psi_{O^+} \times \mathbf{b}) \cdot \nabla n_{O^+} \qquad (27)$$

$$V \cdot \nabla n_{H_2O^+} = \frac{1}{B} (\nabla \psi_{H_2O^+} \times \mathbf{b}) \cdot \nabla n_{H_2O^+} \qquad (28)$$

These equations have the general solution

$$\nabla v_{O^+} = \mathbf{H} + \frac{1}{n_{O^+}} \nabla \Psi_{O^+} \qquad (29)$$

$$\nabla v_{H_2O^+} = \mathbf{G} + \frac{1}{n_{H_2O^+}} \nabla \Psi_{H_2O^+} \qquad (30)$$

where $\mathbf{H}$ and $\mathbf{G}$ are constant vectors related to $\mathbf{V}$ and $\nabla \Psi_{H_2O^+}$ and $\nabla \Psi_{O^+}$ are arbitrary functions of the water ion density and oxygen ion density, respectively. If we substitute these expressions for the potentials in (22), we obtain

$$\nabla^2 (\Psi_{O^+} + \Psi_{H_2O^+}) = \mathbf{M} \cdot \nabla n_{O^+} + \mathbf{N} \cdot \nabla n_{H_2O^+} \qquad (31)$$

where the vectors $\mathbf{M}$ and $\mathbf{N}$ are independent of the densities. We integrate (31) over a volume V bounded by a surface of constant electron density to obtain

$$\int_V \nabla^2 (\Psi_{O^+} + \Psi_{H_2O^+}) \, dV = 0 \qquad (32)$$

Now if we multiply (31) by $\Psi_{O^+} + \Psi_{H_2O^+}$, integrate over the same volume, and use (32) and Green's theorem, we obtain

$$\int_V (\nabla \Psi_{O^+} + \nabla \Psi_{H_2O^+})^2 \, dV = 0 \qquad (33)$$

This is only possible if

$$(\nabla \Psi_{O^+} + \nabla \Psi_{H_2O^+}) = 0 \qquad (34)$$

This indicates that the electron density equation must be of the form

$$\mathbf{V} \cdot \nabla n_e = 0 \qquad (35)$$

The only nonconstant solution to this equation is for the electron density to vary in only one direction in space, which is physically unreasonable. Therefore we can conclude that if the electron density has closed contours then it has no steady state and if there is a steady state then the electron density must be the ambient density everywhere.

REFERENCES

Gatsonis, G. E., L. C. Person, and D. E. Hastings, The interpretation of ... in the measurements of ionic species, *J. Geophys. Res.*, 92, ...

D... P. W., and B. A. Whalen, Thermal ion results from an experiment to produce artificial an ionospheric hole, *J. Geophys. Res.*, 84, 6881-6888, 1979.

Drake, J. F., and J. D. Huba, Convective stabilization of ionospheric plasma clouds, *J. Geophys. Res.*, 91, 10,108-10,116, 1986.

Dungey, J. W., *Cosmic Electrodynamics*, Cambridge University Press, New York, 1958.

Green, B. D., G. E. Caledonia, and T. D. Wilkerson, The shuttle environment: Gases, particulates and glow, *J. Spacecr. Rockets*, 22, 500-511, 1985.

Katz, I., D. E. Parks, D. L. Cooke, and J. R. Lilley, Jr., Polarization of spacecraft generated plasma clouds, *Geophys. Res. Lett.*, 11, 1115-1116, 1984.

Krall, N. A., and A. W. Trivelpiece, *Principles of Plasma Physics*, McGraw-Hill, New York, 1973.

Mitchell, H. G., J. A. Fedder, J. D. Huba, and S. T. Zalesak, Transverse motion of high-speed barium clouds in the ionosphere, *J. Geophys. Res.*, 90, 11,091-11,095, 1985.

Murad, E., and S. T. Lai, Some charge exchange reactions involving H_2O, *Chem. Phys. Lett.*, 126, 427, 1986a.

Murad, E., and S. T. Lai, Effect of dissociative electron-ion recombination on the propagation of critical ionization discharges, *J. Geophys. Res.*, 91, 13,745-13,749, 1986b.

Murphy, G., J. Pickett, N. D'Angelo, and W. S. Kurth, Measurements of the plasma parameters in the vicinity of the space shuttle, *Planet. Space Sci.*, 34, 993-1004, 1986.

Perkins, F. W., N. J. Zabusky, and J. H. Doles, Deformation and striation of plasma clouds in the ionosphere, 1, *J. Geophys. Res.*, 78, 697-709, 1973.

Pickett, J. S., G. B. Murphy, W. S. Kurth, C. K. Goertz, and S. D. Shawhan, Effects of chemical releases by the STS 3 orbiter on the ionosphere, *J. Geophys. Res.*, 90, 3487-3497, 1985.

Reasoner, D. L., S. D. Shawhan, and G. Murphy, Plasma diagnostics package measurements of ionospheric ions and shuttle-induced perturbations, *J. Geophys. Res.*, 91, 13,463-13,471, 1986.

Roach, P. J., *Computational Fluid Dynamics*, Hermosa Publishers, Albuquerque, N. M., 1976.

Sasaki, S., S. Kubota, N. Kawashima, K. Kuriki, M. Yanagisawa, T. Obayashi, W. T. Roberts, D. L. Reasoner, W. W. L. Taylor, P. R. Williamson, P. M. Banks, and J. L. Burch, An enhancement of plasma density by neutral gas injection observed in SEPAC Spacelab-1 experiment, *J. Geomagn. Geoelectr.*, 37, 883-894, 1985.

Zabusky, N. J., J. H. Doles, and F. W. Perkins, Deformation and striation of plasma clouds in the ionosphere, 2, Numerical simulation of a nonlinear two-dimensional model, *J. Geophys. Res.*, 78, 711-724, 1973.

Zalesak, S. T., Fully multidimensional flux-corrected transport algorithms for fluids, *J. Comput. Phys.*, 31, 335-362, 1979.

Zalesak, S. T., A physical interpretation of the Richtmeyer two-step Lax-Wendroff scheme and its generalization to higher spatial order, in *Proceedings of the Fifth (IMACS) International Symposium on Computer Methods for Partial Differential Equations*, edited by R. Vichveretsky and R. S. Stepleman, International Association for Mathematics and Computers in Simulation, New Brunswick, N. J., 1984.

N. A. Gatsonis, D. E. Hastings, and T. Mogstad, Department of Aeronautics and Astronautics, Room 37-441, Massachusetts Institute of Technology, Cambridge, MA 02139.

The Motion of Contaminant Water Plasma Clouds About Large Active Space Structures

D. E. HASTINGS AND N. A. GATSONIS

Department of Aeronautics and Astronautics, Massachusetts Institute of Technology, Cambridge

Large structures in low earth orbit will release neutral water or ions through outgassing, water dumps or thruster firings and thus perturb the ambient ionosphere. Neutrals and ions within the perturbed environment will undergo chemical reactions to form a contaminant cloud. It is assumed that the contaminant cloud consists of ions such as O^+, H_2O^+, H_3O^+ and neutrals such as O, H, OH and H_2O. A two-dimensional model for the motion of the contaminant cloud perpendicular to the magnetic field lines is developed. Numerical solution of the derived model equations examines the effects of Alfvén wave coupling, neutral water density, ion temperature and initial conditions on the cloud motion. In low density neutral water clouds ($\leq 10^9$ cm^{-3}) the shielding of the electric field is small. In neutral water clouds with densities of interest for shuttle conditions ($\sim 10^{10}$ cm^{-3}) the shielding is predicted to be of the order of the motional electric field and the ratios of the line averaged densities of the ions is consistent with experimental data. The effect of ion temperature is negligible for the range of densities and temperatures considered. It is predicted that for symmetric initial conditions, the drifting clouds will develop fingerlike instabilities. Plasma depletions are predicted in the wake of the moving structure with enhancements in the ram direction. Asymmetric initial conditions, such that could result from a thruster firing, rotate the plasma cloud which undergoes a highly asymmetric distortion.

1 INTRODUCTION

With the advent of large active structures in space such as the space shuttle and the planned space station it has been realized that these structures will significantly perturb the ambient ionosphere by the generation of a contaminant plasma cloud. The plasma cloud may arise either by ionization of gases released from the structure due to such mechanisms as outgassing or thruster firings or may be due to the deliberate release of a plasma cloud by the firing of a plasma thruster. It is of interest to understand the dynamic evolution of these clouds for three reasons. One reason is to give of information on the ambient ionosphere and its chemistry. Another reason is to understand the environmental impact that large space structures will have on the ionosphere and thirdly to determine the impact that contaminant clouds may have on the operation of the space structure itself especially if it contains sensitive sensors.

The contaminant plasma cloud about the space shuttle has been studied experimentally by several authors [Pickett et al., 1985; Murphy et al., 1986; Reasoner et al., 1986]. Caledonia et al. [1987] showed that their measurements were consistent with an ion residence time in the vicinity of the shuttle of 40 ms. Theoretical work on the plasma cloud about the space shuttle started with the suggestion that the plasma cloud could be highly polarized leading to a long residence time for the ions in the shuttle frame [Katz et al.,

1984]. A model for the unsteady motion of the plasma cloud was developed by *Hastings et al.* [1988], where it was shown that for the densities around the shuttle the polarization of the cloud was highly dependent upon the ion density. Another study of the plasma cloud which takes into account the effect of Hall and Pederson currents has been undertaken by *Eccles et al.* [1988]. The Hall currents are shown to rotate the polarization field so that it is not antiparallel with the motional electric field.

In this work we extend the model of *Hastings et al.* [1988] to include the coupling of the cloud to Alfvén waves which can carry current parallel to the magnetic field. The cloud equations are studied systematically as a function of the parallel interaction length, neutral density, ion temperature, and the initial conditions.

2 DEVELOPMENT OF THE CLOUD EQUATIONS

We assume that the space structure moves with the orbital velocity of $V_s = 8$ km/s perpendicular to the magnetic field lines and creates a neutral water cloud. In a reference frame attached to the structure (structure frame), the ambient O^+ ions sweep through the water neutrals with energies up to 5 eV. Under such conditions ionic water is formed by the charge exchange reaction
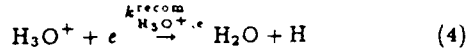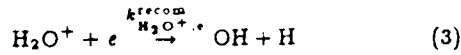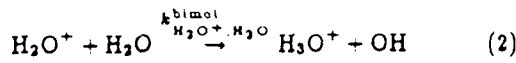
$$O^+ + H_2O \xrightarrow{k_1} O + H_2O^+ \qquad (1)$$
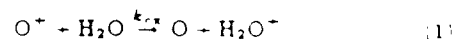
For simplicity we shall consider a plasma cloud consisting of three components, namely, O^+, H_2O^+ and H_3O^+ intermixed with a neutral cloud composed of O, H_2O, OH and H. The ions and neutrals are allowed to interact inelastically through the following reactions,

$$H_2O^+ + H_2O \xrightarrow{k^{bimol}_{H_2O^+,H_2O}} H_3O^+ + OH \qquad (2)$$

$$H_2O^+ + e \xrightarrow{k^{recom}_{H_2O^+,e}} OH + H \qquad (3)$$

$$H_3O^+ + e \xrightarrow{k^{recom}_{H_3O^+,e}} H_2O + H \qquad (4)$$

The charge exchange reaction rate is taken to be $k_{cx} = 2.4 \times 10^{-9}$ cm^3/s [Bolden and Twiddy, 1972] and the bimolecular reaction rate is taken as $k^{bimol}_{H_2O^+,H_2O} = 1.7 \times 10^{-9}$ cm^3/s [Caledonia et al., 1987]. The electron recombination reaction rates are taken as $k^{recom}_{H_2O^+,e} = 3 \times 10^{-7}$ cm^3/s [Murad and Lai, 1986] and $k^{recom}_{H_3O^+,e} = 2.4 \times 10^{-7}$ cm^3/s [Mitchell and McGowan, 1983].

We work in a frame of reference where the space structure is stationary, the magnetic field $\mathbf{B}$ is in the z direction and the ambient wind in the negative x direction with a speed of 8 km/s (Figure 1). In the structure frame and in the absence of any other electric field within the plasma perturbation the observer will see the unshielded motional electric field $\mathbf{E}_m = \mathbf{V}_s \times \mathbf{B}$ in the negative y direction (Figure 1); in that frame the guiding centers of the ions will drift with the $-\mathbf{V}_s$ velocity. However, within a plasma density perturbation the electric field and consequently the drift velocity will be determined by the balance between Pedersen and Hall currents, ambipolar diffusion currents, "pickup" currents as well as parallel currents carried by the Alfvén wings. [Lloyd and Haerendel, 1973; Goertz, 1980; Neubauer, 1980]. Charge buildup due to ion-neutral collisions or "pickup" processes will create a polarization field which will shield the imposed motional electric field. Consequently, the electric field within the plasma cloud will be $|\mathbf{E}| < |\mathbf{E}_m|$ and the ions will drift backward (in the structure frame) with a speed which is less than the orbital. In the case that the motional electric field is entirely shielded, the plasma cloud will be stationary or it will be moving with the structure velocity in a fixed frame [Katz et al., 1984].

The continuity equation for the i-th ion with density N_i is given by

$$\frac{\partial N_{O^+}}{\partial t} + \nabla \cdot (\mathbf{U}_{O^+} N_{O^+}) = -N_{O^+} k_{cx} N_{H_2O} \qquad (5)$$
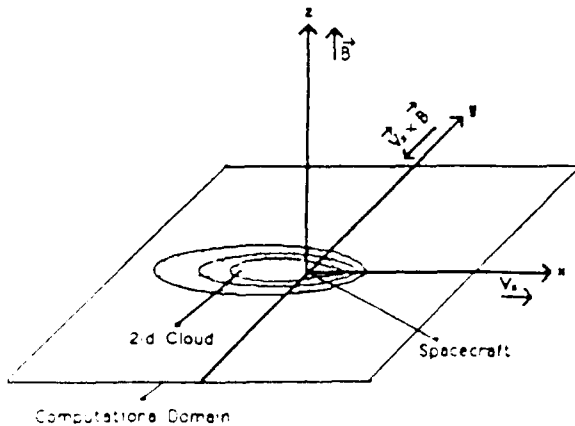
$$\frac{\partial N_{H_2O^+}}{\partial t} + \nabla \cdot (\mathbf{U}_{H_2O^+} N_{H_2O^+}) = N_{O^+} k_{cx} N_{H_2O}$$
$$- N_{H_2O^+} k^{bimol}_{H_2O^+,H_2O} N_{H_2O} - N_{H_2O^+} k^{recom}_{H_2O^+,e} N_e \qquad (6)$$

$$\frac{\partial N_{H_3O^+}}{\partial t} + \nabla \cdot (\mathbf{U}_{H_3O^+} N_{H_3O^+}) =$$
$$N_{H_2O^+} k^{bimol}_{H_2O^+,H_2O} N_{H_2O} - N_{H_3O^+} k^{recom}_{H_3O^+,e} N_e \qquad (7)$$

where the right-hand side terms are the ionic chemical source and loss terms obtained from the chemical reaction equations (Equations (1), (2), (3), and (4)).

The drift velocity of each ion species can be obtained from the ion momentum equation [Hastings et al., 1988; Eccles et al., 1988]. For the i-th ion and if the ion inertia is neglected (which implies that the drift velocity of the ions is smaller than the thermal) the steady state momentum equation is

$$0 = -T_i \nabla N_i + eN_i \left(\mathbf{E} + \frac{\mathbf{U}_i \times \mathbf{B}}{c}\right) - \sum_b \mathbf{R}_i^b$$
$$- m_i N_i \sum_n \nu_{i,n}(\mathbf{U}_i - \mathbf{U}_n) - m_i N_i \sum_j \nu_{i,j}(\mathbf{U}_i - \mathbf{U}_j) \qquad (8)$$

where T_i is the temperature, N_i is the density, $\mathbf{U}_i$ is the bulk velocity, $\mathbf{U}_n$ is the velocity of the neutral n and $\nu_{i,j\ or\ n}$ is the collision frequency of momentum transfer between the species i and j or n. We included the term $\mathbf{R}_i^b$ to account for momentum transfer due to reactive collision of the ion i in reaction b. In general for the ion i created or lost in a reaction b, the momentum transfer operator has the form

$$\mathbf{R}_i^b = S_i^b m_i(\mathbf{U}_i - \mathbf{U}_i^b) \qquad (9)$$

where S_i^b is the rate of production or depletion of the i-th ion in the reaction b and the $\mathbf{U}_i^b$ is the velocity with which the ion is created or lost in the reaction. Clearly, with this definition of the momentum operator, there is no average momentum lost for those ions which are depleted in the reactions considered, since these ions are lost with their average velocity. However, for the ions which are created it is important to establish the velocity with which they leave the reactions. In the charge exchange reaction we assume that the water ions are created with the water neutral velocity, so $\mathbf{U}^{cx}_{H_2O^+} = \mathbf{U}_{H_2O}$. In the bimolecular reaction we assume that the created hydronium ions gain the bulk velocity of the water neutrals, so that we can write $\mathbf{U}^{bimol}_{H_3O^+} = \mathbf{U}_{H_2O}$. A complete model for the momentum transfer operator in a chemically reacting plasma is beyond the scope of this paper [Burgers, 1969; Li, 1966]. However, detailed numerical simulations indicated that the dominant mechanism for momentum transfer are the elastic ion-neutral collisions and not the reactive collisions. We can write then the momentum transfer operators due to reactive collisions as follow

$$\mathbf{R}^{cx}_{O^+} = 0 \qquad (10)$$

$$\mathbf{R}^{cx}_{H_2O^+} = m_{H_2O^+} N_{O^+} k_{cx} N_{H_2O}(\mathbf{U}_{H_2O^+} - \mathbf{U}_{H_2O}) \qquad (11)$$

Fig. 1. Coordinate system and computational domain

$$R^{bimol}_{H_2O^+} = 0 \quad (12)$$

$$R^{recom}_{H_2O^+} = 0 \quad (13)$$

$$R^{bimol}_{H_3O^+} =$$

$$m_{H_3O^+} N_{H_3O^+} k^{bimol}_{H_2O^+, H_2O} N_{H_2O}(U_{H_3O^+} - U_{H_2O}) \quad (14)$$

$$R^{recom}_{H_3O^+} = 0 \quad (15)$$

The perpendicular drift velocity of the ion i then can be written as

$$U_{i\perp} = \frac{A' \times B}{B^2} + \frac{A'}{B}\left(\frac{\nu'}{\Omega_i}\right)\frac{1}{1 + (\nu'/\Omega_i)^2} + \frac{A' \times B}{B^2}\left[\frac{1}{1 + (\nu'/\Omega_i)^2} - 1\right] \quad (16)$$

where the vector A' is given by

$$A' = -c\nabla\left(\phi + \frac{T_i}{e}\right) + \frac{c}{eN_i}F^i_N + \frac{c}{eN_i}F^i_I \quad (17)$$

In (17) the potential is ϕ, the ion temperature is T_i, the ion density is N_i. The neutral force densities which arise from elastic and inelastic ion-neutral collisions are

$$F^{O^+}_N = m_{O^+} N_{O^+}\left(\sum_n \nu_{O^+, n} U_n\right) \quad (18)$$

$$F^{H_2O^+}_N = m_{H_2O^+} N_{H_2O^+}\left(\sum_n \nu_{H_2O^+, n} U_n\right) + m_{H_2O^+} N_{O^+} \nu^{cx} U_{H_2O} \quad (19)$$

$$F^{H_3O^+}_N = m_{H_3O^+} N_{H_3O^+}\left(\sum_n \nu_{H_3O^+, n} U_n\right) + m_{H_3O^+} N_{H_2O^+} \nu^{bimol} U_{H_2O} \quad (20)$$

where $\nu^{cx} = k_{cx} N_{H_2O}$ and $\nu^{bimol} = k^{bimol}_{H_2O^+, H_2O} N_{H_2O}$. The comparable force density for the i-th which arises from ion-ion collisions is

$$F^i_I = m_i N_i \sum_{j \neq i} \nu_{i,j} U_j. \quad (21)$$

The total collision frequency for momentum transfer ν' is defined as

$$\nu' = \sum_n \nu_{i,n} + \nu'_{reaction} + \sum_{j \neq i} \nu_{i,j} \quad (22)$$

where $\nu'_{reaction}$ is the rate of momentum transfer due to chemical reactions where an ion is created or lost. For O^+ we have $\nu^{O^+}_{reaction} = 0$, for H_2O^+ we have $\nu^{H_2O^+}_{reaction} = (N_{O^+}/N_{H_2O^+})\nu^{cx}$ and for H_3O^+ we have $\nu^{H_3O^+}_{reaction} = (N_{H_2O^+}/N_{H_3O^+})\nu^{bimol}$.

We expand the ion drift velocity in the expansion parameter ν'/Ω_i, which is the collisionality, to obtain to lowest order

$$U^{(0)}_{i\perp} = -\frac{c}{B^2}\nabla_\perp \psi_i \times B \quad (23)$$

and to first order

$$U^{(1)}_{i\perp} = -\frac{c}{B}\nabla_\perp \psi_i\left(\frac{\nu'}{\Omega_i}\right) + \frac{c}{B^2}\left[\frac{F^i_N \times B}{eN_i} + \frac{F^i_I \times B}{eN_i}\right] \quad (24)$$

where the pressure modified potential ψ_i is

$$\psi_i = \phi + \frac{T_i}{e}\ln N_i \quad (25)$$

In using the collisionality as an expansion parameter we restrict ourselves to neutral densities below 10^{11} cm^{-3} and neglect the Hall terms which give rise to the rotation seen in the work of *Eccles et al.* [1988]. However, small collisionality allows us to keep finite ion temperature in a consistent manner, since the effect of the ion-ion collisions appears to first order in the velocity which we neglect for the density equations. In the work of *Eccles et al.* [1988] the collisionality is not taken to be small and the ion temperature is taken to be zero. We are interested in keeping a finite ion temperature since we wish to model initial conditions such as thruster firings.

The perpendicular ion current due to collisions is

$$J_{i\perp} = \sum_i eN_i U^{(1)}_{i\perp} = \sum_i \frac{c}{B^2} F^i_N \times B - \sum_i eN_i \frac{c}{B}\frac{\bar{\nu}'}{\Omega_i}\nabla\psi_i \quad (26)$$

where the collision frequency $\bar{\nu}'$ is

$$\bar{\nu}' = \nu' - \sum_{j \neq i} \nu_{i,j} \quad (27)$$

We note that all the ion-ion collision terms have dropped out of the net current, although they have not dropped out of the the individual ion currents. This is due to ion momentum conservation.

The perpendicular ion current due to the polarization drift is

$$J_{i_{pol}} = -\frac{c^2}{v^2_A}\frac{1}{4\pi}\frac{d\nabla\phi}{dt} \quad (28)$$

where the Alfvén velocity is

$$v^2_A = \frac{B^2}{4\pi \sum_i N_i m_i} \quad (29)$$

An expression for the parallel current can be derived from the theory of Alfvén wings [*Goertz*, 1980]. The parallel current is

$$J_\parallel = \pm\frac{c^2}{4\pi v_A}\nabla \cdot E_\perp \frac{B}{B} \quad (30)$$

We use (26), (28), and (30) in the charge conservation equation, keep the largest time derivative terms, neglect the parallel electric field compared to the perpendicular electric field and obtain

53

$$\frac{c^2}{v_A^2} v_A \frac{d}{ds} \nabla \cdot \mathbf{E}_\perp$$

$$+ 4\pi \nabla \cdot \left(\sum_i \frac{c}{B^2} \mathbf{F}_N^i \times \mathbf{B} - \sum_i e N_i \frac{c}{B} \frac{\overline{\nu}'}{\Omega_i} \nabla \psi_i \right) = 0 \quad (31)$$

where d/ds is the derivative along the Alfvén characteristic

$$\mathbf{s} = \frac{\mathbf{U}_\perp \pm v_A \mathbf{B}/B}{v_A}$$

We can integrate (31) along the Alfvén characteristics to obtain the potential equation

$$- \nabla \cdot \left(\nabla \phi \left(1 + \int \frac{ds}{v_A} \sum_i \frac{v_A^2}{v_{A_i}^2} \overline{\nu}' \right) \right.$$

$$+ \int \frac{ds}{v_A} \sum_i \frac{v_A^2}{v_{A_i}^2} \frac{T_i}{e} \overline{\nu}' \nabla \ln N_i - \int \frac{ds}{v_A} \frac{\sum_i \mathbf{F}_N^i \times \mathbf{b}}{e \sum_i N_i/\Omega_i} \right) = 0 \quad (32)$$

where v_{A_i} is the Alfvén velocity of the i-th ion species. The current carried by Alfvén waves is represented by the first term in (32). As can be seen from the second term the Alfvén term is dominant for low collision frequencies while for higher collision frequencies the Pederson terms are dominant. The charge conservation equation can be seen to be of the form

$$\nabla \cdot (\epsilon \nabla \phi) = \rho_{ext} \quad (33)$$

for some dielectric constant ϵ and some external charge density ρ_{ext}. The dielectric constant has the form

$$\epsilon \simeq 1 + \int \frac{ds}{v_A} \overline{\nu}' \quad (34)$$

The parallel interaction length to perform the parallel integration over can be estimated as

$$L_\parallel \simeq 2 r_{cloud} \frac{v_A}{v_\perp} \quad (35)$$

where r_{cloud} is the cloud radius in the perpendicular direction and $v_\perp$ is the average perpendicular drift velocity of the cloud. This expression is the distance an Alfvén wave can travel in the time the cloud takes to convect across a magnetic field line. If we use (35) in (34) we obtain the dielectric constant as

$$\epsilon \simeq 1 + 2 r_{cloud} \frac{\overline{\nu}'}{v_\perp} \quad (36)$$

For plasmas with low neutral water density the collision frequency is small and the drift velocity is of the order of the orbital speed. In this case, $\epsilon \simeq 1$ and the electric field in the plasma is the motional electric field since the plasma does not shield out the field. Physically, the parallel electron current carried by Alfvén waves is so large that no significant field can build up in the plasma cloud to shield out the imposed motional electric field. For a plasma where neutral water density is high, the collision frequency is large and the drift velocity is small. We find that $\epsilon \gg 1$ and so the electric field is highly shielded. In this case the perpendicular

ion current is sufficiently large to give rise to a substantial change in the motional electric field.

The density equation for the i-th ion is given by

$$\frac{\partial N_i}{\partial t} - \frac{c}{B^2} \nabla_\perp \phi \times \mathbf{B} \cdot \nabla N_i = S_i - L_i \quad (37)$$

where the righthand side terms are the ionic chemical source and loss terms (see also (5), (6), (7)). In this equation we neglect the parallel flow terms relative to the perpendicular flow terms. This can be justified by noting that the parallel scale length is expected to be much longer than the perpendicular scale length and if the electric field is not perfectly shielded [Hastings et al. 1988], then the perpendicular ion velocity is much larger than the parallel ion velocity which is in magnitude of the order of the ion acoustic velocity [Caledonia et al., 1987].

The neutral densities (for water, oxygen, hydroxyl and atomic hydrogen) are obtained as the solution of equations of the form

$$\frac{\partial N_n}{\partial t} + \nabla \cdot (N_i \mathbf{U}_n) = S_n - L_n \quad (38)$$

where S_n, L_n are the appropriate neutral source and loss terms. Consistent with our low collisionality limit we take the neutrals to be ballistic and therefore take the neutral velocity as the initial velocity with which they enter the system. For the oxygen and hydrogen this is the orbital speed in the negative $\mathbf{x}$ direction, i.e $\mathbf{U}_{O \text{ or } H} = -\mathbf{V}_s$. This stream of neutrals constitutes the neutral wind in the structure frame of reference. For the water and hydroxyl we assume that their velocity has a radial direction from the moving structure with magnitude equal to the thermal speed, i.e., $\mathbf{U}_{H_2O \text{ or } OH} = \sqrt{2 T_n/m_n} \mathbf{e}_r$.

3   NUMERICAL ANALYSIS OF THE CLOUD EQUATIONS

The density and potential equations have been solved as in Gatsonis [1987] and Hastings et al. [1988]. We briefly review the procedure. The equations are solved for a 5 km by 5 km square region using a uniform 101 by 101 cartesian mesh. The center of the computational domain was fixed on the structure which is assumed to be circular with a radius of 50 m. The magnetic field is in the $\mathbf{z}$ direction and the motional electric field is in the negative $\mathbf{y}$ direction (Figure 1). With $N_{H_2O^+}(x,y), N_{H_3O^+}(x,y)$ and $N_{O^+}(x,y)$ given at some time we calculate the potential from (32) and use that result to obtain the flow field velocities. Then that information is used in the ion density equations ((37)), to advance the densities by one time step. The neutral density equations ((38)) were advanced in a similar manner.

A successive point over relaxation (SPOR) scheme was used to solve the elliptic current balance equation ((32)). Neumann boundary conditions were applied in both the x and y directions. We required the potential to match the following boundary conditions in the far field

$$\nabla_\perp \phi = -\frac{\mathbf{V}_s \times \mathbf{B}}{c}$$

in the $\mathbf{V}_s \times \mathbf{B}$ direction and

$$\nabla_\perp \phi = 0$$

in the direction of motion. The potential of the central structure was taken to be 4 Volts which is consistent with measurements taken from the Shuttle. A potential of this order would arise from spacecraft-ionosphere sheath effects.

For the convective equations ((37), (38)) we used the two–dimensional flux correction method (FCT) of *Zalesak* [1979]. The high order scheme was a leapfrog-trapezoidal with fluxes calculated with the flux formulae developed by *Zalesak* [1984] while a donor-cell scheme was used for the lower scheme to complete the FCT algorithm. Symmetric boundary conditions were applied on the density distributions at the outer boundaries while solid wall boundary conditions on the interior. The flux limiter was applied on every iteration. All simulations were run to a time of 0.2 s ($\sim$ 6 ion gyroperiods) at which time the cloud has moved a significant way towards the edge of the computational grid.

Symmetric Initial Conditions: An Outgassed Cloud

We assumed that the water neutrals are outgassed radially from the moving body with their thermal velocity. Then their initial density can be written like

$$N_{H_2O}(\mathbf{r}) = N_{H_2O}(\mathbf{r} = 0)\left(\frac{r_o}{r}\right)^2 \qquad (39)$$

where $r_o = 50$ m is the radius of the moving structure and r is the distance from its center. The central neutral water density was taken as a variable in the simulations.

For the water ions we assumed that they follow an initial distribution given by

$$N_{H_2O^+}(\mathbf{r}, t = 0) =$$
$$10^{-4} + N_{H_2O^+}(\mathbf{r} = 0)\exp\left[-\left(\frac{|\mathbf{r} - \mathbf{r}_o|}{r_L}\right)^2\right] \qquad (40)$$

The above formula represents a Gaussian distribution falling off at a distance $r_L = 500$ m on the top of a flat distribution. The central water ion density was taken to be $N_{H_2O^+}(\mathbf{r}) = 10^3$ cm^{-3}. For the hydronium ions we assume an initial flat distribution with $N_{H_3O^+}(\mathbf{r}, t = 0) = 10^{-4}$ cm^{-3}. The neutral ambient species were assumed to follow uniform distributions with $N_O(\mathbf{r}, t = 0) = 8 \times 10^8$ cm^{-3}, $N_H(\mathbf{r}, t = 0) = 10^5$ cm^{-3}, and $N_{OH}(\mathbf{r}, t = 0) = 10^{-4}$ cm^{-3}.

For the ion temperatures needed in the potential equation we assumed that the outgassed contaminant cloud is at a temperature of 300° K, so that $T_{H_2O^+} = 0.025$ eV and $T_{H_3O^+} = 0.025$ eV. For the oxygen ions however the temperature was that of the ambient LEO environment taken to be $T_{O^+} = 0.1$ eV.

The ion-neutral collision rates were calculated assuming a hard-sphere collision model. For collisions between H_2O^+ or H_3O^+ and O, H, OH or H_2O the ion temperature was taken to be 0.025 eV. For collisions between O^+ and O or

H we assumed that $T_{O^+} = 0.1$ eV, since most of the collisions will be between the ambient O^+ which is the dominant ion and the background neutrals O and H. However, for collisions between ionic oxygen and neutral water or the hydroxyl radicals it was assumed that the relative energy was 5 eV. For the time scales that we are interested in, the outgassing occurs at a constant rate giving rise to a spherically expanding neutral water cloud. Hence the outgassed neutrals will always see a streaming O^+ with energies almost equal to the ram energy, i.e., 5 eV. We anticipate also that the OH species upon their creation follow the water neutrals and interact with the O^+ in a similar manner like H_2O.

We performed simulations assuming central neutral water density of 10^8 cm^{-3}, 10^9 cm^{-3} and 10^{10} cm^{-3} for both the limits of the parallel interaction length of 50 and 500 km. The lower limit of the parallel length corresponds to a 500 meter in radius cloud, moving with drift velocity of approximately 8 km/s in an environment where the Alfvén velocity is about 400 km/s. The upper limit of the parallel length, taken to be 500 km, is the distance along the lines of force from the cloud in low earth equatorial orbit down to the E-layer of the ionosphere; this is a situation where the cloud should experience strong shielding and, thus should drift with much slower than the orbital velocities. Figures 2, 3 and 4 show results for the three neutral densities and for the maximum parallel interaction length of 500 km.

The three cases shown in Figures 2-4 mark the transition from a practically unshielded cloud (Figure 2) to a cloud with moderate shielding (Figure 3) to a cloud with substantial shielding (Figure 4). This behavior is depicted very clearly in the pictures of the potential. The potential contours start from almost a flat distribution for the low density neutral cloud to end in a highly shielded distribution for the high density neutral water cloud case.

In Figure 2 where the central neutral water is 10^8 cm^{-3} the contaminant cloud drifts backward quickly. The front side of the water ion cloud remains smooth while its back develops fingerlike disturbances. New ionic water is formed with maximum of 1.39×10^3 cm^{-3} at the wake of the mov: structure. The hydronium ions, initially flat, develop a cloud-structure as well. Hydronium ion formation is predicted to be confined at the wake region of the moving structure. The oxygen ion distribution completes the above picture, showing a depletion region which extends almost 2000 m behind the moving structure. This depletion is confined at the region where charge exchange and recombination reactions are important, i.e., the region of new ionic formation.

In Figure 3 the central neutral water density is 10^9 cm^{-3} and shielding effects are important. In that case the central, dense region of the cloud is moving slower than the edges, producing a tadpole shaped formation. In the back side of the cloud a steep gradient is formed, since the back side moves more quicly and catches up with the slowly moving center. The front side however elongates and the whole cloud deforms into a "dumbbell" shape. The front side of the moving cloud remains smooth while its back side develops finger like disturbances. Overall, there is a substantial formation of ionic water, with a maximum of 1.5×10^4 cm^{-3}.

55

H_2O^+ NORMALIZED DENSITY DISTRIBUTION

H_3O^+ NORMALIZED DENSITY DISTRIBUTION

O_+ NORMALIZED DENSITY DISTRIBUTION
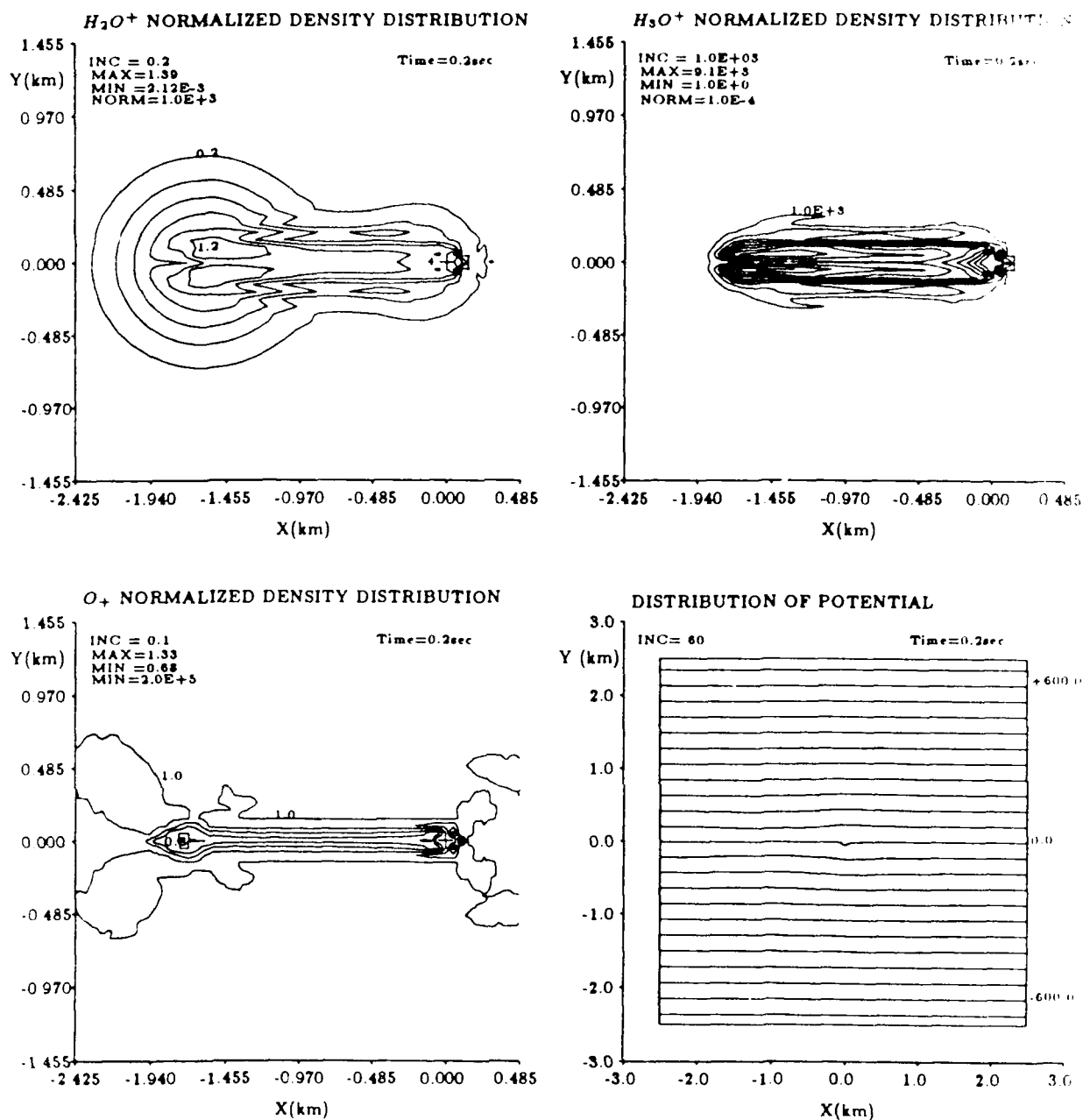

DISTRIBUTION OF POTENTIAL

Fig 2 Ion density contours and potential distribution in a plasma cloud with symmetric initial conditions and central neutral water density of 10^8 cm^{-3} at a time of 0 2 s after release The interaction parallel length is 500 km and the contaminant H_2O^+ and H_3O^+ temperature is 0 025 eV (top-left)Water ion contours. Normalization is to the initial central value of 10^{-3} cm^{-3} (top-right) Hydronium ion contours. Normalization is to the ambient value of 10^{-4} cm^{-3} (bottom-left) Oxygen ion contours Normalization is to the ambient value of 2×10^5 cm^{-3} (bottom-right) Potential distribution in volts as measured in the frame of the moving structure which is located at (0, 0) km

an order of magnitude increase to the initial central density. The hydronium ion species develop a very similar "dumbbell" structure with a maximum at the wake, predicted to be at 1.4×10^2 cm^{-3}. The oxygen ions deforms in a cloud structure forming a depletion region in the wake with a "hole" which levels off at 0.7×10^5 cm^{-3}. In the ram direction, however, an "enhancment" is predicted due to the density

pile-up. The morphological picture of the cloud deformation presented here is very similar to what was predicted in previous work in the discussion of the behavior of dielectric clouds [Perkins et al., 1973]. The potential figures show the shielding behavior of the cloud to be confined at places where neutral density is high. A very important feature is shown in the wake region of the moving structure where the
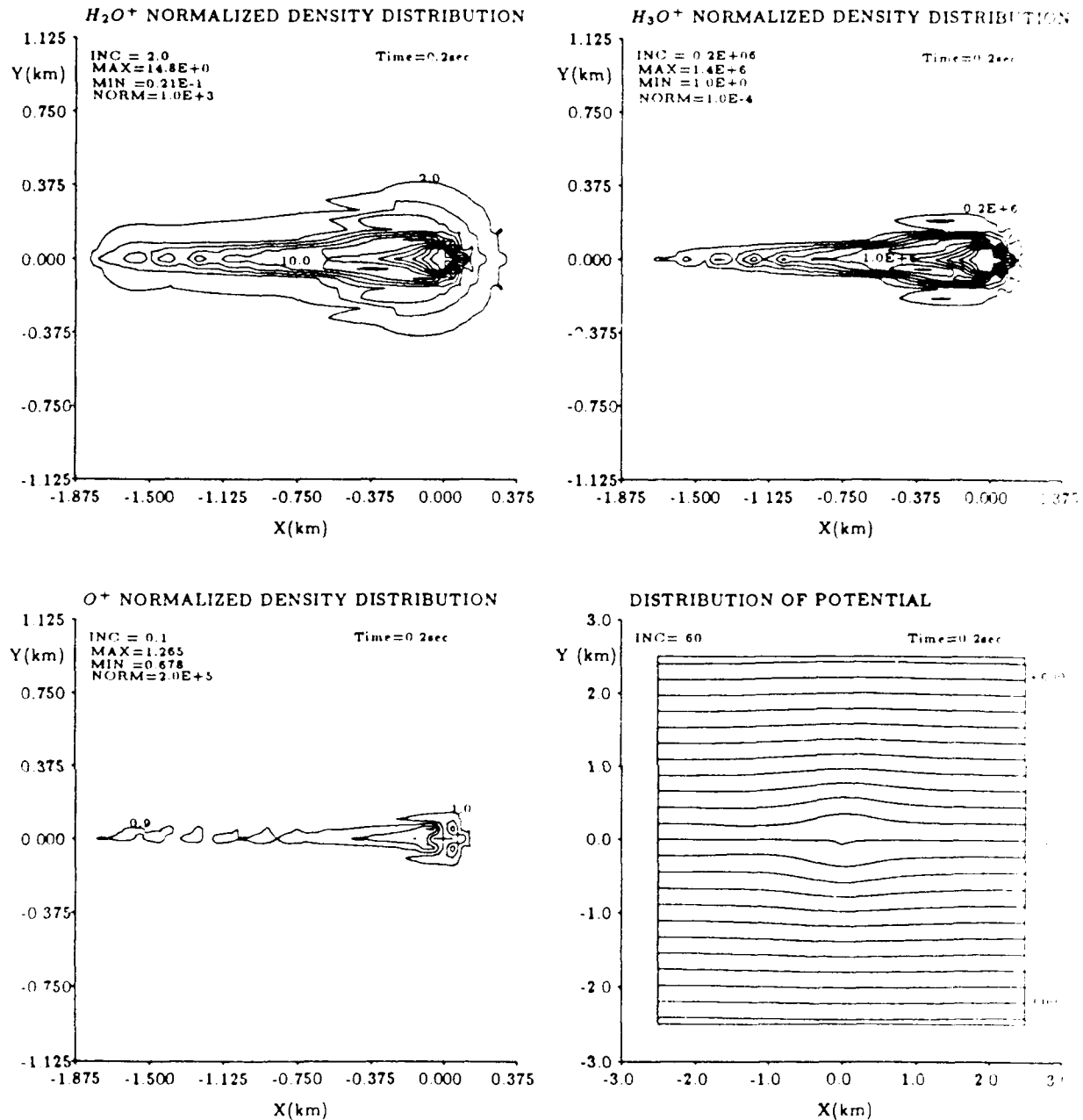
H_2O^+ NORMALIZED DENSITY DISTRIBUTION

```
INC = 2.0                    Time=0.2sec
MAX=14.8E+0
MIN =0.21E-1
NORM=1.0E+3
```

H_3O^+ NORMALIZED DENSITY DISTRIBUTION

```
INC = 0.2E+06                Time=0.2sec
MAX=1.4E+6
MIN =1.0E+0
NORM=1.0E-4
```

O^+ NORMALIZED DENSITY DISTRIBUTION

```
INC = 0.1                    Time=0.2sec
MAX=1.265
MIN =0.678
NORM=2.0E+5
```

DISTRIBUTION OF POTENTIAL

```
INC= 60                      Time=0.2sec
```

Fig 3 Ion density contours and potential distribution in a plasma cloud with symmetric initial conditions and central neutral water density of 10^9 cm^{-3} at a time of 0.2 seconds after release. The interaction parallel length is 500 km and the contaminant H_2O^+ and H_3O^+ temperature is 0.025 eV (top-left) Water ion contours. Normalization is to the initial central value of 10^3 cm^{-3} (top-right) Hydronium ion contours. Normalization is to the ambient value of 10^{-4} cm^{-3} (bottom-left) Oxygen ion contours. Normalization is to the ambient value of 2×10^5 cm^{-3} (bottom-right) Potential distribution in volts as measured in the frame of the moving structure which is located at (0,0) km.

potential contours are shown to steepen in contrast with the ram region where they smoothly fall off to match the boundary conditions. This behavior of the potential is also depicted in Figure 2 and Figure 4. The explanation lies in the equation of the potential and the associated currents. In the wake the water neutral density is low, compared with the ambient, while there is an excessive build-up of ionic species. At high neutral density regions, collision frequencies are large, the drift velocities are small and the electric field is shielded. However, in regions where collision frequencies are low currents due to ion density gradients act with the motional electric field and short-circuit the shielding currents. These regions in turn move very fast with large parallel currents carried by Alfvén waves. A similar
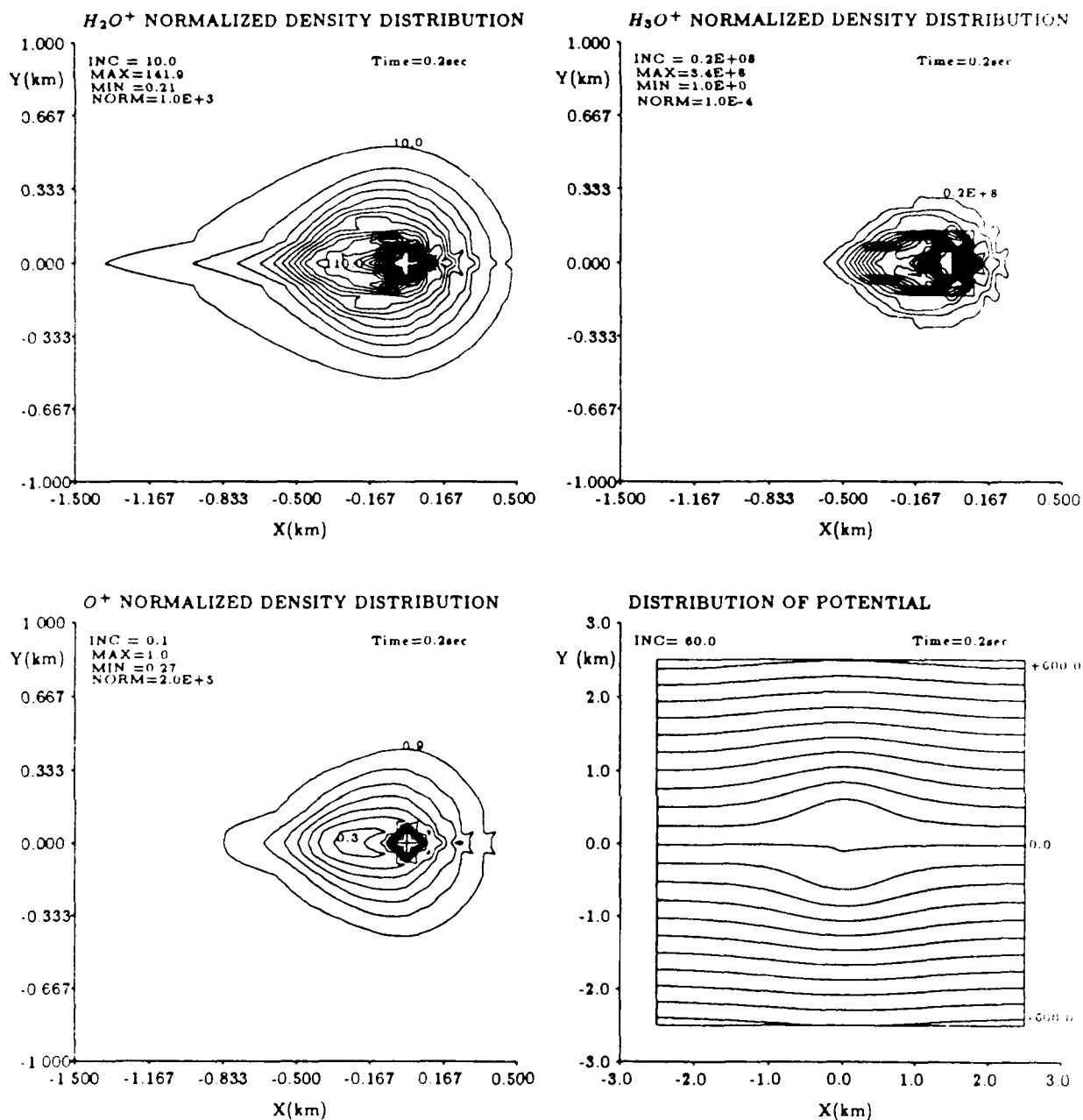
57

H_2O^+ NORMALIZED DENSITY DISTRIBUTION

INC = 10.0
MAX = 141.9
MIN = 0.21
NORM = 1.0E+3

Time = 0.2sec

H_3O^+ NORMALIZED DENSITY DISTRIBUTION

INC = 0.2E+08
MAX = 3.4E+8
MIN = 1.0E+0
NORM = 1.0E-4

Time = 0.2sec

O^+ NORMALIZED DENSITY DISTRIBUTION

INC = 0.1
MAX = 1.0
MIN = 0.27
NORM = 2.0E+5

Time = 0.2sec

DISTRIBUTION OF POTENTIAL

INC = 60.0

Time = 0.2sec

Fig 4 Ion density contours and potential distribution in a plasma cloud for symmetric initial conditions and central neutral water density of 10^{10} cm^{-3} at a time of 0 2 s after release. The interaction parallel length is 500 km and the contaminant H_2O^+ and H_3O^+ temperature is 0 025 eV (top-left) Water ion contours. Normalization is to initial central value of 10^3 cm^{-3} (top-right) Hydronium ion contours. Normalization is to the ambient value of 10^{-4} cm^{-3} (bottom-left) Oxygen ion contours. Normalization is to ambient value of 2×10^5 cm^{-3} (bottom-right) Potential distribution in volts as measured in the frame of the moving structure which is created at (0,0) km

behavior has been observed before in cases where the ion density was larger than the ambient [Hastings et al., 1987].

Figure 4 represents a cloud with central neutral density of 10^{10} cm^{-3}. The shielding effect is dominant at the region of high neutral densities. The water ion cloud drifts backward more slowly than the previous cases. The overall picture of the cloud resembles that of the Figure 3 but on an

earlier state of development. At 0.2 s the cloud just started to develop the "dumbbell" shape. There is a substantial formation of ionic water due to much longer residence time of oxygen ions with a maximum at 142×10^3 cm^{-3}. The fingerlike disturbances are just about to start forming in the central regions, due to the differential streaming of the ions. The hydronium ion also shows significant formation and a
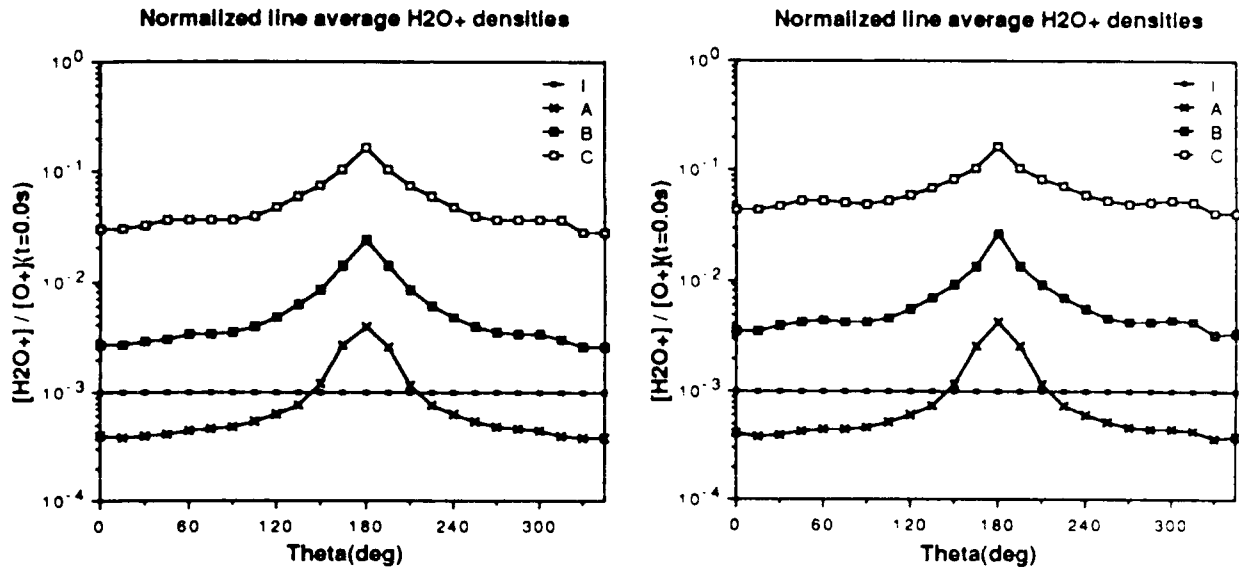
Normalized line average H2O+ densities

Normalized line average H2O+ densities

Fig. 5. Normalized line average H_2O^+ densities as function of the azimuthal angle for different neutral water densities. Normalization is to the initial $[O^+](\theta, t = 0) = 5 \times 10^{10}$ cm^{-2}. I, Normalized $[H_2O^+]$ density at the time of release. A, Normalized $[H_2O^+]$ density at a time of 0.2 s after the release for an initial central neutral water density of 10^8 cm^{-3}. B, Normalized $[H_2O^+]$ density at a time of 0.2 s after the release for an initial central neutral water density of 10^9 cm^{-3}. C, Normalized $[H_2O^+]$ density at a time of 0.2 s after the release for an initial central neutral water density of 10^{10} cm^{-3}. (left) The interaction parallel length is $L_{\parallel} = 50$ km. (right) The interaction parallel length is $L_{\parallel} = 500$ km.

cloud stucture. The maximum at the wake is 3.4×10^4 cm^{-3}. There is also a large depletion of the ionic oxygen with a "hole" at 0.3×10^5 cm^{-3}.

The simulations in the case of an outgassed cloud were performed to study the effects of the initial central water

density, the parallel interaction length and the ion temperature. For comparison of this information we calculated the line average densities as measured from the center of the moving structure as function of the azimuthal angle. For a species s^+ the line average density is defined as
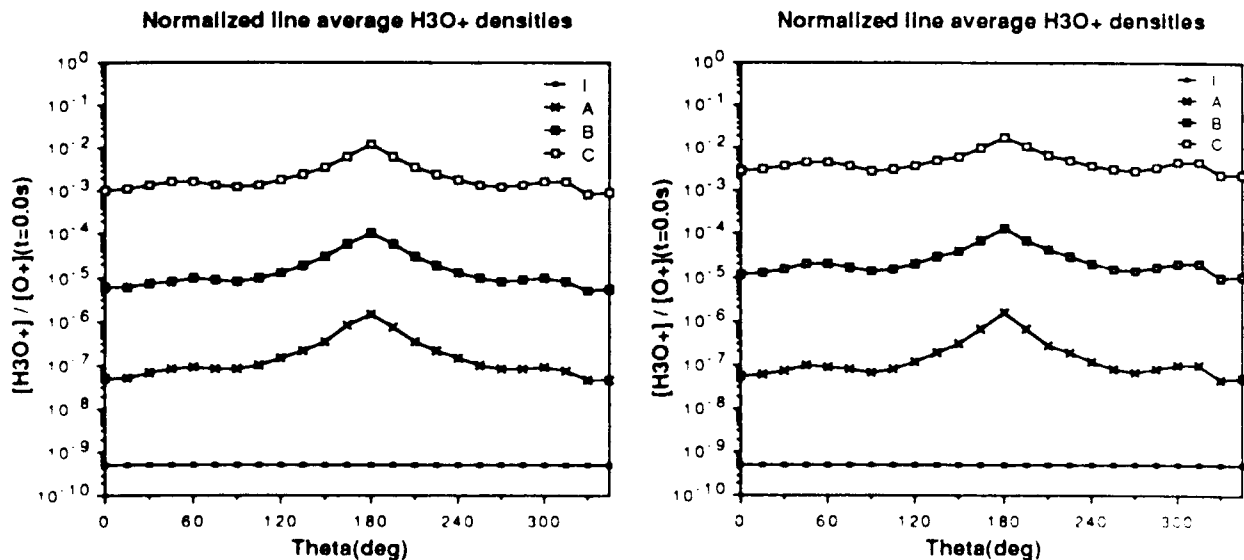
Normalized line average H3O+ densities
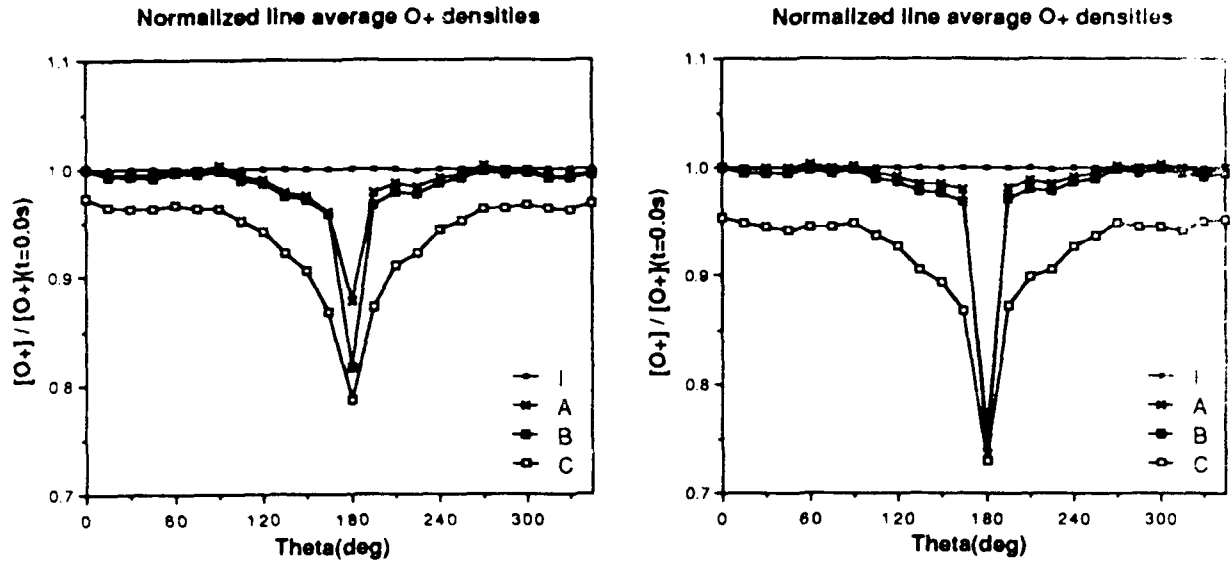

Normalized line average H3O+ densities

Fig. 6. Normalized line average H_3O^+ densities as function of the azimuthal angle for different neutral water densities. Normalization is to the initial $[O^+](\theta, t = 0) = 5 \times 10^{10}$ cm^{-2}. I, Normalized $[H_3O^+]$ density at the time of release. A, Normalized $[H_3O^+]$ density at a time of 0.2 s after the release for an initial central neutral water density of 10^8 cm^{-3}. B, Normalized $[H_3O^+]$ density at a time of 0.2 s after the release for an initial central neutral water density of 10^9 cm^{-3}. C, Normalized $[H_3O^+]$ density at a time of 0.2 s after the release for an initial central neutral water density of 10^{10} cm^{-3}. (left) The interaction parallel length is $L_{\parallel} = 50$ km. (right) The interaction parallel length is $L_{\parallel} = 500$ km.

Normalized line average O+ densities

Normalized line average O+ densities

Fig. 7. Normalized line average O^+ densities as function of the azimuthal angle for different neutral water densities. Normalization is to the initial $[O^+](\theta, t = 0) = 5 \times 10^{10}$ cm^{-2}. I, Normalized $[O^+]$ density at the time of release. A, Normalized $[O^+]$ density at a time of 0.2 s after the release for an initial central neutral water density of 10^8 cm^{-3}. B, Normalized $[O^+]$ density at a time of 0.2 s after the release for an initial central neutral water density of 10^9 cm^{-3}. C, Normalized $[O^+]$ density at a time of 0.2 s after the release for an initial central neutral water density of 10^{10} cm^{-3}. (left) The interaction parallel length is $L_{||} = 50$ km. (right) The interaction parallel length is $L_{||} = 500$ km.

$$[s^+](\theta, t) = \int_0^R N_{o+}(l, \theta, t)dl \qquad (41)$$

where R is the radial distance taken to be 2.5 km and θ is the azimuthal angle measured from the direction of the velocity vector counterclockwise. For all ions the line average density at time 0.2 s after the release was normalized with that of the O^+ at the time of the release. Using the definition of the average and the initial conditions one can show that $O^+(\theta, t = 0) = 5 \times 10^{10}$ cm^{-2}.

The $[H_2O^+]$ densities are shown initially and at time 0.2 s for $L_{||} = 50$ km in Figure 5A and for $L_{||} = 500$ km in Figure 5B. For all the central water densities considered there is ionic water formation in the wake of the moving body. For the $N_{H_2O}(r = 0) = 10^8$ cm^{-3} neutral cloud there is no difference in the levels of ionic water between the two parallel lengths. The shielding is not important for the low-density cloud. However, for high-density neutral clouds the difference becomes more evident, since shielding slows down the cloud, thus making the charge exchange reaction more efficient in producing ionic water.

The $[H_2O^+]$ densities are shown initially and at time 0.2 s for $L_{||} = 50$ km in Figure 6A and for $L_{||} = 500$ km in Figure 6B. In all cases there is production of hydronium ions. The levels of hydronium ions increase with the central neutral density for both the interaction lengths. Again, as for the water ions, the low-density case shows no difference between the two interaction lengths. For high neutral densities however the large interaction length allows more hydronium ion creation due to larger water ion residence times.

The $[O^+]$ densities initially and at time 0.2 s are shown in Figures 7A and 7B, for interaction lengths of 50 and 500 km, respectively. The O^+ depicts a depletion region exactly where new ions are formed, that is, at the wake of the moving structure. The depletion increases with increasing neutral water density for both the parallel lengths. For the dense cloud with $N_{H_2O}(r = 0) = 10^{10}$ cm^3 the depletion extends throughout the structure while for the less dense clouds it is confined between $\theta = 120°$ and $\theta = 240°$. For $N_{H_2O}(r = 0) = 10^{10}$ and $L_{||} = 500$ km the ratio of ionic water to oxygen and the ratio of the hydronium ion to water ion is ~ 0.1 at the wake, which is consistent with measurements indicated by Caledonia et al. [1987].

From the above results we can conclude that at low neutral water densities ($< 10^9$ cm^{-3}) there is no difference in the ionic water formation between the two interaction lengths. The potential field shows no effectively shielding and the ions that are formed are "trapped" in the magnetic field. For high neutral water densities ($> 10^9$ cm^{-3}), shielding occurs, especially for the large parallel interaction lengths. These cases represent slow moving clouds where large parallel current build up at the edges of the cloud, thus diminishing the motional electric field. The reactions, then, basically charge exchange and recombination, build up more ionic species   deplete the ambient oxygen ions. However, as our results indicate, the dominant factor which determines the shielding is not the parallel length but the initial central neutral water density. In the high density neutral clouds the currents due to collisions are large enough to shield the motional electric field. In Figure 8 it is shown the magnitude of the electric field for a cloud with $N_{H_2O}(r = 0) = 10^{10}$ cm^{-3} and $L_{||} = 500$ km, initially

NORMALIZED MAGNITUDE OF ELECTRIC FIELD
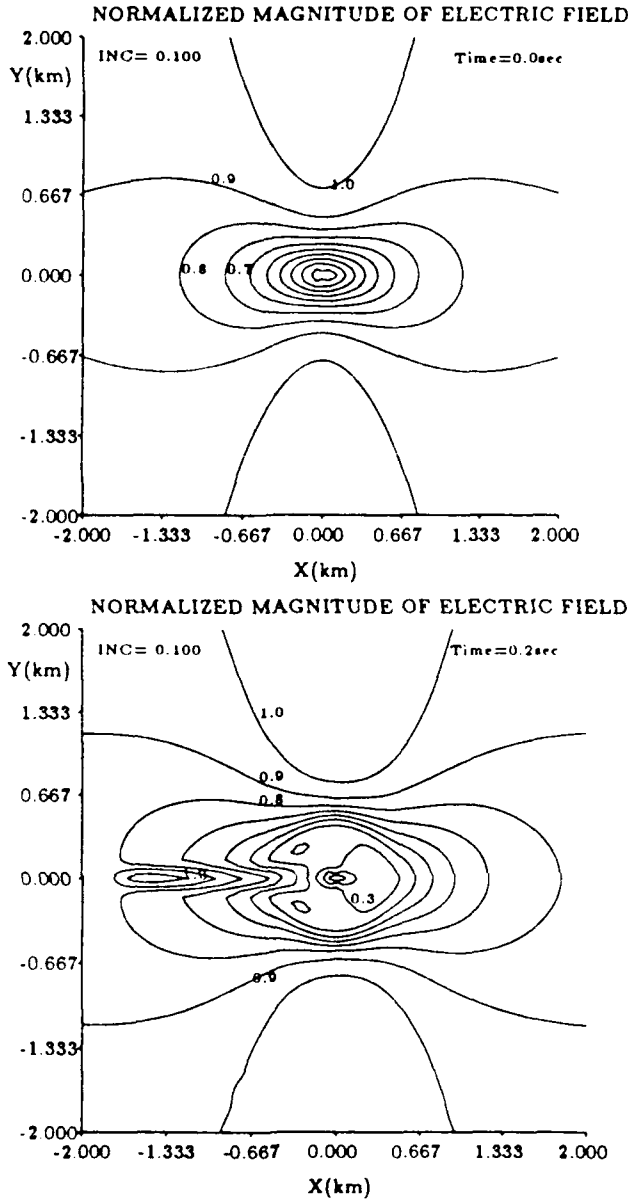

NORMALIZED MAGNITUDE OF ELECTRIC FIELD

Fig. 8. Magnitude of the electric field as measured in the moving frame initial (top) and at a time of 0.2 s after the release (bottom). The initial conditions are symmetric with central neutral water density of 10^{10} cm^{-3}, the interaction length is 500 km and the contaminant H_2O^+ and H_3O^+ temperature is 0.025 eV. Normalization is to the motional electric field of 0.279 V/m.

and at a time of 0.2 s after the release. The magnitude of the electric field has been normalized with that of the motional taken to be $|E_m| \sim 0.28$ V/m. Shawhan et al. [1984] from measurements on STS-3 anticipated reductions on the potential of the order of the motional. Furthermore, Katz et al. [1984] showed that the ions near the vicinity of the space shuttle could be almost stationary with respect to the moving frame. As Figure 8 shows, the electric field is strongly diminished in the near space of the body. Initially, the shielding is symmetric in both directions, a direct result of the symmetry of the initial ion-neutral distributions. At

time of 0.2 s, however, the symmetry of the electric field in the motional direction no longer holds, a direct result of the evolution of the cloud; the increase in the magnitude of the field occurs at the wake of the body, and, as we already speculated, this may be attributed to the high ion density region which is located at the wake. In general the electric field disturbances are shown to be both highly localized, as anticipated from Shawhan et al. [1984], and time dependent. Finally, all cases show fingerlike deformations located in the backside of the drifting clouds in agreement with previous theoretical and experimental data. These disturbances may be attributed to $E \times B$ instabilities.

To study the effect of ion temperature, we performed simulations using the same set of initial conditions as the above but with with a higher ion temperature $(T_i = 0.1$ eV).

In Figure 9 the line average densities for water ion and hydronium ion are shown for two simulations with different ion temperatures but with $N_{H_2O}(r = 0) = 10^9$ cm^{-3} and $L_{\parallel} = 500$ km. The $[H_2O^+]$ are shown to be identical, while $[H_3O^+]$ shows a slight increase with increasing ion temperature. The line average densities for oxygen ion were identical for the two cases. The magnitude of the higher ion temperature was chosen to be consistent with the temperature expected in a thruster firing. The weak dependence on the
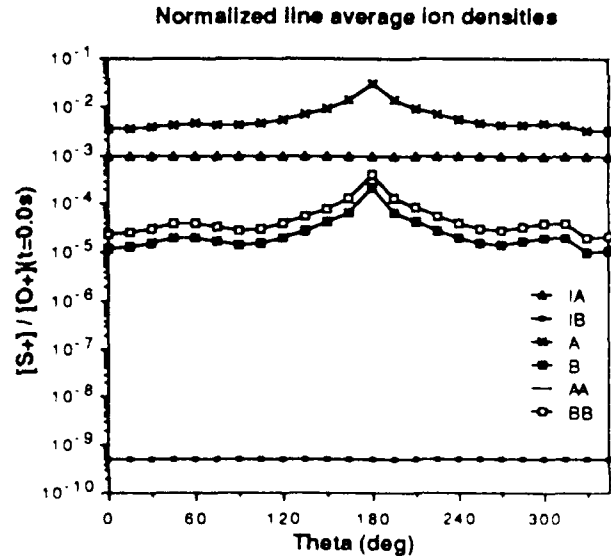
Normalized line average ion densities

Fig. 9. Normalized line average H_2O^+ and H_3O^+ densities as function of the azimuthal angle for different ion temperatures Normalization is to the initial $[O^+](\theta, t = 0) = 5 \times 10^{10}$ cm^{-2} The initial conditions are symmetric with central neutral water density of 10^9 cm^{-3} and the interaction length is 50 km IA, Normalized $[H_2O^+]$ densities at the time of release IB, Normalized $[H_3O^+]$ densities at the time of release A, Normalized $[H_2O^+]$ densities at a time of 0.2 s after the release The contaminant H_2O^+ and H_3O^+ temperature is 0.025 eV B, Normalized $[H_3O^+]$ densities at a time of 0.2 s after the release The contaminant H_2O^+ and H_3O^+ temperature is 0.025 eV AA, Normalized $[H_2O^+]$ densities at a time of 0.2 s after the release The contaminant H_2O^+ and H_3O^+ temperature is 0.1 eV BB, Normalized $[H_3O^+]$ densities at a time of 0.2 s after the release The contaminant H_2O^+ and H_3O^+ temperature is 0.1 eV

ion temperature occurs because in the potential equation the diffusion terms (which contain the temperature) are always subdominant for the ion density ranges explored. The electric field is primarily determined as the $V_s \times B$ field with a modification due to the dielectric shielding. For ion densities higher than the ambient the behavior is different and is illustrated by *Hastings et al.* [1988]. The other major effect of the ion temperature is on the collision frequencies. However for the density ranges considered the dominant collision frequency is that due to oxygen atoms colliding with ions. The relative velocity in this collision frequency is determined by the orbital velocity of the oxygen which is only very weakly dependent on the ion temperature. However, we must state that the conclusions about the temperature are limited from the range of temperatures considered. The newly created ions within the plasma cloud could have temperatures much higher than 0.1 eV. The possible temperature for the H_2O^+ produced in the charge exchange reaction is possibly 1eV or more. There are large source terms in the ion energy equation as a result of the large differential motion of the reactants but this consideration is beyond the limits of the isothermal model assumed in this study.

Asymmetric Initial Conditions: A Thruster Cloud

In order to simulate a directed contaminant release, such that could result from a thruster firing we chose asymmetric initial conditions for the water ions and water neutrals. The neutral water was modeled as

$$N_{H_2O}(\mathbf{r}, t = 0) = 10^{-4}$$

$$+ N_{H_2O^+}(\mathbf{r} = 0) \exp\left[-\left(\frac{|x^* - x_o^*|}{x_L^*}\right)^2 \left(\frac{|y^* - y_o^*|}{y_L^*}\right)^2 \right] \quad (42)$$

where x^* and y^* are the coordinates in the rotated frame, x_L^* is the decay distance in the x^* direction and y_L^* in the y^* direction. The decay distances were chosen so that $x_L^* = 150$ m in the positive x^*, while $x_L^* = 450$ m in the negative x^* direction. The $y_L^* = 150$ m in the y^* direction. The initial profile described by the above is an asymmetric ellipsoidal distribution on the top of a flat profile and is shown in Figure 10. The central water was taken to be 10^9 cm^{-3}. The water ions were following a similar distribution with a central density of 10^3 cm^{-3}. The ion temperature was taken at 0.1 eV, which is consistent with what is expected in a thruster firing and the parallel interaction length was 50 km.

In Figure 11 we show the normalized density distributions of ionic water, hydronium and oxygen ions at time of 0.2 s after the release. The ion density peak has rotated due to the $E \times B$ motion of the ions. In addition, both densities show considerable asymmetry, while hydronium ion has broken up into two discernible cloud structures. The ion clouds drift backward and remain smooth in their front sides with instabilities developing in the back side. In the same figure at a time of 0.2 s the oxygen ion contours depict a depletion
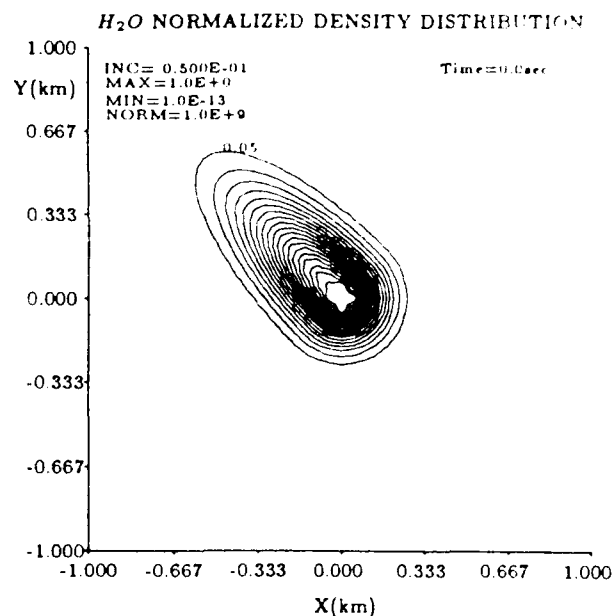

H_2O NORMALIZED DENSITY DISTRIBUTION

INC= 0.500E-01
MAX=1.0E+0
MIN=1.0E-13
NORM=1.0E+9
Time=0.0sec

Fig. 10. Asymmetric (ellipsoidal) initial conditions for a central water density of 10^9 cm^{-3} at initial time and for a parallel interaction length of 50 km. Ion temperature is 0.1 eV.

in the wake of the moving body, while the potential contours shows the shielding and the asymmetry. The rotation of the cloud is confirmed from Figure 1? where we show the line averages for the ions at 0.2 seconds as compared to the initial line averages. The oxygen ion density is seen to undergo a slight reduction behind the body. The water ion density increases by about an order of magnitude from its initial value and shows a broad peak mainly behind the body. The hydronium ion density also shows asymmetry behind the body with the line averaged density having two asymmetric peaks at $\sim 180°$ and $\sim 210°$. This asymmetry is due to the nonlinear coupling of the density and potential fields and suggests that the initial conditions for a water release are very important to understanding the subsequent evolution of the water plasma cloud. This also suggests that mass spectrometer measurements taken from a spacecraft such as the shuttle will see a substantial dependence on the look angle relative to the ram direction. Of course one reason for such a dependence is that the collection of ions is much more efficient in the ram direction than in other directions due to the fact that ions from the ram direction can directly enter the instrument. Here we point out that another reason is the existence of nonlinear distortion of the plasma density contours which is a strong function of angle. From Figure 12 we see that typically there is a factor of 2 to 5 between the line averaged densities for angles less than π and for angles greater than π.

4 SUMMARY AND CONCLUSIONS

A model has been developed for the motion of contaminant water plasma clouds about large space structures. The
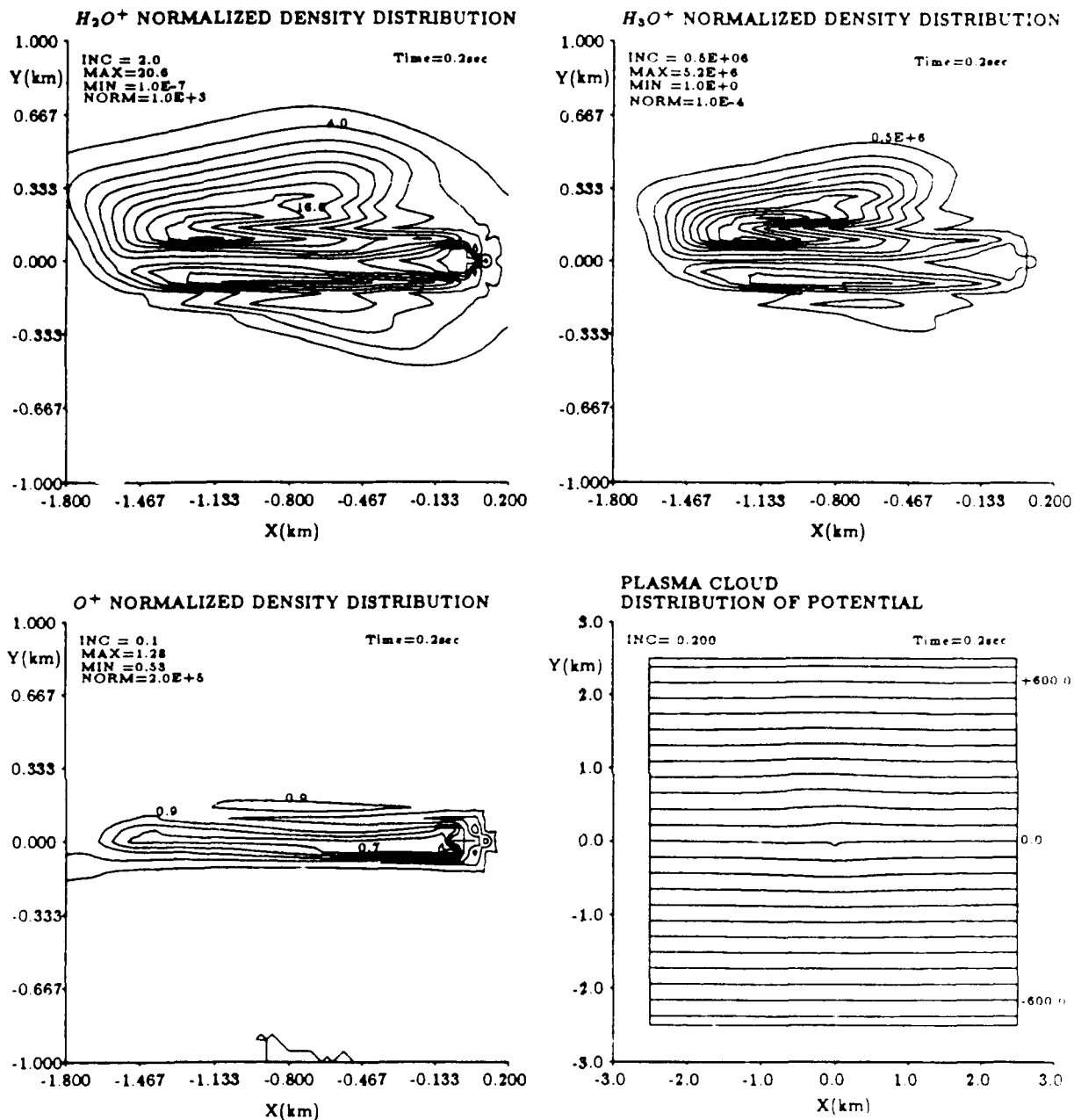
Fig 11 Ion density contours and potential in a plasma cloud for assymetric ellipsoidal initial conditions and central neutral water density of 10^9 cm^{-3} at a time of 0.2 s after release. The interaction parallel length is 50 km and the ion temperature is 0 1 eV (top-left) Water ion density contours. Normalization is to the initial central value of 10^3 cm^{-3} (top-right) Hydronium density contours. Normalization is to the ambient value of 10^{-4} cm^{-3} (bottom-left) Oxygen ion contours. Normalization is to ambient value of 2×10^5 cm^{-3} (bottom-right) Potential distribution in volts as measu ed in the frame of the moving structure which is located at (0,0) km

model includes emission of Alfvén waves from the cloud to carry current along the magnetic field. The ions exhibit $E \times B$ drifts which is determined by the current balance within the plasma cloud. A parallel interaction length scale is derived which represents the coupling of the cloud with the ionosphere via parallel currents carried by the Alfvén waves emitted by the moving cloud. The cloud equations have been studied systematically as a function of the paral-

lel interaction length, neutral density, ion temperature and initial conditions. We conclude that for low density neutral water clouds ($\leq 10^9$ cm^{-3}) the amount of shielding is small and the electric field is the motional. In this case the cloud drifts with almost the orbital speed in the structure reference frame. However, for neutral water densities of interest for shuttle conditions ($\sim 10^{10}$ cm^{-3}) shielding is very significant in the vicinity of the moving structure and is predicted
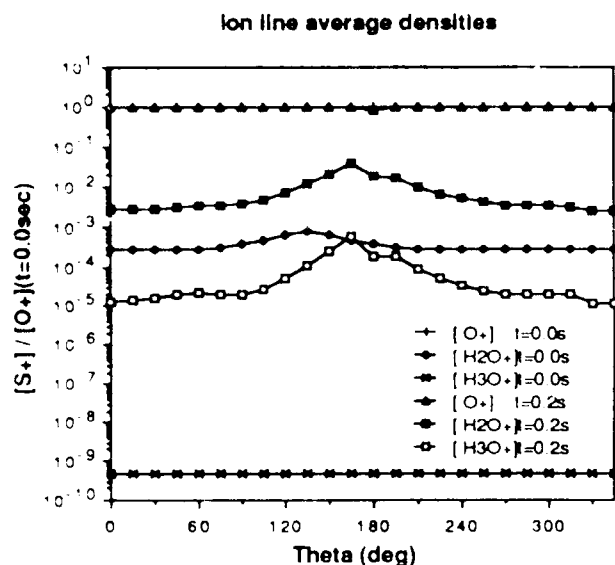
63

Ion line average densities

Fig. 12. Ion line average densities as a function of azimuthal angle, for initial and at time of 0.2 s conditions. The interaction length is 50 km, the ion temperature is 0.1 eV and the initial neutral water density is 10^9 cm^{-3}. Ionic line averages are normalized to the initial line average for ionic oxygen. Asymmetric (ellipsoidal) initial conditions.

to be of the order of the motional electric field, in accordance with experimental data. This represents a case in which the plasma cloud drifts almost with the moving structure. For the highest density neutral cloud the ratios of the line averaged signals is consistent with experimental data. The effect of ion temperature is negligible for the range of densities considered. The effect of different (asymmetric) initial conditions is mainly to allow the plasma cloud that is formed to rotate under the crossed electric and magnetic fields and to undergo a highly asymmetric distortion. In all the cases considered it is predicted that the backward moving clouds will develop fingerlike instabilities in the back-side of the clouds; the appearance of these instabilities is in agreement with theoretical and experimental data.

Future work will be to develop a three-dimensional model of the plasma cloud and will attempt to elucidate the low-frequency stability of the cloud.

REFERENCES

Boden, P. C. and Twiddy, N. D., A flowing afterglow study of water vapor, *Faraday Disc. Chem. Soc.*, 53, 192, 1972.

Burgers, J. M., Flow Equations for Composite Gases, Academic, San Diego, Calif., 1969.

Caledonia, G. E., Person, J. C. and Hastings, D. E., The interpretation of space shuttle measurements of ionic species, *J. Geophys. Res.*, 92, 273-281, 1987.

Eccles, J. V., Raitt, W. J., and Banks, P. M., A numerical model of the electrodynamics of plasma within the contaminant gas cloud of the space shuttle orbiter at LEO, to be published in *J. Geophys. Res.*, 1988.

Gatsonis, N. A., Theory and numerical analysis of plasma clouds surrounding space systems in low earth orbit, Master's thesis, Mass. Inst. of Technol., Cambridge, 1987.

Goertz, C. K., Io's interaction with the plasma torus, *J. Geophys. Res.*, 85, 2949-2956, 1980.

Hastings, D. E., Gatsonis, N. A., and Mogstad, T., A simple model for the initial phase of a water plasma cloud about a large structure in space, *J. Geophys. Res.*, 93, 1961-1973, 1988.

Katz, I., Parks, D. E., Cooke, D. L., and Lilley Jr, J. R., Polarization of spacecraft generated plasma clouds, *Geophy. Res. Lett.*, 11, 1115, 1984.

Li, T. Y., Gas kinetic equations, *Dynamics of Fluids and Plasmas*, edited by S. I. Pai, p. 155, Academic, San Diego, Calif., 1966.

Lloyd, K. H., and Haerendel, G., Numerical modeling of the drift and deformation of ionospheric plasma clouds and their interaction with other layers of the ionosphere, *J. Geophys. Res.*, 78, 7389, 1973.

Mitchell, J. A., and McGowan, J. W., Experimental studies of electron-ion recombination, *Physics of Ion-Ion and Electron-Ion Collisions*, edited by F. Brouillard and J. W McGowan, Plenum, New York, 1983.

Murad, E., and Lai, S. T., Effect of dissociative electron-ion recombination on the propagation of critical ionization discharges, *J. Geophys. Res.*, 91, 13745-13749, 1986.

Murphy, G., Pickett, J., D'angelo, N., and Kurth, W. S., Measurements of the plasma parameters in the vicinity of the space shuttle, *Planet. Space Sci.*, 34, 993-1004, 1986.

Neubauer, F. M., Nonlinear standing Alfvén wave current system at Io: Theory, *J. Geophys. Res.*, 85, 1171-1178, 1980.

Perkins, F. W., Zabusky, N. J., and Doles, J. H., Deformation and striation of plasma clouds in the ionosphere, 1, *J. Geophys. Res.*, 78, 697-709, 1973.

Pickett, J. S., Murphy, G. B., Kurth, W. S., Goertz, C. K., and Shawhan, S. D., Effects of chemical releases by the STS 3 orbiter on the ionosphere, *J. Geophys. Res.*, 90, 3487-3497, 1985.

Reasoner, D. L., Shawhan, S. D., and Murphy, G., Plasma diagnostics package measurements of ionospheric ions and shuttle-induced perturbations, *J. Geophys. Res.*, 91, 13463-13471, 1986.

Shawhan, S. D., Murphy, G., and Pickett, J. S., Plasma diagnostics package initial assessment of the shuttle orbiter plasma environment, *J. Spacecr. Rockets*, 21, 387, 1984.

Zalesak, S. T., Fully multidimensional flux corrected transport algorithms for fluids, *J. Comput. Phys.*, 31, 335-362, 1979.

Zalesak, S. T., A physical interpretation of the Richtmeyer two-step Lax-Wendroff scheme and its generalization to higher spatial order. In *Advances in Computer Methods for Partial Differential Equations*, edited by Vichnevetsky, R., and Stepleman, R. S., Imacs, New Brunswick, N.J., 1984.

N. A. Gatsonis and D. E. Hastings, Department of Aeronautics and Astronautics, Massachusetts Institute of Technology, Room 37-441, Cambridge, MA 02139

A THREE-DIMENSIONAL MODEL FOR AN ARTIFICIAL PLASMA
CLOUD ABOUT A SPACECRAFT IN LOW EARTH ORBIT

Nikolaos A. Gatsonis* and Daniel E. Hastings[+]

Department of Aeronautics and Astronautics
Massachusetts Inst. of Technology, Cambridge, MA 02139

We developed a fully three-dimensional model for an artificial plasma cloud in the ionosphere. Such a cloud could be a result of a deliberate release or contamination about a spacecraft. We took into account finite perpendicular and parallel lengths, all elastic collisions between the considered species, finite temperature effects, variable ionospheric densities, variable neutral winds, ambient electric fields and gravity. The velocities of the charged species were written with the use of transport coefficient tensors. We derived an equation for the self-consisted perturbation potential due to the plasma perturbation which is a three-dimensional, non-self adjoint elliptic type of equation with very dissimilar coefficients. The current balance equation was solved numerically in order to obtain the perturbation potential at the time of the release. We examined the effects of the central density of the ions and the dimensions of the cloud. The perturbation potential increases with increasing ion density. With densities of 10^{15} m^{-3} the cloud shields out the motional electric field. Ion clouds with smaller dimensions result in weaker electric field perturbations. In all cases, the magnetic field lines are not equipotential lines within a region bounded by the density perturbation. The perturbation along the magnetic field lines is stronger for the case of denser and larger clouds. The effect of the presence of neutral was also investigated through the use of a gaussian neutral cloud. The perturbation potential is stronger when neutrals are present. Due to the screening of the motional electric field the cloud is expected to drift with differential speeds which will result in finger-like shaping.

Introduction

The presence of a moving body in the ionosphere represents a disturbance in the ambient environment. The Space Shuttle Orbiter (SSO) flights provided clear evidence of the severe interactions between a space vehicle and the ambient ionosphere. *Carignan and Miller* [1983], *Shawhan et al.* [1984], *Picket et al.* [1985] *Murphy at al.* [1986]. *Caledonia et al.* [1987].

The study of the induced environment about a space vehicle is extremely important as a design parameter. Especially for a vehicle which is expected to remain in space for a long period, like the proposed space station, it is important to understand the characteristics of the induced environment. It is crucial to be able to model this environment for drag calculations, prediction of surface degradation and spacecraft charging, control of electrostatic noise and airglow, estimate of the impact on the ionosphere and the scale of disturbance that it represents.

In this study we will focus our attention to the plasma cloud which surrounds a space vehicle in Low Earth Orbit (LEO). *Hastings et al.* [1988], *Gatsonis,* [1987] ,*Eccles et al.* [1988], *Hastings and Gatsonis* [1989]. The schematic of the process that we study is as follows: we consider a vehicle in LEO which creates a neutral cloud around it. The neutral cloud expands while undergoing chemical reactions which produce ions. The motion and composition of this plasma cloud is then a result of complicated chemical and electrodynamical processes. The schematic that we consider is quite general and thus can be applied to processes like outgassing or a thruster firing. It can also be applied to another class of events, those of ion cloud experiments. The purpose of this study is to obtain a theory and a model for the motion of an artificial high speed plasma cloud in the ionosphere.

A 3-Dimensional Model for an Ion-Neutral Cloud in the Ionosphere

In the present model we assume that there are two neutral and two ion species; s for the ejected neutrals and a for the ambient ionospheric neutrals. Similarly, s^+ designates the contaminant ions and a^+ the ambient ions. Emphasis

---

*Graduate Research Assistant, Student Member AIAA

[+]Associate Professor, Member AIAA

65

will be given on water neutrals and water ions since those two species have been identified as the major contaminants about large space structures. There are subsequently two neutral winds which are taken into account. The ambient neutral wind, $\vec{U}_a$ and the contaminant neutral wind, $\vec{U}_s$.

We adopted a simple chemistry model. The ejected neutrals interact with the ambient stream in ions via charge exchange reaction to form ions and produce neutrals. The charge exchange reaction is

$$a^+ + s \rightarrow a + s^+ \qquad (1)$$

The expansion of the neutral gas in a rarefied environment is by itself a very difficult analytical and computational problem. One expects the neutral cloud to pass through various flow regimes and be highly dependent upon the conditions of its release. Initially we will use simple spherically expanding neutral clouds. This will enable us to develop and validate the ion cloud model.

Fluid Model for the Plasma Motion

Coordinate System

Given the latitude of the release of the neutral cloud we construct an orthogonal coordinate system, the fixed to
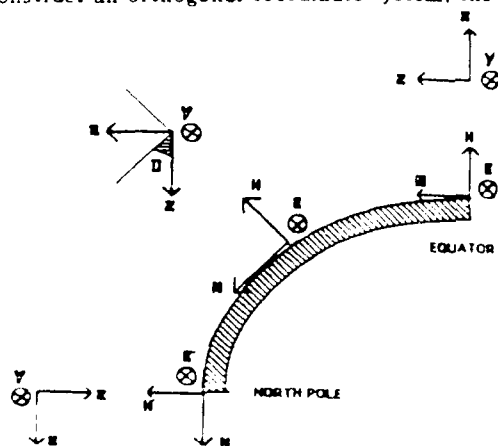
Figure 1. Fixed to earth coordinate system (H,E,N) and the field aligned system (x,y,z)

earth (e s). (Figure 1) In that system the $\vec{E}$ points to the east, N points to the north and H refers to the altitude. This system will bring the spatial variability of the ambient ionospheric parameters. The coordinate system which is suitable for analytical purposes is the field aligned system. Given the latitude and altitude of the release this system has its origin at the point of the release and is orthogonal. The $\hat{z}$ axis is parallel to the local magnetic field line, the $\hat{y}$ axis is parallel to the $\vec{E}$ direction and the $\hat{x}$ direction is the perpendicular to both the $\hat{z}$ and $\hat{y}$ directions.

Continuity and Momentum Equations

Assume that the plasma cloud consists of contaminant ions with density n_{s^+} and velocity $\vec{V}_{s^+}$. The density of ambient ions is n_{a^+} and their velocity is $\vec{V}_{a^+}$. Electrons are shown with a density n_e and velocity $\vec{V}_e$. The continuity equation for any species $t = a^+, s^+, e$ is

$$\frac{\partial n_t}{\partial t} + \nabla \cdot (n_t \vec{V}_t) = P_t + L_t \qquad (2)$$

The terms on the r.h.s of the continuity equation come from the production or loss of the species due to chemical reactions are

$$P_{a^+} = 0 \qquad L_{a^+} = -n_{a^+} k^{cx} n_s$$
$$P_{s^+} = n_{a^+} k^{cx} n_s \qquad L_{s^+} = 0$$
$$P_e = 0 \qquad L_e = 0 \qquad (3)$$

In the momentum balance we take into account electric fields, pressure forces, gravity and elastic collisions. Assuming that the time scales of interest are much larger than collision times the unsteady term can be neglected. This assumption restricts the analysis to the low frequencies. The inertia term $\vec{V} \cdot \nabla \vec{V}$ can be neglected as long as the thermal velocity is much greater than the drift velocity. The momentum equations can be written in the following form

$$\frac{\vec{F}_t}{m_t} + \frac{q_t}{m_t}(\vec{V}_t \times \vec{B}) - (\nu_{te} + \nu_{ta} + \sum_{j \neq t} \nu_{tj})\vec{V}_t = 0 \qquad (4)$$

where the force for the species t is

$$\vec{F}_t = q_t \vec{E} + m_t \nu_{ta} \vec{U}_a + m_t \nu_{ts} \vec{U}_s + \sum_{j \neq t} m_t \nu_{tj} \vec{V}_j$$
$$- \frac{\nabla P_t}{n_t} + m_t \vec{g} \qquad (5)$$

Here m_t is the mass of the species, $\vec{E}$ is the electric field, ν_{ts} is the collision frequency for momentum transfer, P_t is the pressure and $\vec{g}$ is the gravitational acceleration. The ambient neutral wind is denoted by V_a while the neutral wind from the ejected neutrals is V_s.

The momentum equations written in this form allows us to define the total collision frequency for momentum transfer due to elastic collisions for any of the plasma species as

$$\nu_{a^+} = \nu_{a^+a} + \nu_{a^+s} + \nu_{a^+s^+} + \nu_{a^+e}$$
$$\nu_{s^+} = \nu_{s^+a} + \nu_{s^+s} + \nu_{s^+a^+} + \nu_{s^+e}$$
$$\nu_e = \nu_{ea} + \nu_{es} + \nu_{ea^+} + \nu_{es^+} \qquad (6)$$

Implicit Solution of the Momentum Equation

We have shown that the momentum equation for any species can be written in the form

$$\nu \vec{V} - \frac{q}{m}(\vec{V} \times \vec{B}) = \frac{\vec{F}}{m} \qquad (7)$$

66

Here, $\vec{V}$ is the velocity, m is the mass, q is the charge, ν is the total collision frequency and $\vec{F}$ is the force. Take now a coordinate system with its $\hat{z}$ axis aligned to the magnetic field direction $\vec{B}$. For any vector $\vec{A}$ we can write $\vec{A} = \vec{V}_{\perp} + \vec{V}_{\parallel}$

With the use of vector identities we can obtain the velocity components

$$\vec{V}_{\perp} = \frac{1}{qB}\frac{\kappa}{1+\kappa^2}\vec{F}_{\perp} + \frac{1}{qB}\frac{\kappa^2}{1+\kappa^2}\vec{F}_{\perp} \times \vec{B}$$

$$\vec{V}_{\parallel} = \frac{1}{m\nu}\vec{F}_{\parallel} \tag{8}$$

where Ω is the gyrofrequency defined as $\Omega = qB/m$ and $\kappa = \Omega/\nu$ is the ratio of the gyrofrequency to the total collision frequency.

Motion on the Perpendicular Plane

Electron Perpendicular Flow

For the perpendicular component of the electron velocity we can write

$$\vec{V}_{e\perp} = k_{Pe}\vec{F}_{e\perp} + k_{He}\vec{F}_{e\perp} \times \vec{b} \tag{9}$$

This expression can be further simplified by examining the magnitude of the collisionality ratio for electrons at altitudes between $150 - 600$ km. For both the ambient and the cloud conditions the collisionality ratio is very large i.e $\kappa_e \gg 1$. The Pedersen term in the perpendicular electron velocity can be neglected since it will be much smaller than the Hall term. Furthermore since we expect that for both ambient and cloud conditions $\left|\frac{\nu_{ei}}{\nu_{ie}}\right| \ll 1$ we can neglect all the contribution from the ion and neutral collisions as well as from gravity so that the velocity can be written finally as

$$\begin{bmatrix} V_{ex} \\ V_{ey} \end{bmatrix} = \begin{bmatrix} 0 & -\mu_H^e \\ \mu_H^e & 0 \end{bmatrix}\begin{bmatrix} E_x \\ E_y \end{bmatrix} - \begin{bmatrix} D_{Pe}^e & -D_{He}^e \\ D_{He}^e & D_{Pe}^e \end{bmatrix}\begin{bmatrix} \frac{1}{n_e}\frac{\partial n_e}{\partial x} \\ \frac{1}{n_e}\frac{\partial n_e}{\partial y} \end{bmatrix} \tag{10}$$

where $\mu_H^e = -\frac{1}{B}\frac{\kappa_e^2}{1+\kappa_e^2}$ is the electron Hall mobility (in C s kg) and $D_{eH} = -\frac{kT_e}{q_e B}\frac{\kappa_e^2}{1+\kappa_e^2}$ is the Hall electron diffusivity due to electron density gradients (in m^2/s).

Ion Perpendicular Flow

The solution of the system of the ion momentum equations yields the ion velocities. After some manipulation the perpendicular velocity of the ions $V_{t\perp}$ where $t = a^+, s^+$ can be written in the form

$$\begin{bmatrix} V_{tx} \\ V_{ty} \end{bmatrix} = \begin{bmatrix} \mu_P^t & -\mu_H^t \\ \mu_H^t & \mu_P^t \end{bmatrix}\begin{bmatrix} E_x \\ E_y \end{bmatrix}$$

$$\sum_{t=a^+,s^+} \left(-\begin{bmatrix} D_{tP}^t & -D_{tH}^t \\ D_{tH}^t & D_{tP}^t \end{bmatrix}\begin{bmatrix} \frac{1}{n_t}\frac{\partial n_t}{\partial x} \\ \frac{1}{n_t}\frac{\partial n_t}{\partial y} \end{bmatrix} \right)$$

$$+ \begin{bmatrix} W_{e^+ P}^t & -W_{e^+ H}^t \\ W_{e^+ H}^t & W_{e^+ P}^t \end{bmatrix}\begin{bmatrix} U_{ex} \\ U_{ey} \end{bmatrix}$$

$$+ \begin{bmatrix} W_{a^+ P}^t & -W_{a^+ H}^t \\ W_{a^+ H}^t & W_{a^+ P}^t \end{bmatrix}\begin{bmatrix} U_{ax} \\ U_{ay} \end{bmatrix}$$

$$+ \begin{bmatrix} \beta_P^t & -\beta_H^t \\ \beta_H^t & \beta_P^t \end{bmatrix}\begin{bmatrix} j_x \\ j_y \end{bmatrix} \tag{11}$$

The diffusion coefficients of ions a^+ associated with density gradients of a^+ are

$$D_{a^+ P}^{a^+} = \left[-m_{a^+}m_{s^+}\nu_{a^+s^+}\nu_{s^+a^+}k_{s^+P}\left(k_{a^+P}^2 + k_{a^+H}^2\right) + k_{a^+P}\right][kT_{a^+}]/C_{\perp} \tag{12}$$

$$D_{a^+ H}^{a^+} = \left[-m_{a^+}m_{s^+}\nu_{a^+s^+}\nu_{s^+a^+}k_{s^+H}\left(k_{a^+P}^2 + k_{a^+H}^2\right) - k_{a^+H}\right][kT_{a^+}]/C_{perp} \tag{13}$$

The denominator $C_{\perp}$ is given by

$$C_{\perp} = m_{s^+}^2 m_{a^+}^2 \nu_{s^+a^+}^2 \nu_{s^+a^+}^2 \left(k_{a^+P}^2 + k_{a^+H}^2\right)\left(k_{s^+P}^2 + k_{s^+H}^2\right)$$
$$+ 2m_{s^+}m_{a^+}\nu_{a^+s^+}\nu_{s^+a^+} + 1 \tag{14}$$

The diffusion coefficients of ions a^+ associated with density gradients of s^+ are

$$D_{s^+P}^{a^+} = \left[-m_{a^+}^2 m_{s^+}\nu_{a^+s^+}^2\nu_{s^+a^+}\left(k_{s^+P}^2 + k_{s^+H}^2\right)\right.$$
$$\left(k_{a^+P}^2 + k_{a^+H}^2\right) - m_{a^+}\nu_{a^+s^+}\left(k_{a^+H}k_{s^+H} - k_{a^+P}k_{s^+P}\right)$$
$$(kT_{s^+})/C_{\perp} \tag{15}$$

$$D_{s^+H}^{a^+} = \left[-m_{a^+}\nu_{a^+s^+}\left(k_{a^+P}k_{s^+H} + k_{s^+P}k_{a^+H}\right)\right]$$
$$(kT_{s^+})/C_{\perp} \tag{16}$$

The diffusion coefficients of ions a^+ associated with density gradients of electrons are

$$D_{eP}^{a^+} = \left(\left[m_{a^+}^2 m_{s^+}\nu_{a^+s^+}\nu_{s^+a^+}\nu_{a^+e}k_{s^+H}\left(k_{a^+P}^2 + k_{a^+H}^2\right)\right.\right.$$
$$+ m_{a^+}m_{s^+}\nu_{a^+s^+}\nu_{s^+e}\left(k_{s^+P}k_{a^+H} + k_{a^+P}k_{s^+H}\right)$$
$$+ m_{a^+}\nu_{a^+e}k_{a^+H}\left(-\frac{1}{B}\frac{\kappa_e^2}{1+\kappa_e^2}\frac{kT_e}{j_e}\right)\right] C_{\perp} \tag{17}$$

$$D_{eH}^{a^+} = \left(\left[-m_{a^+}^2 m_{s^+}\nu_{a^+s^+}\nu_{a^+e}\nu_{s^+a^+}k_{s^+P}\left(k_{a^+P}^2 + k_{a^+H}^2\right)\right.\right.$$
$$- m_{a^+}m_{s^+}\nu_{s^+a^+}\nu_{a^+e}\left(k_{s^+H}k_{a^+H} - k_{a^+P}k_{s^+P}\right)$$
$$- m_{a^+}^2 m_{s^+}\nu_{a^+s^+}^2\nu_{s^+a^+}\nu_{a^+e}\left(k_{s^+P}^2 + k_{s^+H}^2\right)\left(k_{a^+P}^2 + k_{a^+H}^2\right)$$
$$+ m_{a^+}\nu_{a^+e}k_{a^+P}\left(-\frac{1}{B}\frac{\kappa_e^2}{1+\kappa_e^2}\frac{kT_e}{j_e}\right)\right] C_{\perp} \tag{18}$$

67

The diffusion coefficients of ions s^+ associated with density gradients of s^+ are

$$D_{s^+P}^{s^*} = \left[-m_{a^+} m_{s^+} \nu_{a^+s^+} \nu_{s^+a^+} k_{a^+P} \left(k_{s^+P}^2 + k_{s^+H}^2 \right) \right. $$
$$\left. + k_{s^+P} \right] (kT_{s^+}) / C_\perp \quad (19)$$

$$D_{s^+H}^{s^*} = \left[-m_{a^+} m_{s^+} \nu_{a^+s^+} \nu_{s^+a^+} k_{a^+H} \left(k_{s^+P}^2 + k_{s^+H}^2 \right) \right. $$
$$\left. - k_{s^+H} \right] (kT_{s^+}) / C_\perp \quad (20)$$

The diffusion coefficients of ions s^+ associated with density gradients of a^+ are

$$D_{a^+P}^{s^*} = \left[-m_{a^+} m_{s^+}^2 \nu_{a^+s^+} \nu_{s^+a^+}^2 \left(k_{s^+P}^2 + k_{s^+H}^2 \right) \right. $$
$$\left(k_{a^+P}^2 + k_{a^+H}^2 \right) - m_{s^+} \nu_{s^+a^+} \left(k_{a^+H} k_{s^+H} - k_{a^+P} k_{s^+P} \right) \right]$$
$$(kT_{a^+}) / C_\perp \quad (21)$$

$$D_{a^+H}^{s^*} = \left[-m_{s^+} \nu_{s^+a^+} \left(k_{a^+P} k_{s^+H} + k_{s^+P} k_{a^+H} \right) \right]$$
$$(kT_{a^+}) / C_\perp \quad (22)$$

The diffusion coefficients of ions s^+ associated with density gradients of electrons are

$$D_{eP}^{s^*} = \left\{ \left[m_{a^+} m_{s^+}^2 \nu_{a^+s^+} \nu_{s^+a^+} \nu_{s^+e} k_{a^+H} \left(k_{s^+P}^2 + k_{s^+H}^2 \right) \right. \right. $$
$$+ m_{a^+} m_{s^+} \nu_{s^+a^+} \nu_{a^+e} \left(k_{s^+P} k_{a^+H} + k_{a^+P} k_{s^+H} \right)$$
$$\left. + m_{s^+} \nu_{s^+e} k_{s^+H} \right] \left(-\frac{1}{B} \frac{\kappa_e^2}{1 + \kappa_e^2} \frac{kT_e}{q_e} \right) \right\} C \quad (23)$$

$$D_{eH}^{s^*} = \left\{ \left[-m_{a^+} m_{s^+}^2 \nu_{a^+s^+} \nu_{s^+a^+} \nu_{s^+e} k_{a^+P} \left(k_{s^+P}^2 + k_{s^+H}^2 \right) \right. \right. $$
$$-m_{a^+} m_{s^+} \nu_{s^+a^+} \nu_{a^+e} \left(k_{s^+H} k_{a^+H} - k_{a^+P} k_{a^+P} \right)$$
$$-m_{a^+}^2 m_{s^+}^2 \nu_{a^+s^+} \nu_{s^+a^+}^2 \nu_{a^+e} \left(k_{s^+P}^2 + k_{s^+H}^2 \right) \left(k_{a^+P}^2 + k_{a^+H}^2 \right)$$
$$\left. + m_{s^+} \nu_{s^+e} k_{s^+P} \right] \left(-\frac{1}{B} \frac{\kappa_e^2}{1 + \kappa_e^2} \frac{kT_e}{q_e} \right) \right\} / C_\perp \quad (24)$$

A careful examination of the obtained transport coefficients reveals very important and simple relations among them. First, a generalized *Einstein* relation holds between the mobility and the diffusion coefficients

$$\mu_P^t = D_{s^+P}^t \frac{q_{s^+}}{kT_{s^+}} + D_{a^+P}^t \frac{q_{a^+}}{kT_{a^+}} + D_{eP}^t \frac{q_e}{kT_e} \quad (25)$$

$$\mu_H^t = D_{s^+H}^t \frac{q_{s^+}}{kT_{s^+}} + D_{a^+H}^t \frac{q_{a^+}}{kT_{a^+}} + D_{eH}^t \frac{q_e}{kT_e} \quad (26)$$

The ambient neutral wind transport coefficients relate with the diffusion coefficients as follows

$$W_{aP}^t = D_{s^+P}^t \frac{m_{s^+} \nu_{s^+a}}{kT_{s^+}} + D_{a^+P}^t \frac{m_{a^+} \nu_{a^+a}}{kT_{a^+}} \quad (27)$$

$$W_{aH}^t = D_{s^+H}^t \frac{m_{s^+} \nu_{s^+a}}{kT_{s^+}} + D_{a^+H}^t \frac{m_{a^+} \nu_{a^+a}}{kT_{a^+}} \quad (28)$$

and similar expressions hold between the contaminant neutral wind transport coefficients and the diffusion coefficients

$$W_{sP}^t = D_{s^+P}^t \frac{m_{s^+} \nu_{s^+c}}{kT_{s^+}} + D_{a^+P}^t \frac{m_{a^+} \nu_{a^+c}}{kT_{a^+}} \quad (29)$$

$$W_{sH}^t = D_{s^+H}^t \frac{m_{s^+} \nu_{s^+c}}{kT_{s^+}} + D_{a^+H}^t \frac{m_{a^+} \nu_{a^+c}}{kT_{a^+}} \quad (30)$$

Finally the following relationships hold between the diffusion coefficients and the coefficients for gravity

$$\beta_P^t = D_{s^+P}^t \frac{m_{s^+}}{kT_{s^+}} + D_{a^+P}^t \frac{m_{a^+}}{kT_{a^+}} + D_{eP}^t \frac{m_e}{kT_e} \quad (31)$$

$$\beta_H^t = D_{s^+H}^t \frac{m_{s^+}}{kT_{s^+}} + D_{a^+H}^t \frac{m_{a^+}}{kT_{a^+}} + D_{eH}^t \frac{m_e}{kT_e} \quad (32)$$

Parallel Plasma Motion

The parallel velocity for any species t is given in the implicit solution of the momentum equation in the form

$$\vec{V}_{t\parallel} = \frac{1}{m_t \nu_t} \vec{F}_{t\parallel} \quad (33)$$

From the parallel momentum equations we can write the solution for the parallel velocity of a species $t = a^+, s^+, e$ in the form

$$\vec{V}_{t\parallel} = \mu_\parallel^t \vec{E}_\parallel - D_{a^+\parallel}^t \frac{\nabla_\parallel n_{a^+}}{n_{a^+}} - D_{s^+\parallel}^t \frac{\nabla_\parallel n_{s^+}}{n_{s^+}} - D_{e\parallel}^t \frac{\nabla_\parallel n_e}{n_e}$$
$$+ W_{a\parallel}^t \vec{U}_{a\parallel} + W_{s\parallel}^t \vec{U}_{s\parallel} + \beta_\parallel^t \vec{g}_\parallel \quad (34)$$

The parallel diffusion coefficients of ambient ions due to density gradients of a^+, s^+ and e are

$$D_{a^+\parallel}^{a^+} = \frac{\nu_e \nu_{s^+} - \nu_{es^+} \nu_{s^+e}}{C_\parallel} \frac{kT_{a^+}}{m_{a^+}}$$

$$D_{s^+\parallel}^{a^+} = \frac{\nu_e \nu_{a^+s^+} + \nu_{s^+e} \nu_{a^+e}}{C_\parallel} \frac{kT_{a^+}}{m_{a^+}}$$

$$D_{e\parallel}^{a^+} = \frac{\nu_{a^+s^+} \nu_{s^+e} + \nu_{a^+e} \nu_{s^+}}{C_\parallel} \frac{kT_e}{m_e} \quad (35)$$

The denominator $C_\parallel$ is given by

$$C_\parallel = \nu_e \nu_{a^+} \nu_{s^+} - \nu_e \nu_{a^+s^+} \nu_{s^+a^+} - \nu_{ea^+} \nu_{a^+e} \nu_{s^+}$$
$$- \nu_{ea^+} \nu_{a^+s^+} \nu_{s^+e} - \nu_{es^+} \nu_{s^+e} \nu_{a^+} - \nu_{es^+} \nu_{a^+e} \nu_{s^+a^+} \quad (36)$$

The parallel diffusion coefficients of the contaminant ions due to density gradients in ambient, contaminant and electrons are

$$D_{a^+\parallel}^{s^+} = \frac{\nu_e \nu_{s^+a^+} + \nu_{sa^+} \nu_{s^+e}}{C_\parallel} \frac{kT_{a^+}}{m_{a^+}}$$

$$D_{s^+\parallel}^{s^+} = \frac{\nu_e \nu_{a^+} - \nu_{ea^+} \nu_{a^+e}}{C_\parallel} \frac{kT_{a^+}}{m_{a^+}}$$

$$D_{e}^{s^+} = \frac{\nu_{s^+a^+} \nu_{a^+e} + \nu_{s^+e} \nu_{a^+}}{C_\parallel} \frac{kT_e}{m_e} \quad (37)$$

The parallel diffusion coefficients of the electrons due to density gradients in ambient and contaminant ions and electrons are

$$D_{a^+\parallel}^e = \frac{\nu_{ea^+} \nu_{s^+} + \nu_{es^+} \nu_{s^+a^+}}{C_\parallel} \frac{kT_{a^+}}{m_{a^+}}$$

$$D_{s^+\parallel}^e = \frac{\nu_{es^+} \nu_{a^+} + \nu_{ea^+} \nu_{a^+s^+}}{C_\parallel} \frac{kT_{a^+}}{m_{a^+}}$$

$$D_{e}^e = \frac{\nu_{a^+} \nu_{s^+} + \nu_{a^+s^+} \nu_{s^+a^+}}{C_\parallel} \frac{kT_e}{m_e} \quad (38)$$

68

As in the case of the perpendicular transport coefficients, simple relations hold between the parallel transport coefficients as well. A generalized *Einstein* relation holds between the parallel mobility and the parallel diffusion coefficients

$$\mu_{\parallel}^t = D_{a^+\parallel}^t \frac{q_{a^+}}{kT_{a^+}} + D_{s^+\parallel}^t \frac{q_{s^+}}{kT_{s^+}} + D_{e\parallel}^t \frac{q_e}{kT_e} \qquad (39)$$

Also, the following relation holds between the diffusion coefficient and the ambient and contaminant neutral wind coefficients

$$W_{a}^t = D_{a^+\parallel}^t \frac{m_{a^+}\nu_{a^+a}}{kT_{a^+}} + D_{s^+\parallel}^t \frac{m_{s^+}\nu_{s^+a}}{kT_{s^+}} + D_{e\parallel}^t \frac{m_e\nu_{ea}}{kT_e}$$

$$W_{s}^t = D_{a^+\parallel}^t \frac{m_{a^+}\nu_{a^+s}}{kT_{a^+}} + D_{s^+\parallel}^t \frac{m_{s^+}\nu_{s^+s}}{kT_{s^+}} + D_{e\parallel}^t \frac{m_e\nu_{es}}{kT_e} \qquad (40)$$

Finally, the diffusion coefficients and the gravitaional drift coefficient relate as follows

$$\beta_{\parallel}^t = D_{a^+\parallel}^t \frac{m_{a^+}}{kT_{a^+}} + D_{s^+\parallel}^t \frac{m_{s^+}}{kT_{s^+}} + D_{e\parallel}^t \frac{m_e}{kT_e} \qquad (41)$$

Electric Currents

The current balance within the plasma cloud is the key to the electrodynamical interactions taking place. The current closure between the plasma cloud and the ambient ionosphere will determine the self-consistent potential of the cloud and consequently will determine the dynamical behavior and evolution of the cloud. As a first approach to the problem we will not include polarization and Alfvén currents in the model. The current balance in this model will determined by direct currents , diamagnetic (or diffusion) currents, currents due to both ambient and neutral winds and finally currents due gravitational drifts.

The current is given by direct substitution of the velocities of the plasma species Eqs. (11, 10,77) into the definition of the current density.

$$\vec{J} = n_{a^+}q_{a^+}\vec{V}_{a^+} + n_{s^+}q_{s^+}\vec{V}_{s^+} + n_eq_e\vec{V}_{e\perp} \qquad (42)$$

We can write for the total current density

$$\vec{J} = \vec{J}^{dir} + \vec{J}_{s^+}^{dif} + \vec{J}_{a^+}^{dif} + \vec{J}_e^{dif} + \vec{J}_s^{new} + \vec{J}_a^{new} + \vec{J}^{gra} \qquad (43)$$

where we have taken into account the direct current, the diffusion current due to density gradients of the source ions, the ambient ions, the electrons and the current due to the gravitational field.

The direct total current density is given by

$$\begin{bmatrix} J_x^{dir} \\ J_y^{dir} \\ J_{\parallel}^{dir} \end{bmatrix} = \begin{bmatrix} \sigma_P & -\sigma_H & 0 \\ \sigma_H & \sigma_P & 0 \\ 0 & 0 & \sigma_{\parallel} \end{bmatrix} \begin{bmatrix} E_x \\ E_y \\ E_{\parallel} \end{bmatrix}$$

$$(44)$$

Here, we have defined the total direct conductivities in the Pedersen, Hall and parallel directions, taking into account all the plasma species. They are give by

$$\sigma_P = \sigma_P^{s^+} + \sigma_P^{a^+}$$

$$\sigma_H = \sigma_H^{s^+} + \sigma_H^{a^+} + \sigma_H^e$$

$$\sigma_{\parallel} = \sigma_{\parallel}^{s^+} + \sigma_{\parallel}^{a^+} + \sigma^e \qquad (45)$$

Note also that there is no electron current density in the Pedersen direction, since we assumed that electrons mainly exhibit drifts in the Hall direction.

The total diffusion current density due to gradients of species $t = a^+, s^+, e$ is given by

$$\begin{bmatrix} J_{t,x}^{dif} \\ J_{t,y}^{dif} \\ J_{t,\parallel}^{dif} \end{bmatrix} = -e \begin{bmatrix} D_{tP} & -D_{tH} & 0 \\ D_{tH} & D_{tP} & 0 \\ 0 & 0 & D_{t\parallel} \end{bmatrix} \begin{bmatrix} \frac{\partial n_t}{\partial x} \\ \frac{\partial n_t}{\partial y} \\ \frac{\partial n_t}{\partial z} \end{bmatrix} \qquad (46)$$

where the total diffusion coefficient tensor due to ions s^+ is

$$D_{s^+P} = \frac{n_{s^+}}{n_{s^+}}D_{s^+P}^{s^+} + \frac{n_{a^+}}{n_{s^+}}D_{s^+P}^{a^+}$$

$$D_{s^+P} = \frac{n_{s^+}}{n_{s^+}}D_{s^+H}^{s^+} + \frac{n_{a^+}}{n_{s^+}}D_{s^+H}^{a^+}$$

$$D_{s^+\parallel} = \frac{n_{s^+}}{n_{s^+}}D_{s^+\parallel}^{s^+} + \frac{n_{a^+}}{n_{s^+}}D_{s^+\parallel}^{a^+} - \frac{n_e}{n_{s^+}}D_{s^+\parallel}^e \qquad (47)$$

The total diffusion coefficient tensor due to ions a^+ is

$$D_{a^+P} = \frac{n_{s^+}}{n_{a^+}}D_{a^+P}^{s^+} + \frac{n_{a^+}}{n_{a^+}}D_{a^+P}^{a^+}$$

$$D_{a^+P} = \frac{n_{s^+}}{n_{a^+}}D_{a^+H}^{s^+} + \frac{n_{a^+}}{n_{a^+}}D_{a^+H}^{a^+}$$

$$D_{a^+\parallel} = \frac{n_{s^+}}{n_{a^+}}D_{a^+\parallel}^{s^+} + \frac{n_{a^+}}{n_{a^+}}D_{a^+\parallel}^{a^+} - \frac{n_e}{n_{a^+}}D_{a^+\parallel}^e \qquad (48)$$

The total diffusion coefficient tensor due to electrons

$$D_{eP} = \frac{n_{s^+}}{n_e}D_{eP}^{s^+} + \frac{n_{a^+}}{n_e}D_{eP}^{a^+}$$

$$D_{eP} = \frac{n_{s^+}}{n_e}D_{eH}^{s^+} + \frac{n_{a^+}}{n_e}D_{eH}^{a^+} + \frac{n_e}{n_e}D_{eH}^e$$

$$D_{e\parallel} = \frac{n_{s^+}}{n_e}D_{e\parallel}^{s^+} + \frac{n_{a^+}}{n_e}D_{e\parallel}^{a^+} - \frac{n_e}{n_e}D_{e\parallel}^e \qquad (49)$$

The current density due to the contaminant (source) neutral wind is

$$\begin{bmatrix} J_{s,x}^{new} \\ J_{s,y}^{new} \\ J_{s,\parallel}^{new} \end{bmatrix} = e \begin{bmatrix} W_{sP} & -W_{sH} & 0 \\ W_{sH} & W_{sP} & 0 \\ 0 & 0 & W_{s\parallel} \end{bmatrix} \begin{bmatrix} U_{sx} \\ U_{sy} \\ U_{s\parallel} \end{bmatrix} \qquad (50)$$

where

$$W_{sP} = n_{s^+}W_{sP}^{s^+} + n_{a^+}W_{sP}^{a^+}$$

$$W_{sP} = n_{s^+}W_{sP}^{s^+} + n_{a^+}W_{sH}^{a^+}$$

$$W_{s\parallel} = n_{s^+}W_{s\parallel}^{s^+} + n_{a^+}W_{s\parallel}^{a^+} - n_eW_{s\parallel}^e \qquad (51)$$

69

The current density due to the ambient neutral wind is

$$
\begin{bmatrix} j_{ax}^{neu} \\ j_{ay}^{neu} \\ j_{a\parallel}^{neu} \end{bmatrix} = e \begin{bmatrix} W_{aP} & -W_{aH} & 0 \\ W_{aH} & W_{aP} & 0 \\ 0 & 0 & W_{a\parallel} \end{bmatrix} \begin{bmatrix} U_{ax} \\ U_{ay} \\ U_{a\parallel} \end{bmatrix} \quad (52)
$$

where

$$
W_{aP} = n_{a+} W_{aP}^{a+} + n_{a+} W_{aP}^{a+}
$$

$$
W_{aH} = n_{a+} W_{aH}^{a+} - n_{a+} W_{aH}^{a+}
$$

$$
W_{a\parallel} = n_{a+} W_{a\parallel}^{a+} + n_{a+} W_{a\parallel}^{a+} - n_e W_{a\parallel}^{a} \quad (53)
$$

Finally, the total current density due to gravitational drifts is

$$
\begin{bmatrix} j_x^{gra} \\ j_y^{gra} \\ j_\parallel^{gra} \end{bmatrix} = e \begin{bmatrix} \beta_{aP} & -\beta_{aH} & 0 \\ \beta_{aH} & \beta_{aP} & 0 \\ 0 & 0 & \beta_{a\parallel} \end{bmatrix} \begin{bmatrix} g_x \\ g_y \\ g_\parallel \end{bmatrix} \quad (54)
$$

Equation for the Current Balance

We need now to derive an equation for the potential within the plasma cloud . We make here the assumption that the plasma is quasineutral, that is,

$$
n_{a+} q_{a+} + n_{a+} q_{a+} = n_e q_e \quad (55)
$$

This assumption implies that the Debye length is small compared with the length scales of interest. Also, we assume that the electric fields are electrostatic, that is $\vec{E} = -\nabla\phi$, where ϕ is a scalar potential. This in turn implies that $\partial \vec{B}/\partial t = 0$ which means that the self-consistent plasma currents produce negligible variations in the magnetic field $\vec{B}$. Charge conservation then implies

$$
\nabla \cdot \vec{J} = 0 \quad (56)
$$

In the analysis before we denoted by $\vec{E}$ the self-consistent electric field. We take now the electric field to be

$$
\vec{E}(x,y,z) = \vec{E}_o + \vec{\epsilon} + \vec{E}_m \quad (57)
$$

Here $\vec{E}_o$ is the ambient self-consistent electric field, $\vec{\epsilon}$ is the self-consistent potential due to the presence of the plasma perturbation and $\vec{E}_m$ is the motional electric field used to account for any change of reference frame that we might consider. The equation for charge conservation is now

$$
\nabla \cdot \vec{J}^{dir} + \nabla \cdot \vec{J}_{a+}^{dif} + \nabla \cdot \vec{J}_{a+}^{dif} + \nabla \cdot \vec{J}_{a+}^{dif} + \nabla \cdot \vec{J}_{a}^{dif}
$$
$$
+ \nabla \cdot \vec{J}_a^{neu} + \nabla \cdot \vec{J}_a^{neu} + \nabla \cdot \vec{J}^{gra} = 0 \quad (58)
$$

If we assume that the electric fields are electrostatic then the perturbation potential is ϕ such that $\vec{\epsilon} = -\nabla\phi$. We will concentrate in the divergence of the direct current, since this is the term which will give the differential dependence of the

potential ϕ It is important to recast the above equation in a form of a steady-state advection-diffusion equation for the potential ϕ as follows

$$
\nabla \cdot \vec{J}^{dir} = \frac{\partial}{\partial x}\left(\sigma_P \frac{\partial \phi}{\partial x}\right) + \frac{\partial}{\partial y}\left(\sigma_P \frac{\partial \phi}{\partial y}\right) + \frac{\partial}{\partial z}\left(\sigma_\parallel \frac{\partial \phi}{\partial z}\right)
$$
$$
+ \frac{\partial \sigma_H}{\partial y}\frac{\partial \phi}{\partial z} - \frac{\partial \sigma_H}{\partial x}\frac{\partial \phi}{\partial y}
$$
$$
+ \left(\frac{\partial \sigma_P}{\partial x} + \frac{\partial \sigma_z}{\partial y}\right) E_x + \left(\frac{\partial \sigma_P}{\partial y} - \frac{\partial \sigma_H}{\partial x}\right) E_y + \frac{\partial \sigma_\parallel}{\partial z} E_z
$$
$$
+ \sigma_P\left(\frac{\partial E_x}{\partial x} + \frac{\partial E_y}{\partial y}\right) + \sigma_H\left(\frac{\partial E_x}{\partial y} - \frac{\partial E_y}{\partial x}\right) + \sigma_\parallel \frac{\partial E_z}{\partial z} \quad (59)
$$

where, $\vec{E} = \vec{E}_o + \vec{E}_m$. From inspection we see that all the terms which are not ϕ dependent can be regarded as source terms. Note also that it is only the direct (conductive) current which depends on the potential. Thus, we can consider the divergence of all the other current densities as source terms, in an non-self ajoint elliptic equation for the potential. This can be written as

$$
\nabla \cdot \vec{J} = \frac{\partial}{\partial x}\left(\sigma_P \frac{\partial \phi}{\partial x}\right) + \frac{\partial}{\partial y}\left(\sigma_P \frac{\partial \phi}{\partial y}\right) + \frac{\partial}{\partial z}\left(\sigma_\parallel \frac{\partial \phi}{\partial z}\right)
$$
$$
+ \frac{\partial \sigma_H}{\partial y}\frac{\partial \phi}{\partial z} - \frac{\partial \sigma_H}{\partial x}\frac{\partial \phi}{\partial y} + S = 0 \quad (60)
$$

where $\sigma_P, \sigma_H, \sigma_Z$ and S are functions of x, y, z.

Current closure - Boundary Conditions

To solve the equation for the potential one must supply appropriate boundary conditions. In turns one needs to discuss a current closure model . In the beginning we will describe a closure model which is applicable to the high latitude ionospher outside of the equatorial region. The density distribution of the ambient ionosphere is shown in Figure 2. The conductivities calculated from our model are shown in Figure 3. For comparison we calculated conductivities based on the formulas and the ambient conditions given in *Haerendel et al.*[1967] We can see that the conductivities derived from our model compare well with those presented in Table 1, the differences are due to the adopted model
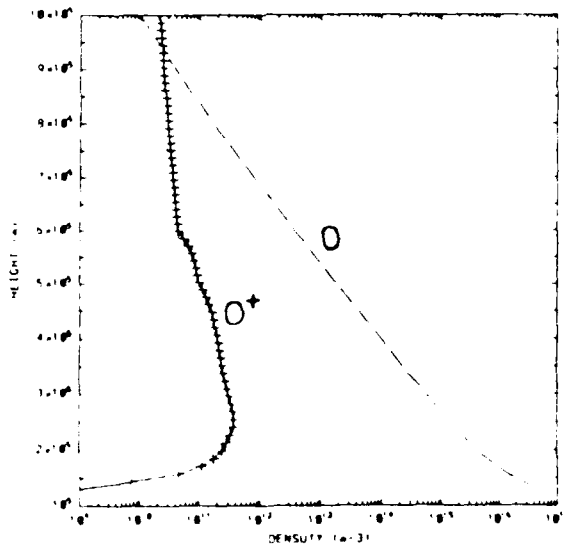
Height	90 km	160 km	160 km	500 km
n	1.5×10^{10}	3×10^{10}	5×10^{10}	2×10^{11}
σ_P	6.4×10^{-6}	6.8×10^{-5}	5×10^{-7}	2×10^{-7}
σ_H	6.8×10^{-6}	2.7×10^{-5}	~ 0	~ 0
$\sigma_\parallel$	2.8×10^{-2}	9.5×10^{-1}	17.9	5.7×10^2

Table 1: Ambient conductivities (in S/m) calculated from *Haerendel et. al*
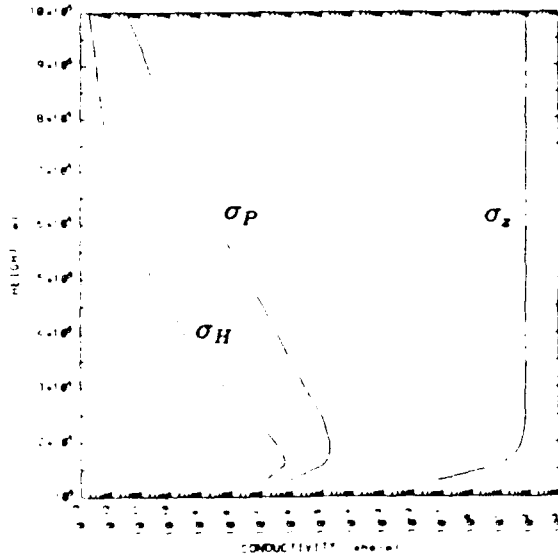
70

Figure 2: The ambient ionospheric densities (m^{-3})

Figure 3: The ambient ionospheric conductivities (in S/m)

ionosphere and the models for collision frequencies. From Figure 3 it is shown that that the maximum of the tranverse conductivities occurs at ~ 180 km. Above and bellow that altitude both Pedersen and Hall conductivities decrease in magnitude significantly. The parallel conductivity increases with altitude and is between 5 and 12 orders higher than the tranverse conductivities. In high latitudes the magnetic field lines will go through the magnetosphere before reaching the conjugate ionosphere. Thus, one can consider that the upper F-region to be a noncunducting boundary since in effect is collisionless. The lower E-region can be also regarded as an insulator. Given that, one can bound the ionospheric plasma between two insulators located at heights h_L and

h_U respectively.

For the disturbed ionosphere we assume that at the upper and lower boundaries the flux will be mainly in the longitudinal direction, and that the electron flux will be equal to the ambient ion flux.

$$\Gamma_{\parallel e} = \Gamma_{\parallel a+}$$
$$\Gamma_{\parallel e+} = 0 \quad z = h_L, h_U \tag{61}$$

If we substitude for the flux from equations (11, 10,34) we can write

$$(\sigma_{e\parallel} - \sigma_{a+\parallel})\frac{\partial \Phi}{\partial z} = -e(D_{a+\parallel} - D_{e\parallel})\frac{\partial n_{a+}}{\partial z} \tag{62}$$

But from the definition of the electric field it will be

$$\Phi(x,y,z) = \Phi_o + \phi(x,y,z) \tag{63}$$

In the undisturbed ionosphere the equality of longitudinal fluxes holds as well so that after manipulating the above equations one gets

$$\frac{\partial \phi}{\partial z} = 0 \quad z = h_L, h_U \tag{64}$$

In other words, we impose the condition that no current will flow peprendicular to the bounding insulators. However, for the equatorial regions the closure occurs between the two conjugate $E-$regions of the ionosphere and the magnetic field lines which cross the perturbation do not neccecerely pass through the magnetosphere; a closure model appliacable to this case is under development.

For the tranverse direction we require that

$$\phi(x,y,z) = 0 \quad (x,y) \rightarrow \infty \tag{65}$$

Numerical Solution of the potential

The equation for the potential (60) is a non-self adjoint elliptic equation, three dimensional, with highly dissimilar coefficients. It is this inherent difficulty that prohibited the solution of the fully three- dimensional problem in the past, and resulted in the well known two- dimensional theories. The difficulties can be revealed further if one recasts the potential equation in the form of a steady-state advection diffusion equation. From a physical and consequently numerical point of view one has to deal with time scales wich are very disimilar, in the the tranverse and parallel directions. One more source of difficulty lies in the Neumman condition which s applied in the parallel direction, which is the direction of the highest conductivity, thus making convergence very difficult to achieve.

Discrete Potential Equation

We descritized the potential equation on a rectangular grid with Δx, Δy and Δz being the grid sizes in the x, y and

71

z directions respectively. In the discrete space the indices i, j, k refer to the computational coordinates, aligned with the x, y and z directions and such that $z_i = i\Delta z$, $y_j = j\Delta y$ and $z_k = k\Delta z$. For a grid point (i, j, k) as shown in Figure (4) the following finite difference operator was used
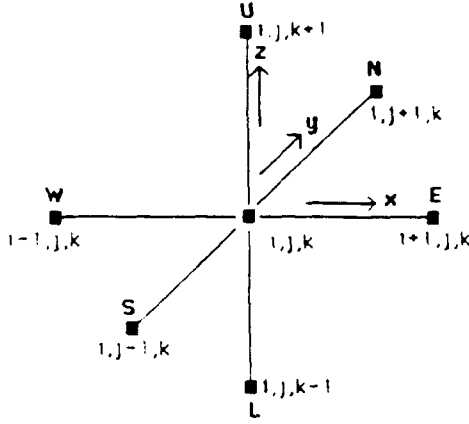

Figure 4: Grid geometry

$$\frac{\partial}{\partial z}\left(A\frac{\partial F}{\partial z}\right) = \frac{A_{i+\frac{1}{2},j,k}(F_{i+1,j,k} - F_{i,j,k})}{\Delta z^2} - \frac{A_{i-\frac{1}{2},j,k}(F_{i,j,k} - F_{i-1,j,k})}{\Delta z^2} \quad (66)$$

Both A and F are functions of x, y, z. The quantities at the interfaces of a cell is defined as

$$A_{i+1/2,j,k} = \frac{A_{i+1,j,k} + A_{i,j,k}}{2} \quad (67)$$

Similar operators applied in the j and k directions. Using the above and expanding in all three directions the finite difference equation for the potential $\phi_{i,j,k}$ at the grid point i, j, k can be written as

$$\phi_{i+1,j,k}\left[\frac{\sigma^P_{i+\frac{1}{2},j,k}}{\Delta z^2} + \frac{\frac{\partial \sigma^H}{\partial y}}{2\Delta z}\right]$$

$$+\phi_{i-1,j,k}\left[\frac{\sigma^P_{i-\frac{1}{2},j,k}}{\Delta z^2} - \frac{\frac{\partial \sigma^H}{\partial y}}{2\Delta z}\right]$$

$$-\phi_{i,j-1,k}\left[\frac{\sigma^P_{i,j+\frac{1}{2},k}}{\Delta y^2} - \frac{\frac{\partial \sigma^H}{\partial z}}{2\Delta y}\right]$$

$$+\phi_{i,j-1,k}\left[\frac{\sigma^P_{i,j-\frac{1}{2},k}}{\Delta y^2} + \frac{\frac{\partial \sigma^H}{\partial z}}{2\Delta y}\right]$$

$$+\phi_{i,j,k+1}\left[\frac{\sigma^t_{i,j,k+\frac{1}{2}}}{\Delta z^2}\right] + \phi_{i,j,k-1}\left[\frac{\sigma^t_{i,j,k-\frac{1}{2}}}{\Delta z^2}\right]$$

$$+\phi_{i,j,k}\left(-\frac{\sigma^P_{i+\frac{1}{2},j,k}}{\Delta z^2} - \frac{\sigma^P_{i-\frac{1}{2},j,k}}{\Delta z^2} - \frac{\sigma^H_{i,j+\frac{1}{2},k}}{\Delta y^2} - \frac{\sigma^H_{i,j-\frac{1}{2},k}}{\Delta y^2}\right.$$

$$\left.\left. -\frac{\sigma^z_{i,j,k+\frac{1}{2}}}{\Delta z^2} - \frac{\sigma^z_{i,j,k-\frac{1}{2}}}{\Delta z^2}\right) = S_{i,j,k} \quad (68)\right.$$

where $S_{i,j,k}$ is the discrete source term obtained through the finite difference of all the source terms in the potential equation. If we work on a grid with nx, ny and nz grid points in the x, y and z direction respectively, applying the above discretization in all the interior grid points we end up with a matrix equation of the form

$$[A_{lm}]\{\phi_p\} = \{S_p\} \quad (69)$$

The subscript p refers to a natural ordering which orders the three dimensional array into a one dimensional vector given by the transformation

$$\phi_{i,j,k} \to \phi_p$$

$$p = (k - 2)(nx - 2)(nz - 2) + (j - 2)(nz - 2) + (i - 1) \quad (70)$$

Consequently l and m of the two-dimensional array denotes the row and column destination of the elements envolved in the finite difference equation at each grid point. The matrix $[A_{lm}]$ is an $N \times N$ sparse, where $N = (nx - 2) \times (ny - 2) \times (nz - 2)$, with only seven nonzero elements in each row. In order to make the problem computationaly tractable we developed a special storage system. We denote as the East,West,North and South grid points as shown in Figure 4. Then for each grid point i, j, k we store the seven nonzero components along with the pointer denoting the column destination in the uncompressed array A_{lm}. In doing so the matrix is compressed into an $N \times 7$ matrix resulting thus in $O(N)$ saving in storage requirements. Solution then of the matrix equation was obtained by a conjugate gradient algorithm, after applying suitable preconditioning on the original matrix.

The unperturbed electric fields

To obtain the equilibrium electric fields we solve equation (68). The problem is to find the potential Φ_o such that the ambient density distribution is in steady state. An approximation to the unperturbed electric field can be obtained by assuming steady state ion and electron continuity equations. With the absence of source and sink terms for the ions and the electrons it is required that

$$\nabla \cdot \vec{\Gamma}_i = \nabla \cdot \vec{\Gamma}_e = 0 \quad (71)$$

If we neglect the ambient neutral wind and gravity and under the assumption that there is no shear in the perpendicular electric field, the above relation becomes

$$\nabla \cdot \vec{\Gamma}_i = \frac{\partial}{\partial z}\left(n\mu_\parallel^+ E_\parallel\right) - \frac{\partial}{\partial z}\left[\left(D^+_{a,\parallel} - D^+_{e,\parallel}\right)\frac{\partial n}{\partial z}\right]$$

$$\nabla \cdot \vec{\Gamma}_e = \frac{\partial}{\partial z}\left(n\mu_\parallel^- E_\parallel\right) - \frac{\partial}{\partial z}\left[\left(D^-_{e,\parallel} + D^-_{a,\parallel}\right)\frac{\partial n}{\partial z}\right] \quad (72)$$

With some manipulation and applying the condition of equal fluxes of ions and electrons at the boundaries we get

$$E_{o\parallel} = \frac{D_e - D_i}{n(\mu_\parallel^+ - \mu_\parallel^-)}\frac{\partial n}{\partial z} \quad (73)$$

72

The numerical solution is shown in Figure 5 in comparison with the analytic Boltzman potential derived from Equation .
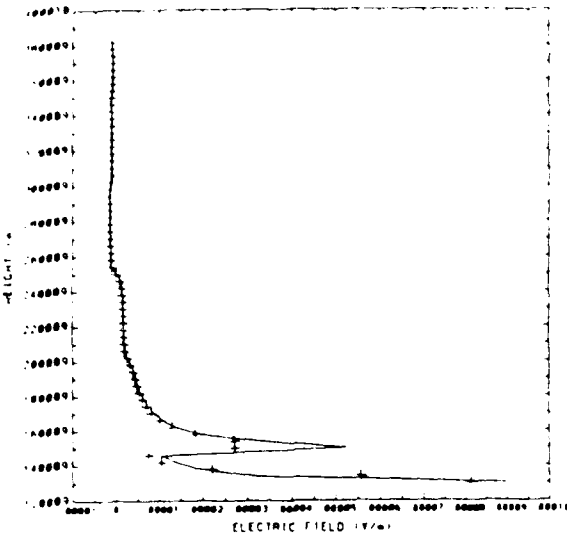

Figure 5: Electric field obtained from the numerical solution (solid line) and the analytical Boltzman potential (symbols)

Neutral Cloud Model-Initial Conditions

In most cases of artificial ion clouds a neutral cloud in present. It is beyond the scope of this study to model completely the neutral cloud. Instead we assume that the basic processes is self-diffusion of the neutrals with losses due to charge exchange reaction. We also assume that the neutral can be described initially by a gaussian profile given by

$$n_e(r, t = 0) = n_{eo} \exp\left[-\left(\frac{x^2 + y^2}{r_\perp^2}\right)\right] \exp\left[-\left(\frac{z^2}{r_\parallel^2}\right)\right] \quad (74)$$

where x, y, z are the distance from the point of release and n_{eo} is the density at the center of the cloud. With this model the mass of the released material is given by $M_e =$ $\pi^{3/2} n_{eo} r_\perp^2 r_\parallel m_e$. For the ion cloud we assume initialy a profile given by a similar gaussian distribution.

Numerical Results

We studied numerically the release of an ion and a neutral cloud at an altitude of 230 km and high latitude. We considred water ions and neutrals, since water was found to be the major contaminant about space structures. However, the analysis could be easily apllied to any other release. The computational grid was orthogonal with 20 × 20 × 64 grid points in the x, y and z directions respectiveiy. The upper

and lower boundaries located appropriately so that there would be no effect on the obtained numerical solution. A uniform mesh was generated with $\Delta x = \Delta y = 3$ km and $\Delta z = 4$ km. The choice of almost equal grid sizes prooved to be necessary since unequal grid sizes would alter and reduce the physical difference between the tranverse and parallel directions. The temperature of the contaminant ions was taken to be $T_{H_2O^+} = 0.025$ eV. The ambient ionosphere was modeled by isothermal oxygen ions with T_{O^+} eV and isothermal electrons with $T_e = 0.2$ eV. In all the simulations we neglected neutral winds and gravity. The results are presented in a reference frame moving with the orbital speed of 8km/sec, so that in this Orbiter frame there is a motional electric field of $|E_m| = 0.35$ V/m. The computational reference frame is shown in Figure (6). In that frame
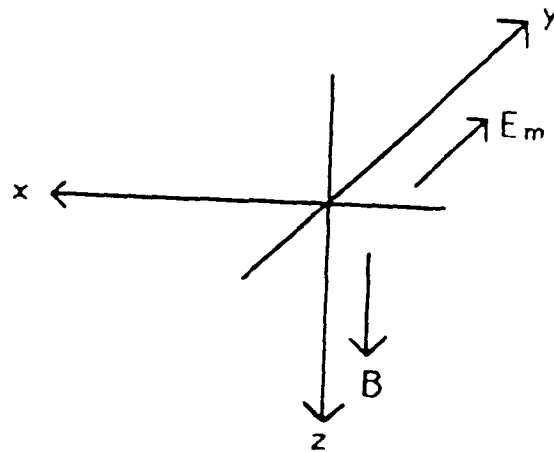
Figure 6: Computational grid

positive z direction points towards lower altitudes, the positive y direction points to the east and is the direction of the motional electric field, and the negative x direction points to the south and is the direction of the orbital motion. In this series of numerical experiments we investigated the effects of the central density, the cloud dimensions and the presence of a neutral cloud on the electrodynamic behavior of the cloud.

Ion cloud

In Figures (7,8,9) we present results from a low density ion cloud. The central density is two orders lower than the ambient and thus, corresponds to a very weak density perturbation. The falling distances of the ion cloud are $r_\perp = 4.5$ km and $r_\parallel = 6$km and the mass of the release water ions is $M_{H_2O^+} = 0.002$ kgr. The perturbation potential at the plane of the release is shown in Figure 7. The potential shows a dipole structure and the perturbation electric field is directed oposite to the motional and tries to screen it out. In the center of the cloud the perturbation electric field is $\epsilon = 4.1 \times 10^{-6}$ V/m. Thus, the total electric field in the Orbital reference frame will be almost the motional. Note

73

that the maximum and minimum of potential are symmetrical since diffusion currents are very small and effects from Hall currents are not important. The $y = 0$ plane shows the very important effects of the three-dimensionality; the magnetic field lines are no longer equipotential lines, an assumption present in all the previous two-dimensional cloud models. The non-equipotential region seems to be confined within the cloud boundaries. Beyond a radius of ~ 9 km in the perpendicular plane and ~ 12 km in the parallel direction the magnetic fild lines become equipotential again. The weak perturbation can be attributed to the very slight modification of the conductivities as it is shown in Figures 8,9).

As the central density increases the potential perturbation increases. In Figure 10 the central density is of the order of the ambient and the perturbed electric field at the center is now $\epsilon = 4.1 \times 10^{-3}$ V/m. The equipotentiality of the B lines holds outside of the cloud boundaries. The conductivities are altered in the cloud region as it is shown in Figures (11,12). Both the Pedersen and the parallel conductivities increase, while the effect of the ion cloud on the Hall conductivity is not so evident.

In Figures (13,14,15) results are shown for a very dense cloud with central ion density of 10^{15} m^{-3} and $M_{H_2O^+} = 15$ kgr. The perturbation electric field is now 0.349 V/m, which shows that the motional electric field is practicaly shielded at the cloud center. There is also a rotation in the perturbation electric field due to the Hall currents. The Hall currents however are flowing to the $\vec{E_m} \times \vec{B}$ direction which implies that the ion Hall conductivity dominates over the electron. As Figure 14 shows the Hall conductivity becomes negative (with our definition of conductivities it is positive when is dominated by the electron conductivity and would imply Hall currents in the $\vec{B} \times \vec{E_m}$ direction). In Figure 15 the Pedersen conductivity shows an increase of almost three order of magnitudes and thus , once expects a significant perturbation to propagate along the B field. The $y = 0$ plane plot in Figure 13 shows that the non- equipotential region extends now to almost 18 km along the magnetic field.

We investigated also the effects of the cloud dimensions on the electrodynamic behavior of the cloud. In Figure 16 the perpendicular and parallel lengths are $r_\perp = 3$ km and $r_\parallel = 4$ km and the perturbation field becomes $\epsilon = 0.341$ V/m at the cloud center. The rotation of the electric field denotes Hall currents in the $\vec{E_m} \times \vec{B}$ direction. In Figure 17 the Hall conductivity is shown to be negative in the outer region of the cloud but remains always smaller than the Pedersen. As the cloud dimensions decrease (Figure 19) to $r_{perp} = 1.5$ km and $r_\parallel = 2$ km, the perturbation electric field at the center of the cloud drops to 0.327 V/m. The dipole structure of the potential prevails again but in this small radius there is an asymmetry in the center caused by the diffusion currents, which are comparable there with the direct currents. The non-equipotential region has also

become smaller and now extends to ~ 9 km along the B lines, and to a radius of ~ 3 km in the perpenicular plane.

Ion and Neutral Clouds

We studied the effects of the presence of contaminant neutrals along with the ions. We considered a neutral cloud with central density of 10^{17} m^{-3} and falling off distances of $r_{perp} = 3$ km and $r_\parallel = 4$ km. This corresponds to a release of 15 kgr of H_2O^+ and 1500 kgr of H_2O. Results are shown in Figures (22,23,24). The perturbation electric field is $\epsilon = 0.3496$ at the center which is larger than the case where only the ion cloud is present. Collisions with the contaminant neutrals are very frequent and the conductivites are much larger than the case where only ions are present as we see by comparing Figures 17 and 23. The effects of Hall currents are also less visible and the Hall conductivity is dominated by the electrons. The maximum and minimum of the perturbation potential are also larger. The region however of nonequipotential B lines seems to extend at ~ 18 km along the B lines, although the disturbance itself appears to be stronger (compare Figures 22 and 16).

Conclusion - Future work

We developed a fully tree-dimensionnal model for an artificial plasma cloud in the ionosphere. Such a cloud could be a result of a deliberate release of neutrals or ions or a result of contamination about a spacecraft. The neutral cloud consists of the ejected neutrals s and the ambient neutrals a. The ejected neutrals undergo charge exchange reaction with the ambient ions to create contaminant ions. It is assumed that the cloud has finite perpendicular and parallel lengths. We take into account all elastic collisions between the considered species and include finite temperature effects. We model the ionosphere and take into account variable densities for ambient neutrals and ions, altitude dependent ambient neutral winds, ambient electric fields and gravity. In the momentum balance of the charged species we include electric fields, forces due to elastic collisions, pressure forces and gravity. The plasma species are assumed to be isothermal. An analytic solution to the system of momentum equations yields the velocities of the charged species in both the perpendicular and parallel plane. The velocities were written with the use of transport coefficient tensors. These transport coefficients account for the mobility, the diffusion due to density gradient of all the charged species, gravity and ambient and contaminant neutral winds. The transport coefficients depend drastically on the direction and are greatly modified by the presence of the plasma cloud. The values for the undisturbed ionosphere calculated from our model compared with simplified models and found to be in good agreement. It is found that generalized Einstein relations hold between the mobility and the diffusion transport coefficients. Simple relations hold between the diffusion and the rest of the transport coefficients.
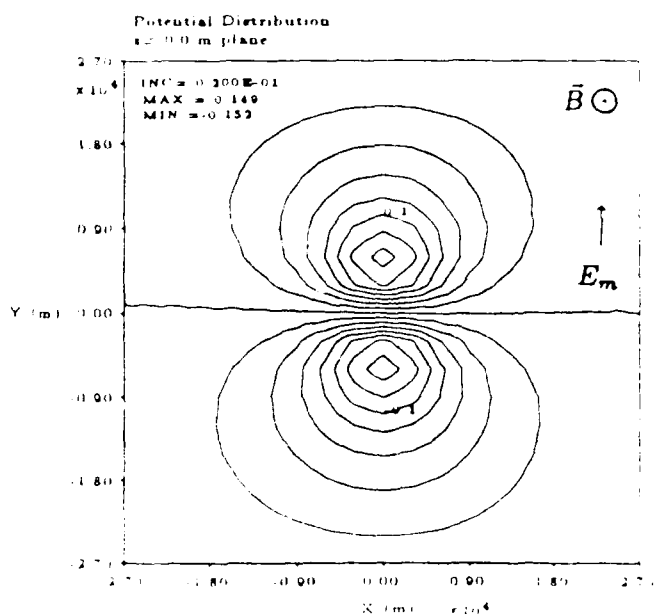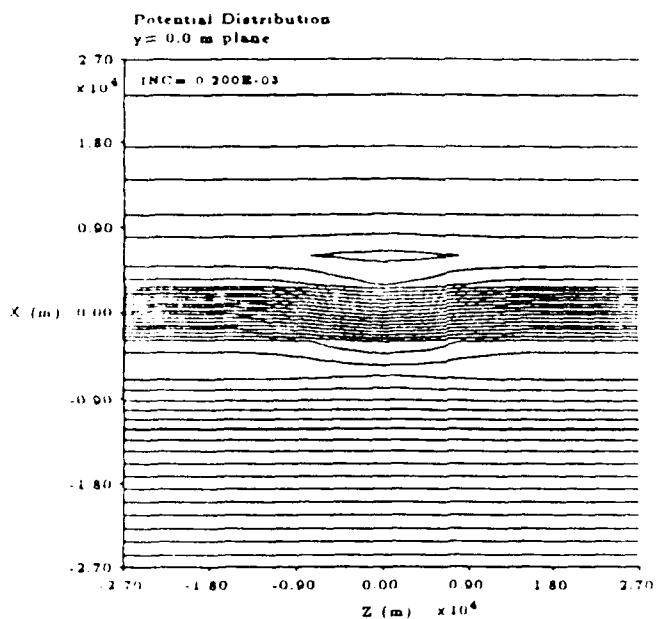
Potential Distribution
y = 0.0 m plane

INC = 0.200E-03

Figure 8: Pedersen at the z=0 plane

Potential Distribution
z = 0.0 m plane

INC = 0.200E-01
MAX = 0.149
MIN = -0.153

$\vec{B} \odot$

E_m

Figure 7: Perturbation potential (Volts). (T_p) At the y plane. (Bottom): At the plane of the release, $z = 0$. The cloud has a central ion density $n_{H_2O^+} = 10^9$ m^{-3} and dimensions $r_\perp = 4.5$ km, $r_\parallel = 6$ km.
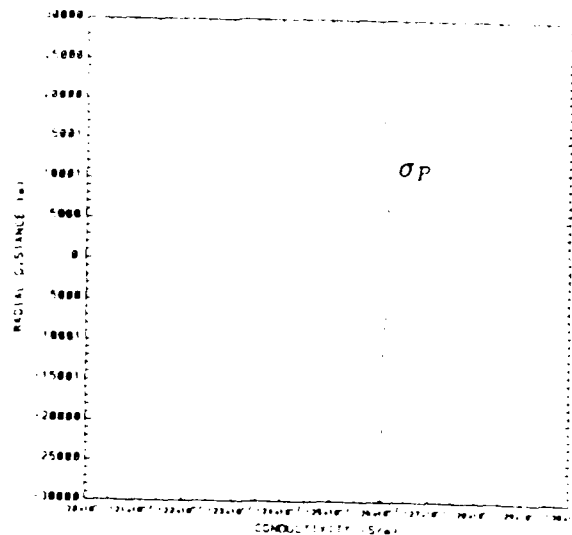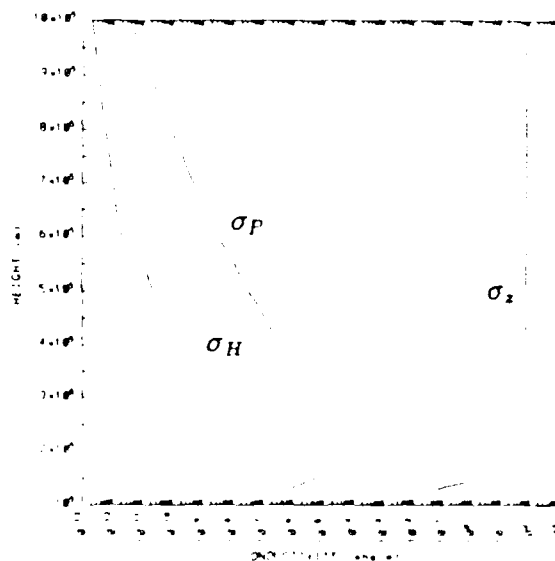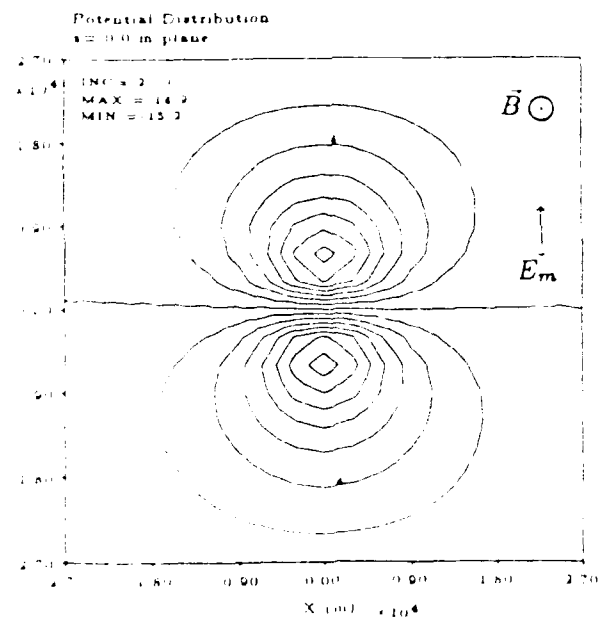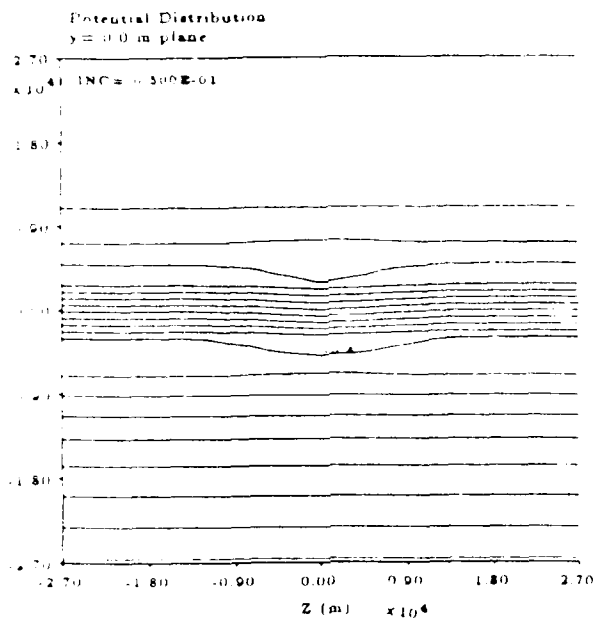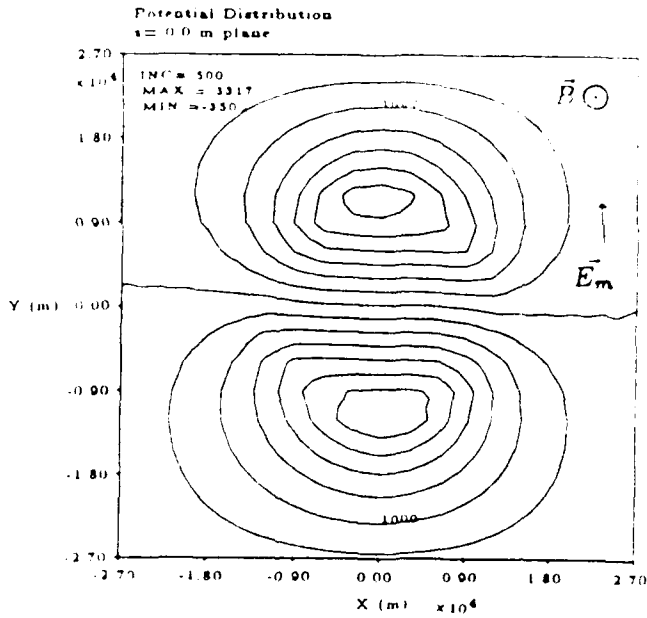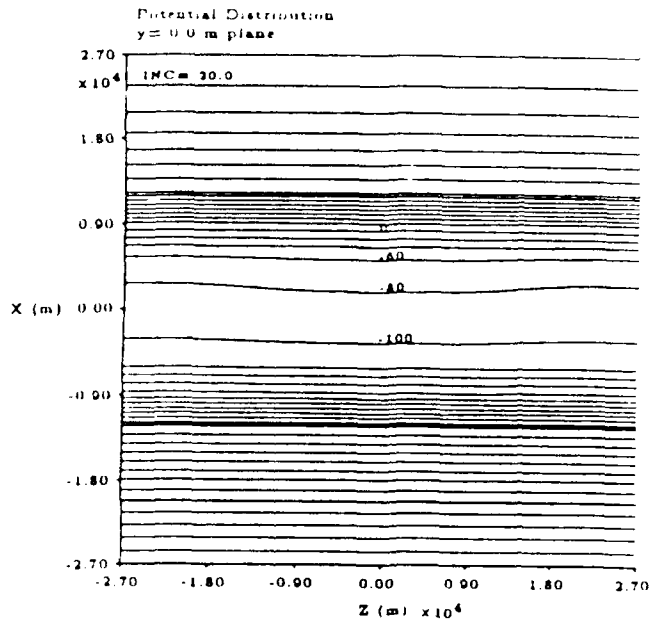
Figure 9: Pedersen, Hall and parallel conductivity at y=0 or x=0 plane

75

Potential Distribution
y = 0.0 m plane

Figure 11: Pedersen and Hall conductivity at the z=0 plane

Potential Distribution
z = 0.0 m plane

$\vec{B} \odot$

$\vec{E}_m$
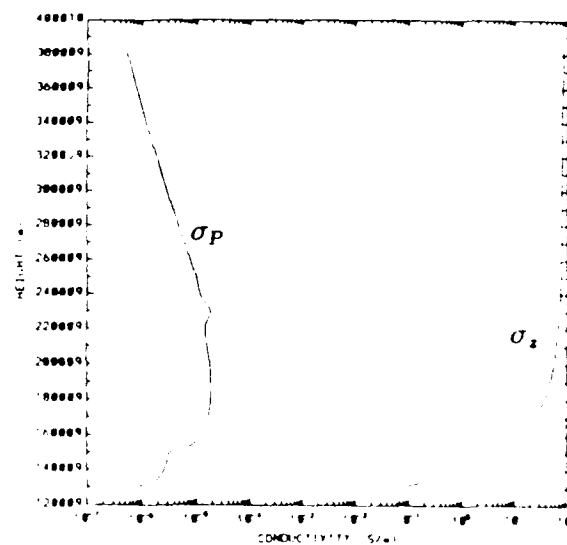
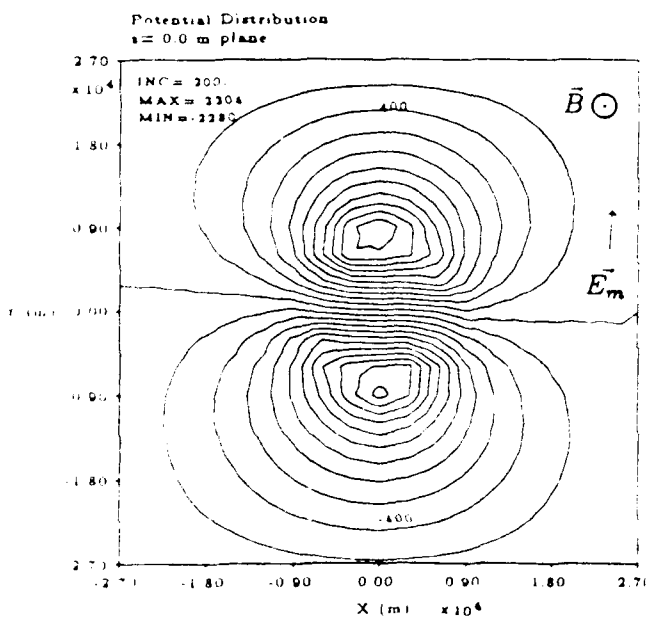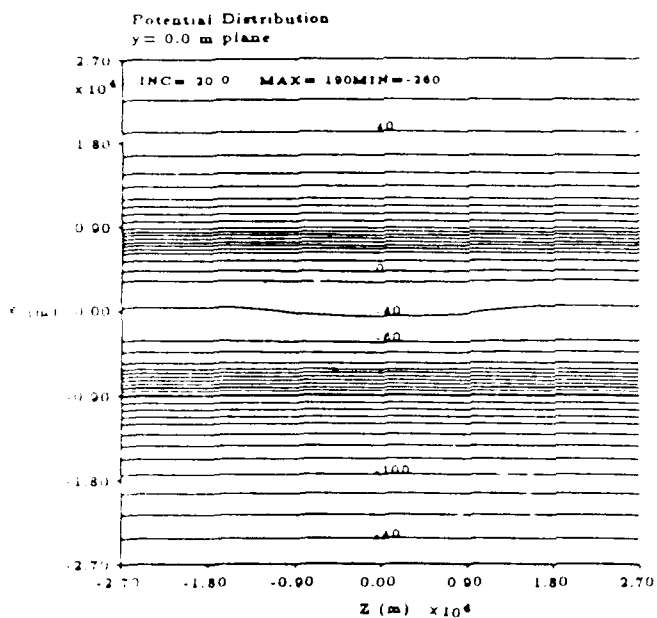Figure 12: Pedersen and parallel conductivity at y=0 or x=0 plane

Figure : Perturbation potential (Volts). (Top) At the z=0 plane. (Bottom) At the plane of the release. The cloud has a central ion density $n_{H_2,0} = 10^{11}$ m^{-3} and dimensions $r_z = 4.5$ km, $r = 6$ km.

76

Potential Distribution
y = 0.0 m plane

INC= 20.0

Figure 14: Pedersen and Hall conductivity at the z=0 plane

Potential Distribution
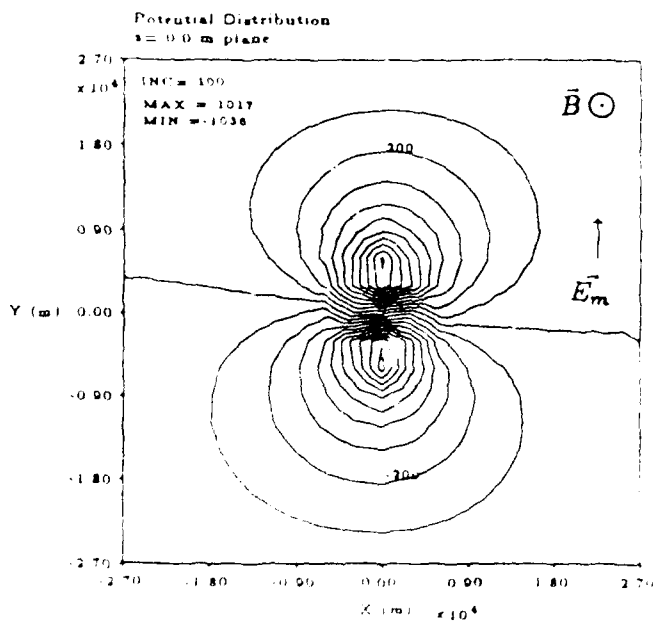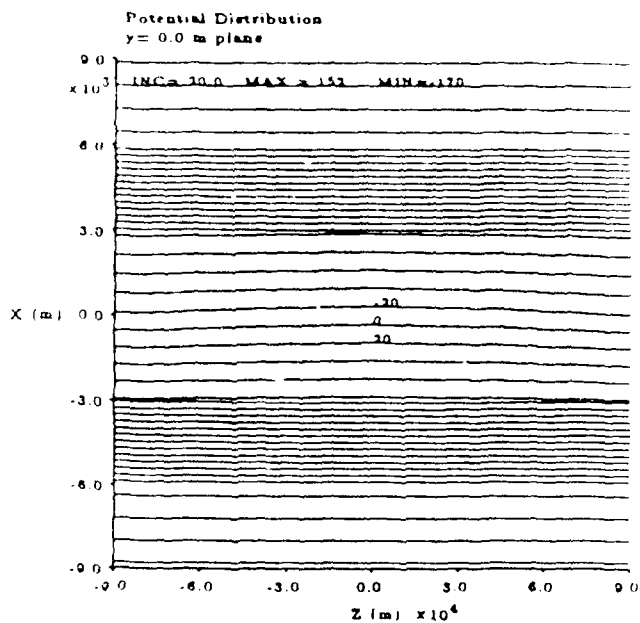z = 0.0 m plane

INC= 500
MAX = 3317
MIN = -350

Figure 13. Perturbation potential (Volts). (Top): At the
y = 0 plane. (Bottom) At the plane of the release. The
lat has a central ion density $n_{H_2O^+} = 10^{15}$ m^{-3} and
dimensions $r_\perp = 4.5$ km, $r_\parallel = 6$ km.
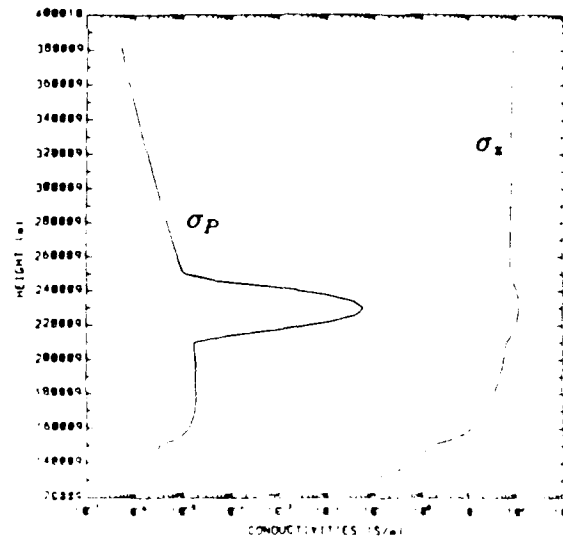
Figure 15: Pedersen and parallel conductivity at y=0 or
x=0 plane

77

Potential Distribution
y = 0.0 m plane

Figure 17: Pedersen and Hall conductivity at the z=0 plane

Potential Distribution
x = 0.0 m plane

Figure 16. Perturbation potential (Volts). (Top): At the y = 0 plane. (Bottom). At the plane of the release. The cloud has a central ion density $n_{H_2O^+} = 10^{15}$ m^{-3} and dimensions $r_\perp = 3$ km, $r_\parallel = 4$ km.
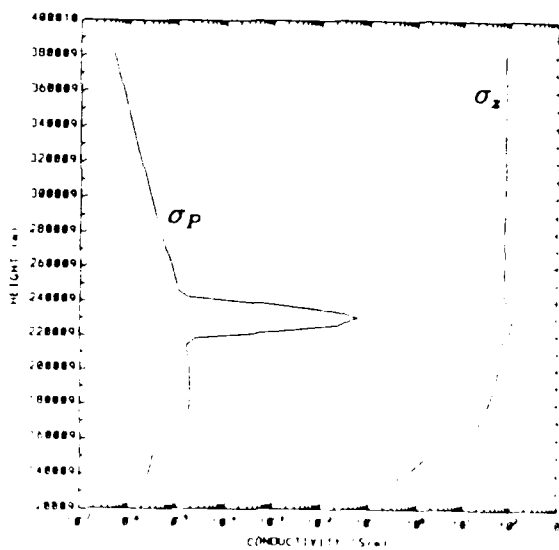
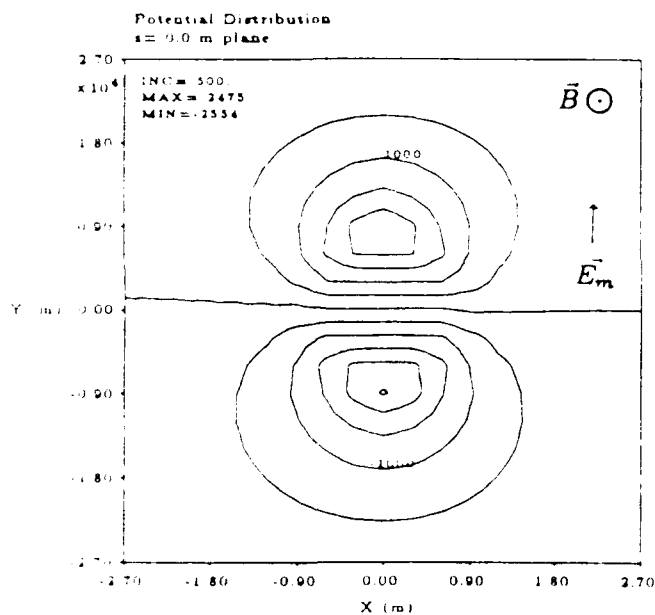Figure 18: Pedersen and parallel conductivity at y=0 or x=0 plane

78

Potential Distribution
y= 0.0 m plane

Figure 20: Pedersen and Hall conductivity at the z=0 plane

Potential Distribution
z= 0.0 m plane

Figure 19: Perturbation potential (Volts) (Top). At the z=0 plane (Bottom). At the plane of the release. The cloud has a central ion density $n_{H_2O^+} = 10^{15}$ m^{-3} and dimensions $r_\perp = 1.5$ km, $r_\parallel = 2$ km.
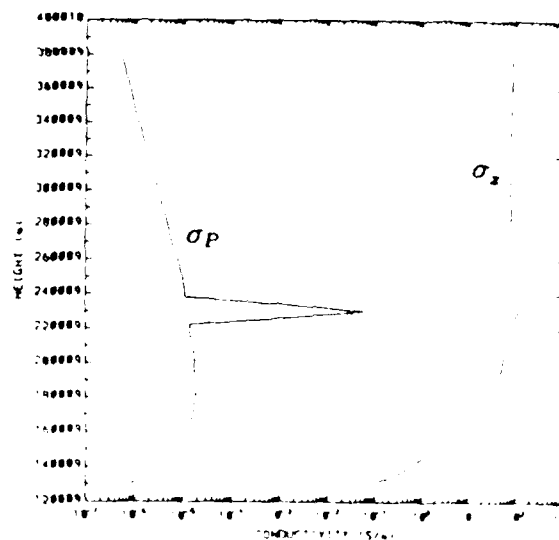
Figure 21. Pedersen and parallel conductivity at y=0, x=0 plane

Potential Distribution
y= 0 0 m plane

INC= 15 0   MAX= 55 MIN=-125

X (m)

Z (m)   x10⁴

Figure 23: Pedersen and Hall conductivity at the z=0 plane

Potential Distribution
z= 0.0 m plane

INC= 500
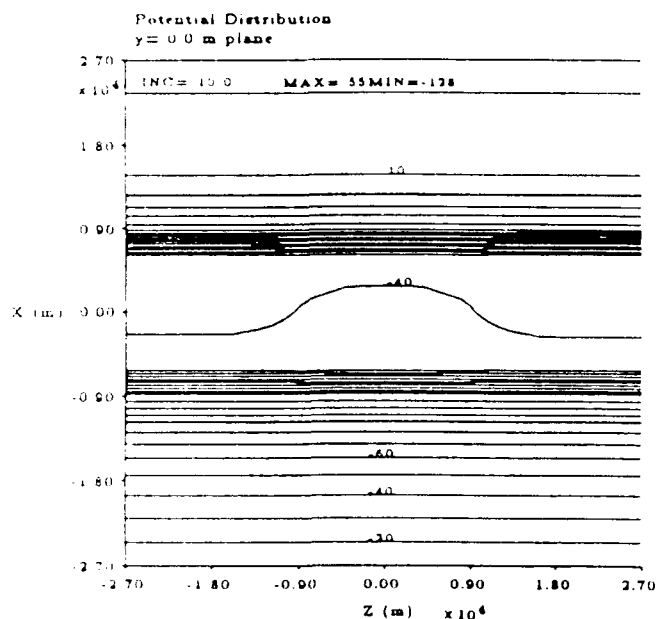MAX= 2475
MIN=-2556

$\vec{B} \odot$

$\vec{E_m}$

X (m)

Figure 22. Perturbation potential (Volts). (Top): At the
y = 0 plane. (Bottom): At the plane of the release. The
cloud has a central ion density $n_{H_2O^+} = 10^{15}$ m^{-3} and
dimensions $r_\perp = 3$ km, $r_\parallel = 4$ km. The neutral cloud has a
central density $n_{H_2O} = 10^{17}$ m^{-3} and dimensions $r_\perp = 3$
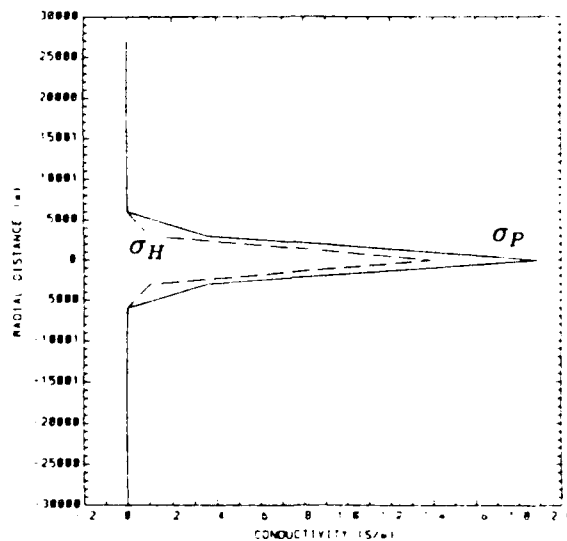km, $r_\parallel = 4$ km.

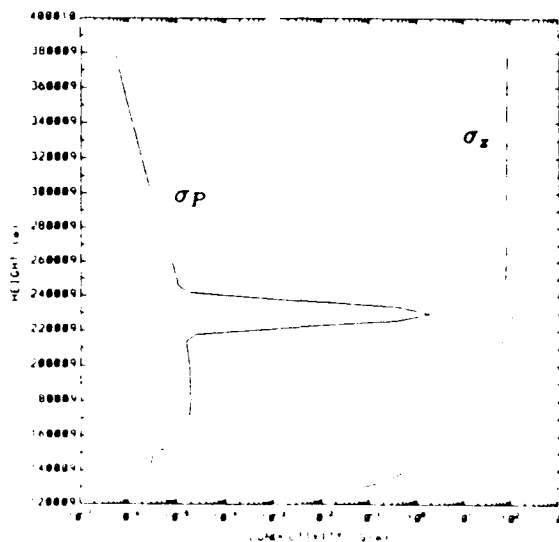
Figure 24. Pedersen and parallel conductivity at y=0 or
x=0 plane

80

The current balance between the cloud and the ambient plasma determines the dynamical behavior of the plasma cloud. It is assumed that the plasma is quasineutral and that the electric fields are electrostatic. On applying charge conservation an equation for the self-consisted potential due to the plasma perturbation is derived. The current balance includes conductive currents, diffusion currents due to density gradients in the ambient and contaminant ions as well as electrons, currents due to the ambient and contaminant neutral winds and gravitational drift currents. The coupling of the plasma cloud to the ambient plasma is examined with the use of a closure model in which insulators are placed in the upper and lower boundaries and coupling is obtained via classical currents only. The equilibrium electric field were obtained and compared with simple analytical solutions. The current balance equation was solved numerically in order to obtain the perturbation potential at the time of the release. We examined the effects of the central density of the ions and the dimensions of the cloud. The perturbation potential increases with increasing ion density. With densities of 10^{16} m^{-3} the cloud shields out the motional electric field. Ion clouds with smaller dimensions result in weaker electric field perturbations. In all cases, the magnetic field lines were not equipotential lines within a region bounded by the density perturbation. The perturbation along the B lines was stronger for the case of denser and larger clouds. The effect of the presence of neutral was also investigated

A gaussian neutral cloud was considered with the same dimensions as the ion cloud. The perturbation potential was stronger than the case where only ions were present. The electric fields will determine the velocities of the ion species. It is expected that for there will be a differential speed within the cloud, which will result in the finger-like shaping of the cloud. Currenlty a numerical model for the solution of the three-dimensional equations for the densities is under development. This will allow to follow in time the motion of the release.

References

[1] G. E. Caledonia, J. C. Person, and D. E. Hastings. The interpretation of space shuttle measurements of ionic species. *J. Geophys. Res.*, 92:273–281, 1987.

[2] G. R. Carignan and E. M. Miller. Induced environment contaminant monitor:gaseous constituents. 87–101, 1983.

[3] J. V. Eccles, W. J. Raitt, and P. M. Banks. A numerical model of the electrodynamics of plasma within the contaminant gas cloud of the space shuttle orbiter at LEO. *J. Geophys. Res.*, 92:273–281, 1987.

[4] N. A. Gatsonis. *Theory and numerical analysis of plasma clouds surrounding space systems in low earth orbit.* Master's thesis, Mass. Inst. of Technol., Cambridge, 1987

[5] G. Haerendel, R. Lust, and E. Rieger. Motion of artificial ion clouds in the upper atmosphere. *Planet. Space Sci.*, 15:1–18, 1967.

[6] D. E. Hastings and N. A. Gatsonis. The motion of contaminant water plasma clouds about large active space structures. 1989.

[7] G. Murphy, J. Pickett, N. D'angelo, and W. S. Kurth. Measurements of the plasma parameters in the vicinity of the space shuttle. *Planet. Space Sci.*, 34:993–1004, 1986.

[8] S. D. Shawhan, G. Murphy, and J. S. Pickett. Plasma diagnostics package initial assessment of the shuttle orbiter plasma environment. *J. Spacecraft and Rockets*, 21:387, 1984.